e-proceedings

IRC 2025 BANGKOK

International Rubber Conference 2025

Rubber Revolution : Balancing Nature and Innovation for a Sustainable Future

1-3 December 2025

Bangkok International Trade & Exhibition Centre, Bangkok, Thailand

Organised by :

Co-organisers :

International Rubber Conference 2025 (IRC 2025)

Organised by :

- The Polymer Society of Thailand (PST)
- International Rubber Conference Organisation (IRCO)

Co-organisers :

- National Metal and Materials Technology Center (MTEC)
- Rubber Industry Club, Federation of Thai Rubber Industry
- Hub of Talents in Natural Rubber, NRCT
- TechnoBiz Communications Co., Ltd.

Sponsors :

Platinum

- National Metal and Materials Technology Center (MTEC)
- Rubber Authority of Thailand (RAOT)

Gold

- Sumitomo Rubber Industries, Ltd.

Silver

- Struktol Company of America, LLC

Bronze

- KOKOKU Innovative Technology Ltd.
- Otani Tire Co.,Ltd.
- Prince of Songkla University
- PT Cabot Indonesia
- Saengthai Rubber Co., Ltd.

Supporting

- Bangkok Synthetics Co., Ltd.
- Behn Meyer Chemicals (T) Co., Ltd.
- MRS-Thailand
- Singha Corporation
- Union Belt Industries Co., Ltd.
- Yokohama Tire Manufacturing (Thailand) Co., Ltd.

Message from Chairman of the Organising Committee

The International Rubber Conference 2025 (IRC 2025) is held for the first time in Thailand, the world's number one supplier of natural rubber, during 1-3 December 2025, although we had previously organised the RubberCon before in 2013. We are honoured to be given an opportunity to host this event on behalf of the rubber societies throughout the world which are members of the IRCO. We promise to do our best to make the IRC 2025 a successful and memorable event as well as being beneficial to all the participants.

As we are well aware, the IRC is one of the leading and most widely known international rubber conference which has been organised since 1966. The Conference provides a forum for sharing new developments in the science, technology and engineering of rubbers and rubber products, including the issues of health, safety and environment in connection with the modern rubber industry. The objectives are to encourage and promote international progress in rubber science, technology and engineering, co-operation as well as involvement of the younger generation for sustainability of the rubber industry.

The theme of IRC 2025 is "Rubber Revolution: Balancing Nature and Innovation for a Sustainable Future". A rather emphatic theme reflects our beliefs that there is an increasing urgency for all of us to work harder and more effectively to achieve sustainability of the rubber industry. Therefore, the IRC 2025 focuses on the innovation of increasing uses of natural raw materials (particularly natural rubber which has unique attributes to help accelerate achievement of net zero emissions goal for the rubber industry), technologies supporting the circular economy of the rubber industry, design and manufacturing technologies for sustainable rubber products with also longer life, raising safety and lowering of negative impact on the environment of the rubber products and unexplored applications of rubbers and rubber composites. As an emphasis on the importance of natural rubber in contributing to sustainability of the rubber industry, a one day Natural Rubber Symposium is also organised in the IRC 2025 under the theme "Sustainability of Natural Rubber : Latest Challenge and Solutions". The NR Symposium provides a platform for discussing and exchanging expert ideas and opinions in order to tackle the critical issues facing the sustainability of natural rubber industry today."

On behalf of the Organising Committee of the IRC 2025, I would like to extend our gratitude to all of you who are actively participating in the IRC 2025, to help make the IRC 2025 a successful event. I also sincerely hope that you will obtain the benefits of learning and exchanging new knowledge and technology relating to the development of sustainable rubber industry, as well as be provided with a rare opportunity to meet, discuss and possibly network with outstanding international researchers.

Welcome to the IRC 2025 and to Thailand.

Dr. Krisda Suchiva
Chairman of the Organising Committee,
International Rubber Conference 2025

Message from the President of the Polymer Society of Thailand

Dear Participants,

On behalf of the **Polymer Society of Thailand**, it is my great pleasure and honour to welcome you to the **International Rubber Conference 2025 (IRC2025)**, held this year under the theme **"Rubber Revolution: Balancing Nature and Innovation for a Sustainable Future."**

It has been nearly ten years since our society first expressed the intention to host this prestigious conference. Today, we are delighted to see IRC return to Thailand — a country recognized as the **world's leading producer of natural rubber** and a vital contributor to the global rubber supply chain. Although the IRC embraces all types of rubber, both natural and synthetic, it is fitting that this year's conference highlights the indispensable role of **natural rubber**, a renewable biomaterial supporting millions of smallholder farmers while meeting the diverse needs of global industries.

We are proud to collaborate closely with the **International Rubber Conference Organisation (IRCO)** in organizing this event, which serves as one of the world's most influential platforms for scientists, technologists, industrial leaders, and policymakers in the rubber field. At a time when the rubber sector faces challenges related to supply, sustainability, climate change, and performance demands from emerging technologies, innovation has never been more crucial. From advanced material design and green processing to circularity and responsible sourcing, our community plays a pivotal role in shaping the future of rubber.

The theme of IRC2025 — balancing nature with innovation — reflects a shared vision: that progress in polymer and rubber science must go hand in hand with environmental stewardship, economic resilience, and the well-being of communities. As a natural, versatile, and high-performance biomaterial, natural rubber remains central to this journey, offering unmatched properties while contributing to a more sustainable future.

I sincerely hope that this conference will inspire new ideas, spark meaningful discussions, and forge lasting collaborations. May IRC2025 serve as a bridge connecting fundamental research, industrial applications, and global strategies for sustainability.

Thank you for joining us in Bangkok. I wish you all a fruitful, engaging, and memorable conference experience.

Sincerely,

Associate Professor Dr. Taweechai Amornsakchai
President, Polymer Society of Thailand

II CONFERENCE COMMITTEE II

Organising Committee

Chairman

Dr. Krisda Suchiva	Mahidol University

Committee

Prof. Pranee Phinyocheep	Mahidol University (Vice-Chairman)
Dr. Ittipol Jangchud	King Mongkut's Institute of Technology Ladkrabang (Vice-Chairman)
Dr. Kannika Sahakaro	Prince of Songkla University (Vice-Chairman)
Dr. Taweechai Amornsakchai	Mahidol University (Secretariat)
Mr. Adisak Kongwaree	Thai Rubber Glove Manufacturers Association
Mr. Boonharn Ou-Udomying	Rubber Industry Group, Federation of Thai Industry
Dr. Charoen Nakason	Prince of Songkla University
Mr. Ekachai Limpichotipong	Rubber Industry Group, Federation of Thai Industry
Dr. Ekwipoo Kalkornsurapranee	Prince of Songkla University
Dr. Kanoktip Boonkerd	Chulalongkorn University
Ms. Pannee Jirabunpaisit	National Research Council of Thailand
Dr. Pasaree Laokijcharoen	National Metal and Materials Technology Center
Mr. Peram Prasada Rao	TechnoBiz
Dr. Sunanta Chuayprakong	King Mongkut's University of technology North Bangkok
Dr. Surapich Loykulnant	National Metal and Materials Technology Center
Dr. Wirasak Smitthipong	Kasetsart University

Scientific Committee

Chairman

Prof. Pranee Phinyocheep	Mahidol University (Chairman)

Committee

Dr. Panya Sunintaboon	Mahidol University (Secretariat)
Dr. Anoma Thitithammawong	Prince of Songkla University
Dr. Chaiwat Raksakulpiwat	Suranaree University of Technology
Prof. Chakrit Sirisinha	Mahidol University
Dr. Charoen Nakason	Prince of Songkla University
Dr. Chorwayakron Phetphaisit	Naresuan University
Dr. Ekwipoo Karnkornsurapranee	Prince of Songkla University
Dr. Ittipol Jangchud	King Mongkut's Institute of Technology Ladkrabang
Prof. Jitladda Sakdapipanich	Mahidol University
Dr. Kannika Sahakaro	Prince of Songkla University
Dr. Kanoktip Boonkerd	Chulalongkorn University
Dr. Pongdhorn Sae-oui	National Metal and Materials Technology Center
Prof. Pramuan Tangboriboonrat	Mahidol University
Prof. Rathanawan Magaraphan	Chulalongkorn University
Dr. Sombat Thanawan	Mahidol University
Dr. Supa Wiraset	Mahidol University
Dr. Supitta Suethao	Kasetsart University
Dr. Surapich Loykulnant	National Metal and Materials Technology Center
Dr. Taweechai Amornsakchai	Mahidol University
Dr. Wirasak Smitthipong	Kasetsart University

International Advisory Committee

Dr. Amir Hashim Yatim	Malaysian Rubber Glove Manufacturers Association, Malaysia
Dr. Amit Das	Leibniz-Institut Fur Polymerforschung Dresden, Germany
Prof. Anke Blume	University of Twente, Netherlands
Prof. Bagdagul Karaagac	Kocaeli University, Turkiye
Prof. Baochun Guo	South China University of Technology, China
Prof. Changwoon Nah	Jeonbuk National University, Korea
Dabo Philippe	AFICEP, France
Prof. Jacques W.M. Noordermeer	The Dutch Natural Rubber Foundation, Netherlands
Prof. James Busfield	Queen Mary University of London, UK
Prof. Jean Francois Pilard	Le Mans Université, France
Prof. Keon-Soo Jang	University of Suwon, Korea
Prof. Kinsuk Naskar	Indian Institute of Technology, Kharagpur, India
Prof. Liqun Zhang	Xi'an Jiaotong University, China
Prof. Markus Susoff	University of Applied Science of Osnabrück, Germany
Prof. Mikihito Takenaka	Kyoto University, Japan
Prof. Murat Sen	Hacettepe University, Turkiye
Dr. Nadras Othman	Universiti Sains Malaysia, Malaysia
Dr. Phan Trung Nghia	Hanoi University, Vietnam
Prof. Sabu Thomas	Mahatma Gandhi University, India
Prof. Seiichi Kawahara	Nagaoka University of Technology, Japan
Prof. Shinichi Sakurai	Kyoto Institute of Technology, Japan
Prof. Ulrich Giese	German Institute for Rubber Technology, Germany

Polymer Society of Thailand Committee

Advisory board

Prof. Supawan Tantayanon	Chulalongkorn University
Prof. Suda Kiatkamjornwong	Chulalongkorn University
Prof. Pattarapan Prasassarakich	Chulalongkorn University
Dr. Krisda Suchiva	Mahidol University
Prof. Suwabun Chirachanchai	Chulalongkorn University
Prof. Pranee Phinyocheep	Mahidol University
Dr. Chaya Chandavasu	PTT Global Chemical PCL

President

Dr. Taweechai Amornsakchai	Mahidol University

Committee

Dr. Amorn Chaiyasat	Rajamangala University of Technology Thanyaburi
Dr. Amornrat Lertworasirikul	Kasetsart University
Dr. Anucha Euapermkiati	PTT Global Chemical Public Co., Ltd.
Dr. Ittipol Jangchud	King Mongkut's Institute of Technology Ladkrabang
Dr. Kannika Sahakaro	Prince of Songkla University
Mr. Kongsak Dokbua	Plastics Institute of Thailand
Dr. Nattakarn Honsriphan	Silpakorn University
Dr. Pakorn Opaprakasit	Thammasat University
Dr. Panya Sunintaboon	Mahidol University
Dr. Pasaree Laokijcharoen	National Metal and Materials Technology Center
Dr. Sararat Mahasaranon	Naresuan University
Dr. Sunanta Chuayprakong	King Mongkut's University of technology North Bangkok
Mr. Thongchai Oranrigsupak	The Federation of Thai Industries
Dr. Varawut Tangpasuthadol	Chulalongkorn University
Dr. Winita Punyodom	Chiang Mai University
Dr. Wonchalerm Rungswang	SCG Chemicals Company Limited

Content

Green Rubber Compounding and Processing

IRC 2025
BANGKOK, THAILAND

International Rubber Conference 2025 (IRC 2025)

Application of stearic acid-modified silica in PCR tread compound

FARSHID ZOLALA[1]

[1]*Process Engineering Specialist (compounding),Barez Industrial Group, Kerman, Ian.*

E-mail: Zolala_f@barez.org

Abstract

Silica is a key reinforcing filler in the rubber industry, particularly for high-performance tire tread applications. However, it has poor compatibility with nonpolar elastomers limit its dispersion and reinforcing efficiency. Surface modification of silica with stearic acid has been explored as an effective method to enhance its performance in tire tread compounds. This study investigates the effects of stearic acid-modified silica on the physical and mechanical properties of PCR tread compound. The modification process involves the esterification reaction between the hydroxyl groups (–SiOH) on the silica surface and the carboxylic acid group (–COOH) of stearic acid, resulting in a hydrophobic surface, containing 5% stearic acid modification, that improves better filler dispersion and polymer-filler interaction. This leads to reduce silica agglomeration due to decreased surface polarity, and better filler-matrix compatibility. Increase tensile strength, abrasion resistance, lower rolling resistance and wet skid properties.

Keywords: Silica, Stearic acid, Rolling resistance, Tread compound

1. Introduction

The tire industry has undergone a major transformation over the past two decades, with an increasing emphasis on developing high-performance, energy-efficient, and environmentally sustainable products. The concept of "green tires" has become central to this effort, aiming to reduce rolling resistance, enhance fuel economy, and maintain superior traction and durability [1, 2].

Silica (SiO_2), a reinforcing filler, has played a key role in this transformation. Unlike conventional carbon black, silica provides better control over viscoelastic properties and offers the potential to decouple rolling resistance and wet grip — two properties that are traditionally difficult to balance [3]. However, silica's widespread adoption is hindered by its intrinsic surface chemistry. The surface of precipitated silica is covered with silanol (Si–OH) groups, which form strong hydrogen bonds with each other, leading to extensive filler–filler networking (the "Payne effect") [4,5]. This network reduces filler dispersion and increases compound viscosity, negatively affecting processing and dynamic properties.

1.1 The challenge of silica–rubber incompatibility

In non-polar elastomers such as SBR and BR, the high polarity of silica results in poor interfacial adhesion, leading to void formation and stress concentration under dynamic loading. To enhance compatibility, silane coupling agents such as bis-(3-triethoxysilylpropyl) tetrasulfide (TESPT) have been extensively used.

1.2 Stearic acid as a surface modifier

Stearic acid ($C_{18}H_{36}O_2$) is a long-chain saturated fatty acid containing a hydrophilic carboxylic head and a hydrophobic alkyl tail. When stearic acid interacts with the silica surface, the carboxylic group reacts or adsorbs onto the silanol groups, while the long hydrocarbon chain extends outward, imparting hydrophobicity [7, 8]. The result is a core–shell structure in which the silica surface is coated by an organic layer that reduces filler–filler interactions and enhances compatibility with non-polar polymers.

1.3 Advantages of stearic acid modification

Stearic acid modification offers several advantages: Simple processing (no need for hydrolysis or condensation control).

Low cost and easy scalability.

Improved processability and dispersion without compromising mechanical strength [9, 10].

2. Chemical Structure of Stearic Acid-Modified Silica

Stearic acid ($C_{18}H_{36}O_2$) contains a polar carboxyl group (-COOH) and a long hydrophobic alkyl chain. Its interaction with silica occurs via:

Hydrogen bonding between the -COOH and surface Si–OH groups.

Covalent ester-like linkages (Si–O–C=O–R) formed through condensation under heat.

Surface hydrophobization by alkyl chains extending outward, lowering surface energy and enhancing compatibility with elastomers [11, 12].

The ultimate goal is to establish stearic acid-modified silica in silica-filled tread compounds. This modification is expected to contribute to the development of green tires with reduced rolling resistance, enhanced wet traction, and maintained abrasion resistance [1–3].

3. Experimental methods

Materials

Silica: Precipitated silica (Ultrasil VN3 or equivalent, specific surface area ~170 m^2/g).

Stearic acid: Analytical grade (98% purity).

Elastomers: Solution styrene-butadiene rubber (SSBR) and butadiene rubber (BR).

Other ingredients: Sulfur, ZnO, accelerator (CBS, DPG), wax, silane, antioxidant (6PPD), process oil.

Surface modification procedure

Drying of silica: The silica was pre-dried at 120 °C for 2 hours to remove surface moisture and activate silanol groups.

Stearic acid solution preparation: Stearic acid was dissolved in ethanol at 60 °C with constant stirring to form a homogeneous solution.

Surface modification: The dried silica was gradually added to the stearic acid solution under mechanical stirring at 70 °C. The mixture was refluxed for 3 hours to promote adsorption and esterification between –COOH and –Si–OH groups.

Separation and drying: The modified silica was filtered, washed with ethanol to remove excess unreacted acid, and dried at 100 °C for 12 hours in a vacuum oven. The final product, stearic acid-modified silica, appeared as a light hydrophobic powder that exhibited excellent dispersibility in rubber compounds.

Chemical reaction mechanism

The modification reaction can be represented as:

Si–OH (on silica) + HOOC–R (stearic acid) ⟶ Si–O–C(=O)–R + H2O

Where R represents the $C_{17}H_{35}$ alkyl chain. The reaction results in the partial substitution of silanol groups by ester bonds, while additional acid molecules may physically adsorb on the surface through hydrogen bonding.

4. Characterization Techniques

To confirm surface modification, several analytical tools are used:

FTIR spectroscopy: detects C=O stretching (~1700 cm^{-1}) and C–H bands (~2850–2920 cm^{-1}), indicating stearic acid attachment [13].

TGA: quantifies organic content and grafting density by measuring weight loss of stearic acid upon heating [14].

SEM/TEM: observes morphological differences and improved dispersion.

Table 1. Sample compositions

Components [Phr]	Sample notations	
	N1	N2
SSBR 27.5 %Oil	110	110
BR	20	20
Silica	75	-
Modified Silica(5% stearic acid modification)	-	75
X50S (TESPT 50%)	12	12
Stearic Acid	1	1
Wax	1.5	1.5
ZnO	2.5	2.5
6PPD	2	2
DPG	1.2	1.2
CBS	1.7	1.7
Sulfur	1.6	1.6

5. Results and Discussion

Table 2. Test results

properties	Sample notations	
	N1	N2
T10 @160°C (min)	1.37	1.28
T50 @160°C (min)	4.45	4.14
T90 @160°C (min)	9.32	9.24
MH @160°C (lb.in)	12.2	12.8
Hardness (Shore A)	64	65
Modulus 300% (MPa)	8.4	8.5
Tensile Strength (MPa)	14.3	15.1
Elongation at Break (%)	347	332
Resilience @ 0 °C (%)	13	11.5
Resilience @ room temp. (%)	26	29
Resilience @ 70 °C (%)	60	63

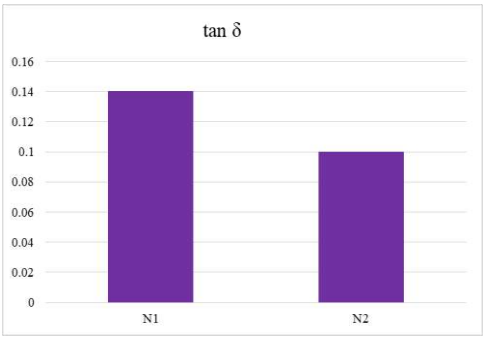

Figure 1. tan δ at 70°C , 10 Hz

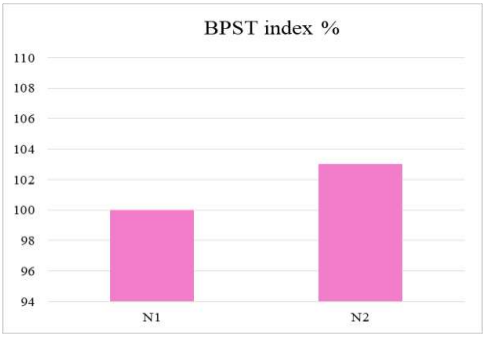

Figure 2. Wet skid resistance

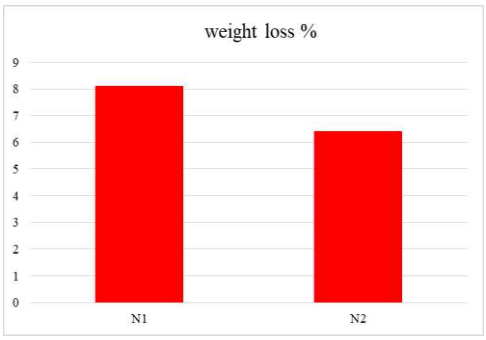

Figure 3. Abrasion resistance

Research has consistently demonstrated that stearic acid modification leads to:

Improved dispersion: reduced aggregation of silica in SBR/BR matrices.

Lower viscosity: reduced Mooney viscosity, enhancing processing.

Stronger filler–rubber interactions: increased storage modulus and reduced filler networking.

Dynamic property improvements:

Lower tan δ at 60 °C (reduced rolling resistance).

Higher tan δ at 0 °C (improved wet traction).

Improve durability: abrasion resistance improves in comparison with unmodified silica-filled compounds.

6. Conclusion

Comparison was made between silica and modified silica in terms of properties and characteristics in the PCR tread compound. Characterization confirms the successful chemical interaction between stearic acid and silica. Based on the performance in the laboratory, the global compromise between rolling resistance, abrasion resistance and wet skid resistance for the tread compounds can be improved by replacing the silica with the modified silica. This is due to the improvement of polymer-filler interaction.

The key outcomes of using stearic acid-modified silica in tread compounds are:

Enhanced compound processability due to lower viscosity.

Optimized performance balance: simultaneous reduction in rolling resistance and improvement in wet traction.

Contribution to green tire technology, enabling tires with lower fuel consumption and reduced environmental footprint.

7. References

1. Wolff, S., Wang, M.J., Rubber Chem. Technol., 1992.
2. Heinrich, G., Klüppel, M., Adv. Polym. Sci., 2002.
3. Donnet, J.B., Custodero, E., Science and Technology of Rubber, 2013.
4. Wang, M.J., Rubber Chem. Technol., 1998.
5. Bokobza, L., J. Appl. Polym. Sci., 2004.
6. Colomines, G., et al., Composites Sci. Technol., 2008.
7. Luo, Y., et al., Materials Chem. Phys., 2015.
8. Li, Y., et al., J. Appl. Polym. Sci., 2017.
9. Zhou, Y., et al., Thermochimica Acta, 2016.
10. Chen, F., et al., Colloids and Surfaces A, 2014.
11. Li, Y., et al. Surface modification of silica with fatty acids and its effect on dispersion in rubber matrix. Journal of Applied Polymer Science, 2017.
12. Luo, Y., et al. Hydrophobization of silica with stearic acid for rubber reinforcement. Materials Chemistry and Phys-ics, 2015.
13. Zhang, M., et al. Characterization of silica modified by fatty acids for rubber applications. Applied Surface Science, 2018.
14. Zhou, Y., et al. Thermal and structural analysis of fatty acid-modified silica particles. Thermochimica Acta, 2016.

Enhancing Durability and Performance of Rubber Products

IRC 2025
BANGKOK, THAILAND

International Rubber Conference 2025 (IRC 2025)

Influences of Sulfur Vulcanization System and Curative Content on Properties of Tire Tread Compounds Filled with Carbon Black/Silica Hybrid Filler

Puchong Thaptong*[1], Pongdhorn Sae-oui[1], Chakrit Sirisinha[2]

[1] *MTEC, National Science and Technology Development Agency (NSTDA), 111 Thailand Science Park, Phahonyothin Road, Khlong Nueng, Khlong Luang, Pathum Thani, Thailand.*

[2] *Rubber Technology Research Centre, Faculty of Science, Mahidol University, Salaya Campus, Phutthamonthon 4 Road, Salaya, Nakhon Pathom, Thailand.*

*E-mail: puchongt@mtec.or.th

Abstract

Properties of 40/60 carbon black (CB)/silica (SiO_2)-filled tire tread compounds were investigated. Two sulfur vulcanization systems, i.e., conventional vulcanization (CV) and semi-efficient vulcanization (semi-EV), were evaluated with relative curative contents ranging from 100% to 140%. Cure characteristics, crosslink density, mechanical properties, tire performance, and thermal aging properties were examined. Based on the tread formulations in this study, an increase in curative content led to enhancements in both the cure rate index (CRI) and crosslink density. However, higher curative contents adversely affected the tensile strength (TS), elongation at break (EB), and thermal aging resistance, while exerting positive influences on key tire performance indicators, i.e., wet grip (WG), fuel saving (FS), and abrasion resistance. Compared with the semi-EV system, the CV system exhibited inferior TS, EB, abrasion resistance, and thermal aging resistance, but superior WG and FS. Overall, the CV system with a relative curative content of 120% provided an optimal balance between tire performance and thermal aging resistance. These findings provide useful guidance for developing advanced tread compounds to meet the stringent requirements of modern, especially electric, vehicles.

Keywords: Sulfur vulcanization system, Curative content, Tread, Properties

1. Introduction

Tire tread plays a crucial role in overall tire performance. It not only functions to evacuate water to prevent hydroplaning, but also influences key performance aspects such as traction, fuel saving (FS), road noise, and service life [1]. Apart from tread pattern, tread compound has a significant impact on tire performance. Continuous efforts have been made to develop tread compounds providing excellent wet grip (WG), low rolling resistance, and high abrasion resistance, that aim to meet the performance requirements of modern vehicles, particularly electric vehicles. Among the various factors affecting tread compound performance, the vulcanization system plays an important role in determining the final performance of tire. Conventional vulcanization (CV), semi-efficient vulcanization (semi-EV), and efficient vulcanization (EV) systems differ primarily in the sulfur-to-accelerator ratio, which directly affects crosslink structure [2], crosslink density, and consequently, tire performance. Therefore, the selection and optimization of the curing system and curative content to meet specific performance targets is a subject of considerable interest.

In this work, tire tread compounds filled with a 40/60 carbon black (CB)/silica (SiO_2) hybrid filler were investigated using two sulfur vulcanization systems: CV and semi-EV. For each system, the relative curative contents—consisting of N-tert-butyl-2-benzothiazole sulfenamide (TBBS), tetrabenzylthiuram disulfide (TBzTD), and sulfur—were varied from 100% to 140%. The mechanical properties, tire performance, and thermal aging behavior were compared, and the optimal vulcanization system and curative level for balancing tire performance and thermal aging resistance were identified.

Table 1. The tread formulae used in this study

Ingredient	Content (parts per hundred rubber, phr)					
	CV			Semi-EV		
	100%	120%	140%	100%	120%	140%
Oil-extended SSBR	137.50	137.50	137.50	137.50	137.50	137.50
CB	28.00	28.00	28.00	28.00	28.00	28.00
SiO_2	42.00	42.00	42.00	42.00	42.00	42.00
TESPT	4.20	4.20	4.20	4.20	4.20	4.20
6PPD	1.50	1.50	1.50	1.50	1.50	1.50
TMQ	1.00	1.00	1.00	1.00	1.00	1.00
Paraffin wax	2.00	2.00	2.00	2.00	2.00	2.00
ZnO	3.00	3.00	3.00	3.00	3.00	3.00
Stearic acid	2.00	2.00	2.00	2.00	2.00	2.00
TBBS	1.20	1.44	1.68	1.20	1.44	1.68
TBzTD	0.20	0.24	0.28	0.20	0.24	0.28
Sulfur	2.20	2.64	3.08	1.20	1.44	1.68

2. Experimental methods

2.1 Materials

All mixing ingredients were used as-received. Oil-extended solution polymerized styrene butadiene rubber (SSBR, SOLC6450SL with 27.1% treated distillate aromatic extract (TDAE) oil content, 34.6% styrene content, 40.1% vinyl content, and 54.5-ML(1+4) at 100°C) was manufactured by Kumho Petrochemical, South Korea. N-(1,3-dimethylbutyl)-N’ -phenyl-p-phenylenediamine (6PPD), 2,2,4-trimethyl-1,2-dihydroquinoline (TMQ) and N-tert-butyl-2-benzothiazole sulfenamide (TBBS) were supplied by Monflex Pte. Ltd., Singapore. Paraffin wax was produced by Nippon Seiro Co., Ltd., Japan. Bis[3-(triethoxysilyl)propyl]tetrasulfide (TESPT) was supplied by Innova (Tianjin) Chemical, China. Other additives were obtained from suppliers in Thailand. Silica (SiO_2, Tokusil 255 with 166 m^2/g BET specific surface area) was manufactured by OSC Siam Silica Co., Ltd. Carbon black (CB, N234 with 126 m^2/g BET specific surface area, 124 ml/100g DBPA number, and 119 mg/g iodine number) was produced by Thai Carbon Black Public Co., Ltd. Zinc oxide (ZnO, white seal) was manufactured by Thai-Lysaght Co., Ltd. Stearic acid was purchased from Kij Paiboon Chemical Ltd., Part. Tetrabenzylthiuram disulfide (TBzTD) was obtained from Behn Meyer Chemicals (T) Co., Ltd. Sulfur was manufactured by Siam Chemicals Public Co., Ltd.

2.2 Preparation and testing of tread compounds

The tread formulae used in this study are shown in Table 1. Tread compounds were prepared in an internal mixer (Brabender-Plasticorder 350E, Germany) equipped with cam rotors. Rotor speed and fill factor were kept constant at 40 rpm and 0.75, respectively. Mixing was carried out in three steps. In the 1st step, all ingredients, except the curatives (TBBS, TBzTD, and sulfur), were mixed with rubbers at the initial chamber temperature of 60°C for 10 minutes to achieve satisfactory degree of filler dispersion. The compounds were then sheeted on two-roll mill (Labtech LRM150, Thailand) and cooled down to room temperature. In the 2nd step, the compounds were remixed at the initial chamber temperature of 140°C for 5 minutes to promote the silanization reaction. In the final step, the compounds were mixed with curatives at the initial chamber temperature of 60°C for 3 minutes. After mixing, the compounds were sheeted on a two-roll mill and kept overnight at room temperature prior to being vulcanized and tested.

Measurement of cure characteristics, i.e., scorch time (t_{s1}), optimum cure time (t_c90), and cure rate index (CRI), was done using a moving die rheometer (TechPro MD+, USA) at 160°C in accordance with ISO 6502-3. CRI is calculated using the following equation:

$$CRI=\frac{100}{t_c90-t_{s1}} \quad (1)$$

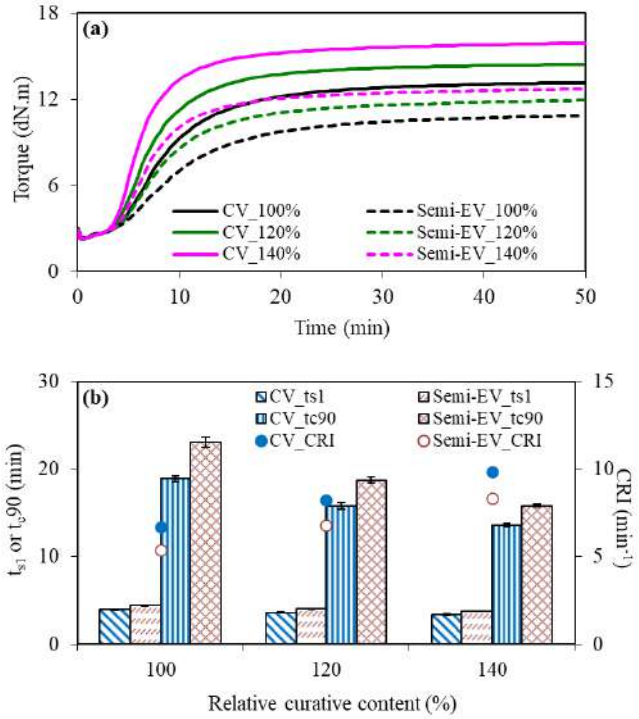

Figure 1. Cure characteristics of the tread compounds: (a) cure curves and (b) t_{s1}, t_c90 and CRI

Vulcanization was carried out using a compression molding technique at 160°C based on the t_c90 measured from MDR. Crosslink density was determined using an indirect method, namely, a swelling test. Rubber test pieces were immersed in toluene for 5 days. The test pieces were then taken out, blotted with filter paper, and weighed. Finally, the test pieces were dried at 70°C until a constant weight was gained before reweighing. The crosslink density was calculated based on the Flory-Rehner equation as follows [3]:

$$-\left[ln(1-v_2)+v_2+\chi_1 v_2^2\right] = v_1 n\left(v_2^{\frac{1}{3}}-\frac{v_2}{2}\right) \qquad (2)$$

where χ_1 is the polymer-solvent interaction parameter (0.446 for SBR-toluene) [4]; v_1 is the molar volume of toluene (106.3 cm^3/mol); n is the number of elastically active chains per unit volume; v_2 is the volume fraction of polymer in the swollen test piece which is calculated as follows:

$$v_2 = \frac{m_0\varphi\frac{(1-\alpha)}{\rho_p}}{m_0\varphi\frac{(1-\alpha)}{\rho_p}+\frac{(m_1-m_2)}{\rho_s}} \qquad (3)$$

where m_0, m_1, and m_2 are the weights of the test piece before swelling, after swelling, and after drying, respectively; φ is the weight fraction of polymer in the test piece; α is the weight loss fraction of the test piece after the swelling test; ρ_p and ρ_s are densities of polymer and solvent, respectively.

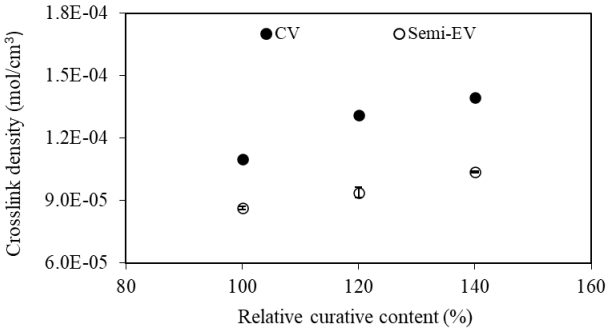

Figure 2. Crosslink density of the tread vulcanizates

Determination of hardness was performed using a Shore A durometer (Wallace H17A, UK) following ISO 48-4. Tensile properties, i.e., tensile strength (TS) and elongation at break (EB), were measured by a universal testing machine (Instron 3366, USA) according to ISO 37 (die type 1). Abrasion resistance, represented in terms of volume loss per 1,000 revolutions, was evaluated by Akron-type abrasion tester (Gotech GT-7012-A, Taiwan) as per BS 903-Part A9 (method B). Dynamic mechanical properties were tested in a tension mode using a dynamic mechanical analyzer (Gabo, Eplexor 25N, Germany). To indirectly measure the WG and FS, the specimens were deformed at static strain, dynamic strain, and frequency of 1%, 0.15% and 10 Hz, respectively, while the temperature was scanned from -60 to 80°C at 2°C/minute. Values of tan δ at 0°C and 60°C were selected to represent the WG and FS of a tread, respectively. The higher the tan δ value at 0°C, the greater the WG [5]. The lower the tan δ value at 60°C, the better the FS [6]. Investigation of thermal aging resistance was carried out by aging the specimens in an air-circulated oven at 100°C for 120 hours. The ratio of TS and EB after aging to those before aging, namely relative properties, was used to represent the thermal aging resistance of the treads.

3. Results and Discussion

Figure 1 presents the cure curves and cure characteristics, i.e., t_{s1}, t_c90, and CRI, of the tread compounds. Both t_{s1} and t_c90 decreased with increasing relative curative content, while CRI showed an opposite

Table 2. Mechanical properties of the tread vulcanizates

Relative curative content (%)	CV				Semi-EV			
	Hardness (Shore A)	TS (MPa)	EB (%)	Volume loss (mm^3)	Hardness (Shore A)	TS (MPa)	EB (%)	Volume loss (mm^3)
100	62.3±0.3	21.9±0.9	444±14	20.3±0.6	58.2±0.3	23.0±1.3	582±33	18.6±0.6
120	64.0±0.0	21.3±0.5	386±10	15.1±0.6	60.3±0.3	22.3±0.7	508±15	15.1±0.6
140	65.6±0.2	20.6±0.8	353±16	13.8±1.2	61.4±0.2	21.6±1.2	462±31	12.5±0.6

Table 3. Values of tan δ at 0°C and 60°C

Relative curative content (%)	CV		Semi-EV	
	tan δ at 0°C	tan δ at 60°C	tan δ at 0°C	tan δ at 60°C
100	0.5599	0.1231	0.4935	0.1383
120	0.5822	0.1118	0.5134	0.1290
140	0.5997	0.1082	0.5256	0.1215

trend. Moreover, the CV system exhibited shorter t_{s1} and t_c90 values, together with a higher CRI, compared to the semi-EV system. These results indicate that the vulcanization process can proceed more rapidly when the sulfur content and/or the sulfur/accelerator ratio increase.

Crosslink density of the tread vulcanizates measured by the swelling technique is depicted in Figure 2. As expected, increasing the relative curative content led to the enhanced crosslink density. This can be explained that increasing the amounts of sulfur and accelerators not only accelerates the vulcanization rate but also generates more crosslink sites. At any given curative content, the CV system exhibited a higher crosslink than the semi-EV system, attributed mainly to its greater sulfur content.

Mechanical properties, i.e., hardness, TS, EB, and volume loss, of the tread vulcanizates are tabulated in Table 2. Regardless of the vulcanization system, hardness increased with increasing relative curative content, attributed mainly to the enhancement in crosslink density. Clearly, the CV system exhibited greater hardness than the semi-EV system, which can be attributed to its higher crosslink density. An increase in relative curative content, however, led to the negative effect on TS. This is likely caused by an excessively high crosslink density beyond the optimum level, leading to brittle behavior of the vulcanizates [7]. Surprisingly, the CV system demonstrated slightly lower TS than the semi-EV system despite the fact that CV system generally provides greater

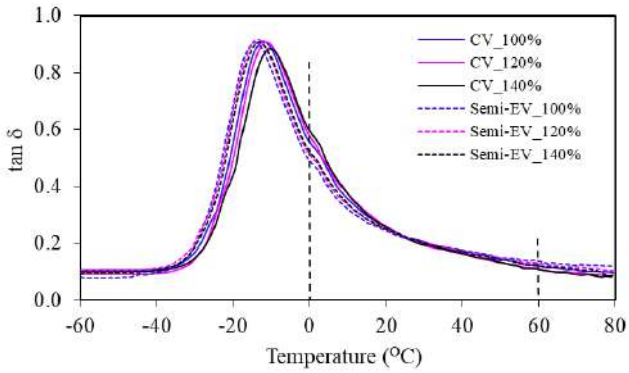

Figure 3. Values of tan δ as a function of test temperature

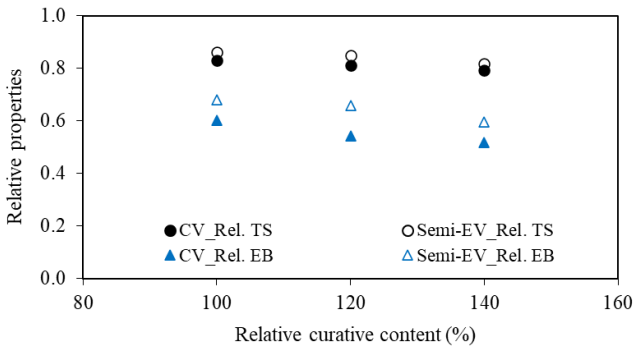

Figure 4. Thermal aging resistance of the tread vulcanizates

amount of polysulfidic linkages, which enables crosslink exchange under stress. Compared to C-S bonds usually found in EV and semi-EV systems, the S-S bonds in the CV system have lower bond energy, facilitating bond breakage and reformation, resulting in higher TS. However, in this case, the brittle behavior from excessively high crosslink density might have overridden the crosslink

structure effect, thereby leading to lower TS in the CV system. Results also showed that EB tended to decrease with increasing relative curative content, and the CV system showed lower EB than the semi-EV system. Obviously, the volume loss reduced with increasing relative curative content, indicating improved abrasion resistance due to higher crosslink density. Nevertheless, the semi-EV system exhibited slightly better abrasion resistance than the CV system, which can be attributed to its higher tensile strength, as discussed earlier.

Figure 3 exhibits the variation of tan δ as a function of test temperature. The tan δ values at 0°C and 60°C, analyzed from Figure 3, are summarized in Table 3. Evidently, increasing the relative curative content led to the improved WG. At any given relative curative content, the CV system showed better WG than the semi-EV system. The FS tended to increase with increasing relative curative content, arising from the enhanced crosslink density. The CV system provided better FS than the semi-EV system, attributed to its greater crosslink density.

Thermal aging resistance of the tread vulcanizates is shown in Figure 4. Both relative TS and relative EB decreased with increasing relative curative content, revealing the adverse effect on thermal aging resistance. This might be owing to enhanced post-curing reactions at higher curative contents. As expected, the semi-EV system exhibited better thermal aging resistance than the CV system.

Figure 5 presents the normalized graph of thermal aging resistance (evaluated from relative TS) and tire performance. Compared with the reference tread vulcanizate—i.e., the CV system with a relative curative content of 100% (normalized to 100% for all properties and represented by the blue solid line)—the most balanced properties were observed for the CV system with a relative curative content of 120% (represented by the pink solid line). This formulation noticeably enhanced wet grip (≈4%), fuel saving (≈9%), and abrasion resistance (≈26%) without a significant sacrifice in thermal aging resistance (≈2%).

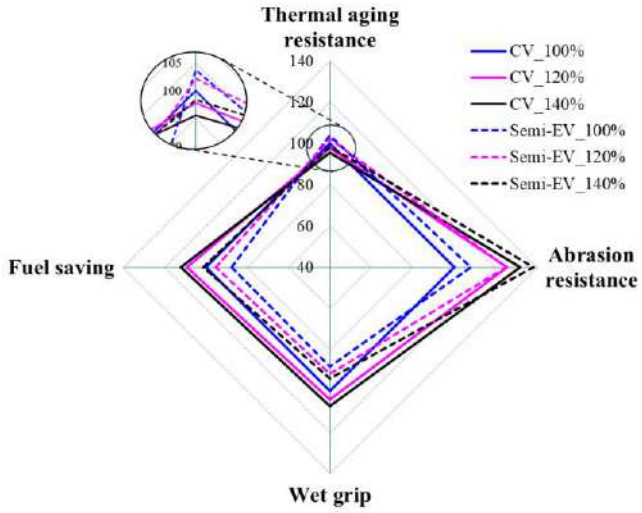

Figure 5. Normalized graph of thermal aging resistance and tire performance at various relative curative contents and sulfur vulcanization systems

4. Conclusion

Regardless of the sulfur vulcanization system, increasing the curative content enhanced the cure rate, crosslink density, hardness, wet grip (WG), fuel saving (FS), and abrasion resistance, while adversely affecting tensile strength (TS), elongation at break (EB), and thermal aging resistance. At any given curative content, the CV system exhibited higher crosslink density, hardness, WG, and FS, whereas the semi-EV system showed superior TS, abrasion resistance, and thermal aging resistance. Overall, the CV system with a relative curative content of 120% is proposed as the optimal formulation, offering a good balance between tire performance and thermal aging resistance.

5. Acknowledgment

Sincere appreciation is expressed to Thailand Research Fund (TRF) via Research and Researcher for Industries (RRi) and Siam Rubber Ltd., Part. for the financial support to this research (Grant No. PHD56I0074).

6. References

1. Giechaskiel, B.; Ferrarese, C.; Grigoratos, T. *Vehicles* **2025**, *7(2)*, 29.
2. Kratina, O.; Pöschl, M.; Stoček, R. *Polym. Degrad. Stab.* **2024**, *227*, 110871.

3. Flory, P. J.; Rehner, J. *J. Chem. Phys.* **1943**, *11(11)*, 521.
4. Li, M. C.; Ge, X.; Cho, U. R. *Macromol. Res.* **2013**, *21*, 793.
5. Lim, K.; Hong, S.; Lee, H.; Jung, J.; Kim, K.; Park, J.; Bang, J. *Sustainable Mater. Technol.* **2024**, *42*, e01156.
6. Ko, J. Y.; Prakashan, K.; Kim, J. K. *J. Elastomers Plast.* **2012**, *44*, 549.
7. Tavakoli, M.; Peyzari, P.; Tamaddon F.; Zare-Banadkouki, B. *Polym. Eng. Sci.* **2025**, *65(5)*, 2699.

Experimental Analysis of the Mixing Behavior of Ethylene-Propylene-Diene Rubber (EPDM) in a Rubber Pin Extruder under Variation of Process Parameters and Mixing Elements

Leon Schmidt[1], Jonas Petzke[1], Dennis Kleinschmidt[1], Florian Brüning[1]

[1] *Kunststofftechnik Paderborn, Paderborn University, Warburger Straße 100, 33098 Paderborn, Germany*

*E-mail: leon.schmidt@ktp.uni-paderborn.de

Abstract

Efficient distributive and dispersive mixing of rubber compounds remains a critical challenge in rubber extrusion, particularly due to the highly viscous, multiphase nature of elastomeric materials. In this study, the mixing behavior of an ethylene–propylene–diene rubber (EPDM) compound is experimentally investigated in a cold-fed rubber pin extruder under systematic variation of process parameters and mixing elements. Two modular screw-tip geometries—a pineapple mixing section and a tip with interrupted flights—are examined, in addition to variations in pin length (10 mm, 12 mm), screw speed (10–30 rpm), and barrel/screw temperature (60 °C, 90 °C). A dual-colored EPDM system enables quantitative analysis of material homogeneity via the green fraction formed during mixing. Thermal homogeneity is assessed using a multi-point temperature probe installed downstream of the screw.

The results show that material homogeneity is strongly affected by screw speed and temperature. Higher screw speeds decrease distributive mixing quality, while elevated temperatures (90 °C) significantly reduce material homogeneity due to viscosity gradients and cold-core formation. In contrast, thermal homogeneity improves with increasing screw speed but remains substantially lower than material homogeneity, demonstrating that both metrics must be evaluated independently. Compared to the pineapple mixing section, the pin-based design provides higher material homogeneity but slightly lower thermal uniformity. Throughput increases with temperature for both mixing elements but behaves differently with respect to screw speed depending on geometry. Overall, the study provides detailed insights into the interplay between process parameters, mixing element design, and resulting mixing quality, establishing a foundation for improved process design in rubber extrusion.

Keywords: Rubber extrusion, Mixing, Pin extruder, Mixing section, Ethylene-propylene-diene rubber (EPDM)

1. Introduction

The rubber processing industry is increasingly confronted with challenges related to resource and energy efficiency in production. A major factor contributing to this issue is the inadequate mixing and poor homogeneity of rubber compounds during the extrusion process, which negatively affects the quality of the final products. In particular, both the thermal and material homogeneity of the compound at the die exit significantly influence the dimensional stability and uniform property distribution of the extrudate. Due to the highly viscous and multi-component nature of rubber compounds, achieving effective dispersive and distributive mixing in rubber extrusion is a non-trivial task. The current state of the art includes cold-fed pin extruders equipped with cylindrical pins that extend radially into the screw channel, continuously deforming and reorienting the rubber melt.

Given the high relevance of mixing quality in rubber extrusion, the topic has already been addressed in the literature. Röthermeyer et al. [1] and Köster et al. [2] described the fundamental mixing mechanisms in rubber extruders in their technical publications. Building on this, Sun et al. [3] conducted studies comparing the mixing behavior of extruders with and without pins. Schöppner et al. [4] and Yao et al. [5] further investigated mixing

mechanisms in more detail, analyzing different rubber compounds under varying pin geometries.

This study focuses on the further analysis of the mixing behavior of a rubber compound based on ethylene–propylene–diene rubber (EPDM). The mixing quality was investigated under variation of key process parameters such as barrel and screw temperature, screw speed, and the screw design including the pin geometry. The latter was enabled by a modular screw equipped with an exchangeable screw tip.

2. Experimental Methods

2.1 Materials

For the investigations presented here, two identical EPDM rubber compounds were used, which differed only in the addition of different colour pigments. The composition of the compound is given in **Error! Reference source not found.**

Table 1: Composition of the yellow and blue EPDM-compounds

Component	**Proportion [phr]**
EPDM	100
Fillers	116
Plasticizers	78
Small chemicals	22
Dyes	17.3 (yellow) 16.85 (blue)
Cross-linking system	16.05

Two identical EPDM compounds, pigmented in yellow and blue respectively, were used to assess mixing performance. The coloration allows for visual detection of the degree of mixing based on the formation of a green color upon blending.

2.2 Process

The compounds were simultaneously fed as strips into a cold-fed pin extruder from TROESTER GmbH & Co. KG (Hannover, Germany) with a 60 mm screw diameter. During the experiments, screw speeds of 10, 20, and 30 rpm as well as barrel and screw temperatures of 60 °C and 90 °C were tested. The screw consisted of a base body with two flights and a pitch of 80 mm and was configured with a conveying thread and an exchangeable screw tip. Two tip designs were used: one with a pineapple mixing section and the other with interrupted flights. The geometries are shown in Figure 1 and Figure 2.

Figure 1: Pineapple mixing section

Figure 2: Tip with interrupted flights

Additionally, the length of the pins in the barrel (10 mm and 12 mm) was varied, while the diameter remained constant at 6 mm. The process parameters used for the investigations are listed in Table 2.

Table 2: Process parameters

Parameter	**Parameter setting**
Screw speed	10 / 20 / 30 rpm
Barrel / Screw temperature	60 / 90 °C

Due to the high experimental effort and material consumption associated with each operating point, all experiments were conducted as single-point measurements. Consequently, no systematic reproducibility or statistical variance analysis was performed, and each data point represents a single experimental run under the specified conditions.

To analyze the mixing behavior, a steady-state extrusion process was first established. A “dead-stop” method was then applied, in which the extrusion was abruptly halted, and the compound was vulcanized in-situ along the entire screw length. The screw was then pushed out of the barrel, and the vulcanized rubber was unwound. Cross-sectional cuts and subsequent color analysis allowed for evaluation of the material homogeneity along the screw. A higher green fraction indicated a higher degree of

material mixing. Therefore, this parameter was used for the analysis of the investigations.

Furthermore, a temperature probe was installed downstream of the screw to assess the thermal homogeneity across the extrudate cross-section. It consisted of a metal web extending across the channel, with temperature sensors embedded at defined positions, enabling the temperature profile across the cross-section to be determined. The temperature probe is shown in Figure *3*.

Figure 3: Temperature probe

In addition to mixing quality, throughput was monitored over time to evaluate the economic efficiency of each process setting.

3. Results

3.1 Material mixing analysis

The analysis of the mixing behavior of the pineapple mixing section at a barrel temperature of 60 °C and under variation of the screw speed is shown in Figure 4. The dashed black line indicates the position at which the mixing section begins. It becomes evident that a pronounced degree of mixing of the EPDM has already occurred upstream of the mixing section (700 mm). For screw speeds of 10 rpm and 20 rpm, the green fraction already exceeds 90 % in this region. The data point for 30 rpm lies clearly below the green fraction observed at the lower screw speeds. This suggests that an increased screw speed leads to a reduced degree of material mixing. However, within the actual mixing section, the material processed at 30 rpm is also brought to a green fraction of nearly 100 %, thereby compensating for this effect.

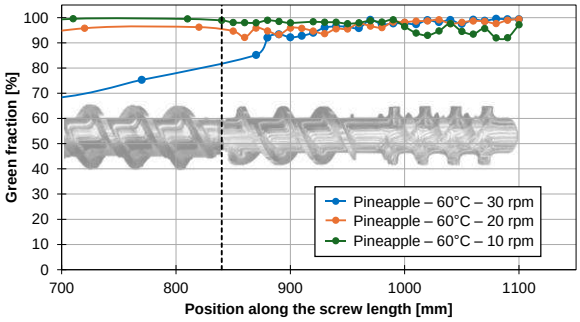

Figure 4: Green fraction along the screw length at 60 °C under variation of the screw speed with pineapple mixing element

The same investigation point at a higher barrel and screw temperature of 90 °C, shown in Figure 5, differs significantly in terms of the green fraction from the samples processed at 60 °C. The green fraction is considerably lower both upstream of and within the mixing section, indicating that elevated temperatures lead to a deterioration of material mixing. A possible reason for this effect is a reduction in viscosity in the outer regions of the screw channel, which promotes the formation of a cold core and thus results in plug flow.

Furthermore, it can again be observed that an increase in screw speed leads to lower green fractions. This effect can also be explained by a viscosity reduction in the boundary regions. In this case, however, the increased shear input is the dominant factor.

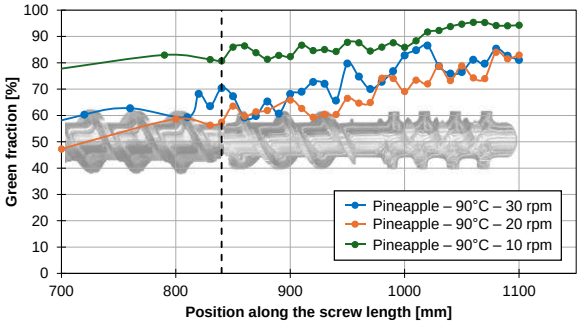

Figure 5: Green fraction along the screw length at 90 °C under variation of the screw speed with pineapple mixing element

In addition to the investigations using the pineapple mixing section, further experiments were conducted using pins. The results at 60 °C for the 12 mm pins are shown in Figure 6. At 60 °C, the green fraction—similar to the pineapple mixing section—is already distinctly high

before the pinned mixing section. For all screw speeds, the values are already above 80 %.

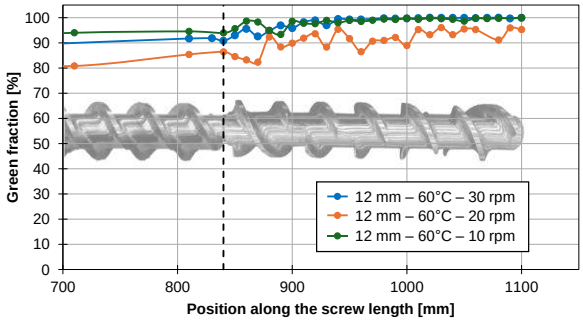

Figure 6: Green fraction along the screw length at 60 °C under variation of the screw speed with 12 mm pins

For the pinned screw, the green fraction was also evaluated at a barrel temperature of 90 °C. Once again, it becomes evident that the degree of mixing—particularly before the mixing section—is lower at the elevated temperature. In this region, the green fraction ranges between 60 and 80 %. However, within the mixing section, the material is mixed significantly better than in the pineapple mixing element. Moreover, the mixing behavior is less dependent on screw speed, with only the 30 rpm condition showing isolated downward deviations in the green fraction.

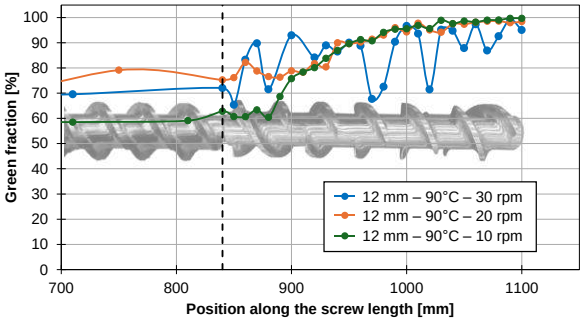

Figure 7: Green fraction along the screw length at 90 °C under variation of the screw speed with 12 mm pins

3.2 Thermal homogeneity analysis

The temperature probe described in Section 2.2 was installed directly upstream of the screw tip, and the temperature profile across the cross-section was recorded. The results of the investigations on the pineapple mixing element at 60 °C under variation of screw speed are shown in Figure 8. It can be observed that the temperature profile forms a parabolic shape with a maximum in the center of the channel. This profile occurs independently of screw speed; however, higher screw speeds lead to increased temperatures, with the temperature maximum in particular rising significantly. In contrast to the material homogeneity, the temperature distribution at the end of the mixing element is non-uniform. Therefore, good material mixing does not necessarily imply high thermal homogeneity.

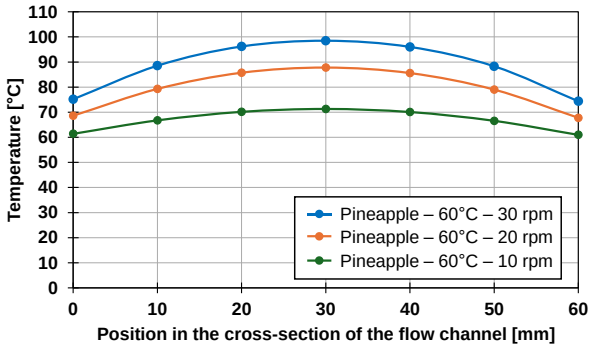

Figure 8: Temperature profile across the cross-section at 60 °C under variation of the screw speed with pineapple mixing element

In the next step, the temperature profile graphs are reduced to a thermal homogeneity index. Equation 1 is used for this purpose, where T_{max} represents the maximum temperature, T_{min} the minimum temperature, T_{med} the mean temperature, and T_0 the temperature of the rubber prior to feeding (23 °C). An index value H_T close to 1 indicates a high degree of thermal homogeneity.

$$H_T = \left(1 - \frac{T_{max} - T_{min}}{T_{med} - T_0}\right) * 100\ \% \qquad (1)$$

Figure 9 presents a comparison of the thermal homogeneity index with the green fraction, which is used as the material homogeneity metric. It becomes evident that material homogeneity is generally significantly higher than thermal homogeneity, particularly at lower temperatures. However, the overall trends of both metrics appear to agree, such that lower screw speeds lead to higher material and thermal homogeneity.

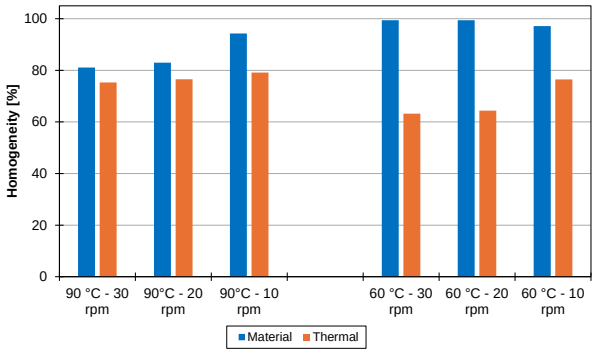

Figure 9: Comparison of material and thermal homogeneity of the process points for the pineapple mixing element

The same behavior can also be observed when using the 12 mm pins, as shown in Figure 10.

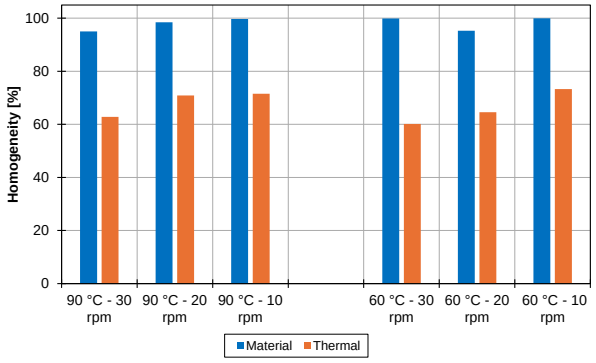

Figure 10: Comparison of material and thermal homogeneity of the process points with 12 pins

Here, too, the material homogeneity is significantly higher than the thermal homogeneity, and the trends with respect to the process parameters are consistent. However, compared to the pineapple mixing section, the material homogeneity is slightly higher, while the thermal homogeneity is somewhat lower. In general, it can be stated that material homogeneity is not a direct indicator of thermal homogeneity, nor vice versa. Nevertheless, corresponding trends can be identified.

3.3 Throughput analysis

The specific throughput for the different process parameters using the pineapple mixing section is shown in Figure 11. It becomes evident that throughput increases with rising screw speed at higher temperatures. In contrast, at the lower temperature of 60 °C, the throughput remains nearly constant. In general, however, the specific throughput is higher at elevated temperatures due to the reduced viscosity of the compound.

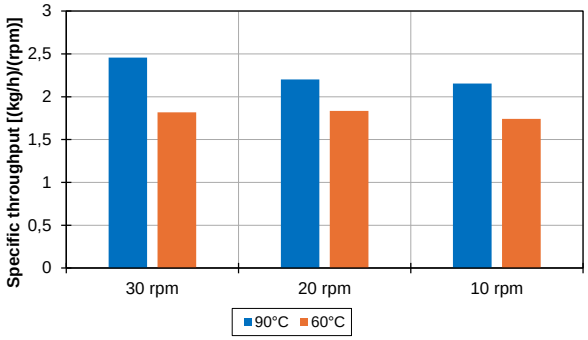

Figure 11: Specific throughput of the pineapple mixing element for different temperatures and screw speeds

The specific throughput of the pinned mixing element, shown in Figure 12, exhibits a similar overall trend. However, at the lower processing temperature, the specific throughput decreases with increasing screw speed. Nevertheless, as with the pineapple mixing section, the specific throughput is higher at elevated temperatures.

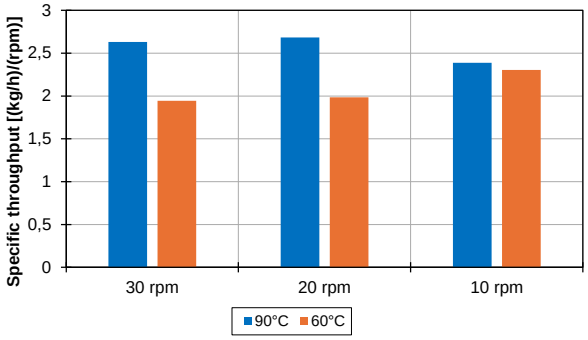

Figure 12: Specific throughput of the 12 mm pins for different temperatures and screw speeds

4. Conclusion

This study presents a comprehensive experimental evaluation of the mixing behavior of an EPDM compound in a cold-fed rubber pin extruder under systematic variation of process parameters and mixing geometries. The combination of a dual-colored material system, the dead-stop technique, and a multi-point temperature probe enabled parallel assessment of both material and thermal homogeneity along the screw and at the die exit. The results demonstrate that material homogeneity is significantly influenced by screw speed and compound temperature. Higher temperatures reduce homogeneity due to pronounced viscosity gradients and cold-core formation, while increasing screw speed leads to less effective

distributive mixing. Nevertheless, both the pineapple mixing section and the pin-based design achieve near-complete material homogeneity at the end of the mixing zone under suitable conditions. The pin configuration, however, consistently provides higher material homogeneity than the pineapple section, particularly at elevated temperatures. In contrast, thermal homogeneity is generally lower and more sensitive to shear-induced heating, increasing with screw speed but deteriorating at low temperatures. Importantly, material and thermal homogeneity do not correlate directly, highlighting the necessity of evaluating both independently when optimizing extrusion processes. Throughput analysis reveals that higher barrel and screw temperatures consistently increase specific throughput for all geometries, whereas the influence of screw speed depends strongly on the mixing element design. Overall, the findings underline the interplay between geometry-induced flow structures and thermo-mechanical process conditions. These insights enable targeted optimization of rubber extrusion processes and provide a validated experimental foundation for future modeling and scale-up activities.

5. Acknowledgement

The authors gratefully acknowledge the financial support provided by the German Aerospace Center (DLR) (IGF No. 01IF22861N). This research was funded by the Federal Ministry for Economic Affairs and Climate Action (BMWK). Furthermore, we would like to thank the companies represented in the project advisory committee for their valuable support and constructive collaboration.

6. References

1. Röthemeyer F, Sommer F, *Kautschuktechnologie*, 2013
2. Köster L, Perz H, Tsiwikis G, *Praxis der Kautschukextrusion*, 2007
3. Sun Y, Wang S, Huang S, Pan W, He Y, Jian R, *Polymers*, 2024; 16(13)
4. Schöppner V, Schadomsky M, Hopman C, Lemke F, *PROCEEDINGS OF PPS-31: The 31st International Conference of the Polymer Processing Society – Conference Papers*, 2015
5. Yao W, Takahashi K, Koyama K, Dai G, *Chemical Engineering Science*, 1997; 13: 21

Durazone D37 as a potential alternative to 6PPD: balancing ozone resistance and dynamic performance

Chutima Saeheng*, Puchong Thaptong

National Metal and Materials Technology Center (MTEC), NSTDA, Pathum Thani, Thailand.

*E-mail: chutima.sae@mtec.or.th

Abstract

Rubber tires require antidegradants to ensure durability against oxidative and ozone-induced degradation, with N-(1,3-dimethylbutyl)-N´-phenyl-p-phenylenediamine (6PPD) being the most widely used. However, its transformation product, 6PPD-quinone, has been identified as highly toxic to aquatic organisms. Tire wear particles containing 6PPD enter waterways through road dust and runoff, where 6PPD-quinone has been linked to acute mortality in coho salmon and related species. This challenge highlights the urgent need to identify safer alternatives that can maintain tire performance while reducing environmental impact. This study investigated 2,4,6-tris-(N-1,4-dimethylpentyl-p-phenylenediamino)-1,3,5-triazine (Durazone D37), a triazine-based antidegradant, as a potential substitute for 6PPD in natural rubber (NR) compounds reinforced with carbon black (CB). NR/CB compounds were formulated with either individual antidegradants or blended systems of 6PPD and D37. Experimental evaluation covered curing behavior, mechanical properties, abrasion resistance, dynamic viscoelastic behavior, and ozone resistance under both static and dynamic modes. Results showed that D37 was fully compatible with sulfur vulcanization and maintained tensile strength, hardness, and abrasion resistance comparable to 6PPD. Notably, D37 provided superior ozone resistance, preventing surface cracking even under dynamic strain. Dynamic mechanical thermal analysis (DMTA) revealed an additional relaxation at 40-60°C in D37-containing compounds, attributed to restricted chain mobility in interfacial bound-rubber regions. This increased hysteresis suggests a potential rise in rolling resistance, however, blended antidegradant systems reduced this effect while maintaining improved ozone durability. In conclusion, D37 demonstrates strong technical feasibility as a partial replacement for 6PPD in NR-based tire compounds. Further pilot-scale evaluation and environmental fate studies are recommended to validate industrial applicability.

Keywords: 6PPD, Durazone D37, antiozonant, ozone resistance, dynamic performance

1. Introduction

The durability and performance of rubber tires depend critically on the incorporation of antidegradants that protect vulcanized elastomers against oxidative and ozone-induced degradation during service. Among these, N-(1,3-dimethylbutyl)-N´-phenyl-p-phenylenediamine (6PPD) (Figure 1(a)) has been the predominant antiozonant in global tire manufacturing for decades due to its strong efficacy in preventing crack initiation under both static and dynamic strain. However, the recent identification of its transformation product, 6PPD-quinone, as an acutely toxic contaminant in aquatic ecosystems has raised significant environmental and regulatory concerns. In particular, 6PPD-quinone has been implicated as the causal toxicant responsible for acute mortality in coho salmon and other salmonid species, with its presence in waterways primarily attributed to tire-wear particles that enter surface runoff and stormwater systems [1]. Consequently, tire manufacturers, especially those with products distributed in California, are now required under the Safer Consumer Products (SCP) regulation to evaluate and adopt safer alternatives to 6PPD, thereby accelerating research into more environmentally benign antidegradant systems [2].

A triazine-based antidegradant, namely 2,4,6-tris-(N-1,4-dimethylpentyl-p-phenylene-diamino)-1,3,5-

triazine, commonly known as Durazone D37 (Figure 1(b)), has recently gained attention due to its oxidative stability and strong ozone protection. However, comprehensive evaluation of D37's performance in tire compounds relative to 6PPD remains limited. This study investigated the technical feasibility of replacing 6PPD partially or fully with D37 in natural rubber (NR) compounds filled with N339 carbon black. Experimental study focused on curing behavior, mechanical properties, wear, dynamic viscoelasticity, and ozone durability under both static and dynamic conditions.

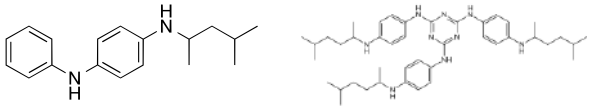

(a) (b)

Figure 1: *Chemical structures of (a) 6PPD and (b) Durazone D37.*

2. Experimental methods

Materials used in the present study and formular of NR-compounds are summarized in Table 1 and in Table 2, respectively. Natural rubber (STR 5L) was used as the base elastomer and compounded with N339 carbon black along with fixed amounts of zinc oxide (ZnO), stearic acid, treated residual aromatic extract (TRAE) oil, polymerized 2,2,4-trimethyl-1,2-dihydroquinoline (TMQ), paraffin wax, *N*-tert-butyl-2-benzothiazolesulfenamide (TBBS), *N,N'*-bis(tert-butyl)benzothiazole disulfide (TBzTD), and sulfur. The antidegradant system varied among five formulations: 6PPD (100%), D37 (100%), and binary 6PPD/D37 blends at weight ratios of 75/25, 50/50, and 25/75. All ingredients were incorporated using a Haake internal mixer (Thermo Fisher Scientific, Karlsruhe, Germany) operated at 60°C, using a masterbatch mixing stage followed by the addition of curatives in a subsequent short stage to minimize premature crosslinking. The mixed compounds were then sheeted on a two-roll mill and stored at room temperature for at least 16 hours before curing. Vulcanization was performed via compression molding at 150°C for the optimum cure time (t_c90), which was determined for each formulation using a Moving Die Rheometer (MDR; Alpha Technologies, Akron, OH, USA) in accordance with ISO 6502-3.

The Mooney viscosity of the uncured compounds was measured using a Mooney viscometer (MV 2000, Alpha Technologies, Akron, OH, USA) in accordance with ISO 289-1. Mechanical properties, including hardness and tensile strength, were evaluated following ISO 48-4 and ISO 37, respectively, using a durometer hardness tester (Shore A; MonTech HT 3000, USA) and a universal testing machine (Instron 3366 series, Instron Corp., Norwood, MA, USA). Abrasion resistance was assessed using an Akron abrasion tester (Gotech GT-7012-A, Taiwan) according to BS 903 A9.

Dynamic mechanical behavior was characterized by using a dynamic mechanical thermal analyzer (DMTA; GABO, model EPLEXOR QC 100, Germany) with a temperature sweep from −80 to 80 °C to determine tan δ values at 0 °C and 60 °C, corresponding to wet traction and rolling resistance, respectively. Ozone resistance was evaluated according to ISO 1431-1 under both static conditions (20% strain, 50 pphm ozone, 40 °C for 72 h) and dynamic conditions (±10% strain, 0.5 Hz, 50 pphm ozone, 40 °C for 72 h), using an ozone test chamber (TOYOSEIKI/PPHM-SD, Tokyo, Japan).

Table 1*: Materials used in the present study.*

Material	Description
Natural rubber	STR 5L/Union Rubber Product Co., Ltd., Thailand
Carbon black	N339/Thai Carbon Black Public Co., Ltd., Thailand
Treated residual aromatic extract Oil **(**TRAE)	Flavex 595/The Shell Company of Thailand Ltd., Thailand
Stearic acid	Palmata 1810/Thanachem (Bangkok) Co., Ltd., Thailand
N-(1,3-dimethylbutyl)-N'-phenyl-p-phenylenediamine (6PPD)	4020/Cenpont Technology Co., Ltd., Hong Kong
Polymerized 2,2,4-trimethyl-1,2-dihydroquinoline (TMQ)	Cenpont Technology Co., Ltd., Hong Kong
Paraffin wax blend	RW287/Guangzhou Anzhan Chemical Technology Co., Ltd., China
Zinc oxide **(**ZnO)	White seal/Zhiyi Zinc Industry (Thailand) Co., Ltd., Thailand
N-tert-butyl-2-benzothiazole sulfenamide (TBBS)	S. Sumpran Chemicals Co., Ltd., Thailand
N,N'-bis(tert-butyl)benzo-thiazole disulfide (TBzTD)	Reliance Technochem Co., Ltd., Thailand
Sulfur	Numchai Industry Co., Ltd., Thailand

***Table 2**: Formula of NR compound.*

Ingredient	Content (phr)
NR	100
CB (N339)	40
TRAE oil	4
ZnO	5
Stearic acid	2
Wax blend	2
TMQ	1.5
Antidegradants	3
TBBS	1.5
TBzTD	0.3
Sulfur	2

3. Results and Discussion

The vulcanization behavior of all compounds (Figure 2) was comparable, with scorch times (t_{s1}) ranging from approximately 2.6 to 3.2 minutes and optimum cure times (t_c90) between 4.7 and 5.5 minutes. Both D37 and the blended systems demonstrated full compatibility with sulfur vulcanization, producing maximum torque values similar to those of the 6PPD reference compound. These similarities indicate that D37 does not interfere with crosslink formation and that the underlying curing network remains largely unaffected by the full or partial replacement of 6PPD with D37. Mooney viscosities (ML(1+4)@100°C) for all compounds were also similar, falling within a narrow range of 52-54 MU, confirming that the selected antidegradants did not significantly influence processability of the rubber compounds.

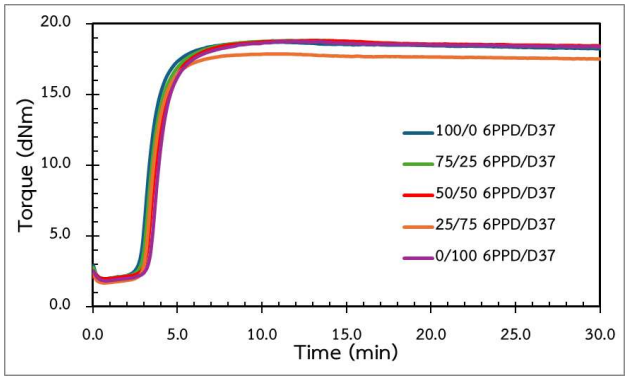

***Figure 2:** Cure curves of NR compounds with different antidegradant systems.*

Mechanical testing revealed that hardness values of all vulcanizates ranged from 62 to 65 Shore A, while tensile strengths remained within 25-28 MPa with elongations at break between 430% and 450% (Table 3). These results demonstrate that the substitution of 6PPD with D37, whether partially or fully, does not significantly affect the crosslink density or mechanical integrity of the vulcanizates. Abrasion resistance also remained within similar bounds, with volume losses ranging from approximately 137 to 160 mm^3. Although D37 alone exhibited slightly higher abrasion volume loss compared to 6PPD, the blended systems, particularly the 75/25 and 50/50 ratios, showed wear properties nearly identical to those of the 6PPD-containing compound.

***Table 3:** Physical and mechanical properties of NR vulcanizates with different antidegradants.*

Antidegradant ratio 6PPD/D37	Hardness (Shore A)	Akron abrasion volume loss (mm^3)	Tensile properties		
			Tensile strength (MPa)	Elongation at break (%)	M100 (MPa)
100/0	63.9±0.6	138.6±3.1	27.7±0.4	441±10	3.6±0.1
75/25	62.7±0.4	147.5±3.3	27.2±0.6	424±10	3.4±0.1
50/50	63.4±0.9	136.9±3.9	26.4±0.7	431±8	3.3±0.1
25/75	63.9±0.7	156.8±4.6	27.2±0.8	448±11	3.3±0.1
0/100	65.2±0.5	159.8±2.5	25.1±0.4	434±7	3.4±0.1

Dynamic mechanical thermal analysis (Figure 3) provided deeper insight into the viscoelastic behavior of the vulcanizates. All formulations exhibited a glass-transition tan δ peak corresponding to the α-relaxation of natural rubber at approximately -60 to -40°C, indicating that the bulk polymer mobility remained unaffected by antidegradant substitution. However, D37-containing vulcanizates displayed an additional relaxation process between 40 and 60°C, with peak intensity increasing proportionally to D37 content. This secondary relaxation is attributed to restricted chain mobility in interfacial regions near the carbon black surface, likely resulting from strong interactions involving the bulky triazine structure of D37 [3-4]. The presence of this relaxation peak implies increased energy dissipation, which correlates with higher hysteresis and potential rolling-resistance penalties. Blended formulations mitigated this effect, with the 75/25 and 50/50 blends exhibiting reduced secondary peak intensity relative to pure D37, thus balancing ozone protection with more acceptable dynamic performance.

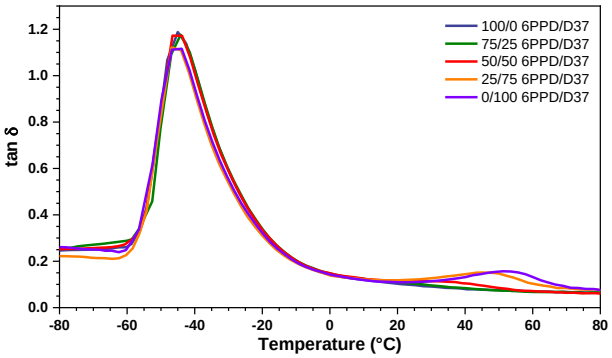

Figure 3: *Relationship between tan δ and temperature (temperature sweep) of the vulcanizates.*

Ozone resistance testing revealed the most notable differences among the antidegradant systems (Table 4). Under static ozone exposure at 20% strain, all vulcanizates remained crack-free. Under dynamic conditions, however, clear distinctions emerged. The 6PPD vulcanizate showed minor edge cracking detectable only under magnification, while D37-containing vulcanizates, including both the pure and blended systems, provided superior surface crack resistance caused by ozone. Pure D37 and the 50/50 and 25/75 blends remained completely crack-free even under dynamic strain, demonstrating outstanding protection against ozone attack. The 75/25 blend also showed improved performance relative to pure 6PPD, developing only extremely minor microscopic edge cracks. These findings confirm that D37 offers enhanced ozone durability, and that blended antidegradant systems effectively preserve this benefit while minimizing any undesirable effects on dynamic mechanical performance.

The results indicate that while D37 improves ozone resistance, its strong interfacial interactions contribute to increased hysteresis. Blended systems offer a practical compromise: they maintain significantly enhanced ozone durability relative to 6PPD while reducing the hysteresis effects associated with pure D37. This balance suggests that D37 can be used most effectively as a partial rather than complete replacement in carbon black–filled NR compounds.

Table 4: *Ozone-induced cracking evaluation of NR-vulcanizates according to ISO 1431-1 under static and dynamic modes.*

Samples	Static mode	Dynamic mode
100/0 6PPD/D37	 0 (No cracks)	 E(1/S)
75/25 6PPD/D37	 0 (No cracks)	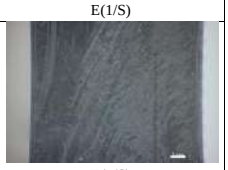 E(1/S)
50/50 6PPD/D37	 0 (No cracks)	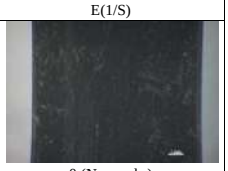 0 (No cracks)
25/75 6PPD/D37	 0 (No cracks)	 0 (No cracks)
0/100 6PPD/D37	 0 (No cracks)	 0 (No cracks)

Note: Ozone crack grading of size = 1, density = S, and location = E indicates very small cracks that are visible only under magnification and are scattered mainly along the exposed edge. The crack size rating of 0 indicates that no ozone cracks were observed, even under magnification.

4. Conclusion

The present study demonstrates that Durazone D37 is a technically viable and environmentally promising antidegradant for natural rubber compounds reinforced with carbon black. D37 fully supports efficient sulfur vulcanization and preserves the mechanical strength, hardness, and abrasion resistance normally associated with 6PPD. Its most significant advantage lies in its superior ozone resistance, particularly under dynamic strain, where D37-containing vulcanizates remained completely free of cracks. However, the enhanced interfacial interactions generated by D37 also increase hysteresis, as reflected by the appearance of a secondary relaxation peak between 40 and 60 °C in dynamic mechanical testing. This effect has

implications for rolling resistance and should be carefully managed in tire applications that require low energy dissipation. Binary blends of 6PPD and D37 successfully mitigate hysteresis while retaining enhanced ozone protection, with the 50/50 and 25/75 blends performing especially well. These results indicate that an optimal D37 loading in the range of approximately 1.0–1.5 phr is likely sufficient to balance ozone durability with acceptable dynamic mechanical behavior.

To fully validate D37 as a practical replacement for 6PPD in commercial tire compounds, further investigations at pilot scale, including rolling resistance measurements, road simulation testing, and environmental fate studies, are recommended. Nonetheless, the present findings provide strong evidence that D37-based antidegradant systems represent a promising pathway toward reducing the environmental impact of tire wear particles while maintaining essential performance attributes.

5. Acknowledgement

The authors gratefully acknowledge the financial and technical support provided by SVIZZ-ONE CORPORATION LTD. This partnership between research and industry played a vital role in shaping the objectives of the study, providing essential resources, and ensuring that the outcomes address both scientific advancement and practical relevance to tire manufacturing.

6. References

1. Z. Tian, M. Gonzalez, C. A. Rideout, H. N. Zhao, X. Hu, J. Wetzel, E. Mudrock, C. A. James, J. K. McIntyre, E. P. Kolodziej, *Environ. Sci. Technol. Lett*., **2022**; 9: 140.
2. DTSC, *Adopted Priority Product: Motor Vehicle Tires Containing 6PPD* https://dtsc.ca.gov/scp/motor_vehicle_tires_containing_6ppd/ (accessed January, 2024)
3. C. G. Robertson, C. M. Roland, *Rubber Chemistry and Technology*, **2008**; 81: 506.
4. V. Arrighia, I. McEwena, H. Qiana, M. Serran, *Polymer*, **2003**; 44: 6259.

Enhancing Mechanical and Antibacterial Properties of Natural Rubber/Tire Waste Blends through Dual-phase Processing Techniques

Napasorn Kingkohyao[1], Tanit Boonsiri[2], Yeampon Nakaramontri*[1]

[1] *Sustainable Polymer & Innovative Composite Materials Research Group, Department of Chemistry, Faculty of Science, King Mongkut's University of Technology Thonburi, Bangkok 10140, Thailand.*

[2] *Department of Microbiology, Phramongkutklao College of Medicine, Bangkok 10400, Thailand.*

*E-mail: yeampon.nak@kmutt.ac.th

Abstract

Rubber composites were developed using incorporating recycled tire waste (TW) a filler-like recycled rubber component, epoxidized natural rubber (ENR), natural rubber (NR) and zinc oxide nanoparticles modified with nanosilica (ZnO-SiO_2) as a multifunctional filler to improve antibacterial activity and mechanical properties. The TW/ENR/ ZnO-SiO_2 blends, with a formulation ratio of 50/50/10 phr, with and without 10 phr NR, were prepared via two processing techniques—melt blending and latex blending—to investigate the influence of processing routes on cure characteristic, mechanical properties, antibacterial activity, and morphology. The latex-blended composites, fabricated through a two-step hybrid method in which ZnO-SiO_2 was dispersed in ENR with or without NR latex, exhibited shorter scorch time (T_{s2}) and optimum cure times (T_{c90}) together with higher torque difference (M_H-M_L), reflecting increased crosslink density due to improved filler dispersion and stronger filler–rubber interactions. In contrast, the melt-blended composites showed higher tensile strength and elongation at break, attributed to heterogeneous crosslink networks rich in polysulfidic linkages that promote strain-induced crystallization. Both composites demonstrated over 90% antibacterial activity against *Escherichia coli* and *Staphylococcus aureus* within 8 h, resulting from zinc ion (Zn^{2+}) release and reactive oxygen species (ROS) generation at the ZnO-SiO_2 interface. Slightly greater antibacterial activity was observed in latex-blended samples owing to the residual acidity of ENR latex and enhanced nanofiller dispersion. These results highlight the critical trade-offs between processing strategies in tailoring the performance of NR-based composites. Latex blending promotes faster curing and greater antibacterial functionality, while melt blending offers superior mechanical strength and durability. The findings provide valuable insight for selecting optimal processing routes to design high-performance, sustainable rubber materials for rubber industrial applications.

Keywords: Latex mixing, Melt blending, Antibacterial, Natural rubber, Tire waste

1. Introduction

In the recent years, the development of high-performance and sustainable elastomeric materials has become a central focus in polymer science and engineering. Natural rubber (NR) remains an indispensable raw material owing to its excellent elasticity, resilience, and renewability. However, its applications are constrained by inherent drawbacks such as poor thermal stability, limited resistance to non-polar solvents, and the absence of intrinsic antibacterial properties [1]. These limitations restrict its use in advanced or hygienic applications that demand both durability and antimicrobial performance. To overcome these challenges, epoxidized natural rubber (ENR) has been introduced as a chemically modified form of NR. The incorporation of epoxy groups into the NR backbone enhances polarity, promotes compatibility with polar fillers, and improves oxidative resistance [2]. In addition, the incorporation of the functional nanoparticles has further expanded the potential of NR-based composites. Zinc oxide (ZnO), a well-known antibacterial agent effective against *Staphylococcus aureus* and *Escherichia coli* [3], often suffers from particle

agglomeration, which reduces its surface reactivity and antibacterial efficiency, in particular the ZnO nanoparticles. To address this issue, modification with nanosilica (SiO_2) has proven to be an effective strategy for stabilizing ZnO nanoparticles, enhancing dispersion, and strengthening filler–rubber interactions [4]. The resulting modified zinc oxide with nanosilica (ZnO-SiO_2) fillers not only reinforce the rubber matrix but also provide durable antibacterial functionality. At the same time, recycled tire waste (TW) has gained attention as a cost-effective and reinforcing filler for NR-based composites which contained ZnO inside the bulk matrix. The incorporation of TW improves stiffness and abrasion resistance while supporting circular-economy principles by converting end-of-life tires into value-added materials [5].

While formulation design defines the composition of the composite, the processing technique ultimately governs its structure–property relationships. Processing determines filler dispersion, filler–matrix adhesion, and crosslink-network uniformity all of which influence the balance between mechanical strength and functional properties. In rubber manufacturing, melt blending is widely adopted for its scalability and strong shear mixing, particularly in dry-rubber applications. However, high processing temperatures may induce filler agglomeration and thermal degradation [6]. In contrast, latex blending allows nanoscale dispersion in the liquid phase, leading to more uniform filler distribution, improved interfacial bonding, and accelerated vulcanization [7]. A systematic comparison of these two approaches is therefore essential to clarify how processing governs structural evolution and overall material performance.

Therefore, this study focuses on the fabrication of TW/ENR blends, with and without NR, filled with ZnO-SiO_2 (ZnO:SiO_2 = 90:10), with particular emphasis on the influence of the processing route—melt blending and latex blending as a hybrid process on cure characteristics, mechanical properties, morphology, and antibacterial activity. The findings provide valuable insight into the crucial role of processing in designing sustainable, multifunctional rubber composites for industrial and hygienic applications.

2. Experimental methods

2.1 Materials

Epoxidized natural rubber (ENR) latex containing 25 mol% epoxide was supplied by Muang Mai Guthrie Co., Ltd. (Surat Thani, Thailand). High-ammonia (HA)-grade natural rubber (NR) latex was obtained from Geefin Rubbertach Co., Ltd. (Songkhla, Thailand). Recycled tire waste (TW) was supplied by Thai Rubb Tech Co., Ltd. (Bangkok, Thailand) as a filler-like recycled rubber component. It exhibited a specific gravity of 1.15, an ash content of 6.62 wt%, and a moisture content of 0.49 wt%. Modified zinc oxide with nanosilica (ZnO-SiO_2), prepared at a ZnO:SiO_2 ratio of 90:10 wt%, was obtained from Global Chemical Co., Ltd. (Samut Prakan, Thailand). Stearic acid was purchased from Imperial Chemical Co., Ltd. (Pathum Thani, Thailand), while dibenzothiazyl disulfide (MBTS) and sulfur were supplied by Flexsys Inc. (Termoli, Italy).

2.2 Preparation of the TW/ENR/ZnO-SiO_2 blend with and without NR prepared using melt and latex processes.

Two different processing routes were used in this study: conventional melt blending and latex blending (hybrid process). The formulation ratio was 50/50/10 phr for TW/ENR/ZnO–SiO_2, with and without 10 phr NR, as summarized in Table 1. Melt-blended samples TW, ENR, NR, and ZnO–SiO_2 were directly compounded in an internal mixer. The rubber was first masticated for 4 min, followed by the sequential addition of stearic acid (1 min), MBTS (1 min), and sulfur (1 min). Mixing was carried out at 80 °C with a fill factor of 75% and a rotor speed of 60 rpm. The compound was then sheeted using a two-roll mill and vulcanized by compression molding at 160 °C. In contrast, latex-blended samples, ZnO–SiO_2 was first dispersed in ENR latex, with or without NR latex, at room temperature using mechanical stirring at 360 rpm for 30 min. The mixture was cast into sheets and dried at 60 °C for 24 h to obtain a pre-dispersed rubber–filler masterbatch. This dried masterbatch was then compounded with TW and addition of stearic acid (1 min), MBTS (1 min), and sulfur (1 min) in an internal mixer under the same

conditions described above. The compound was subsequently sheeted and vulcanized at 160 °C.

In this study, L refers to latex (hybrid) processing, where filler dispersion is first performed in the latex state before internal mixing. In contrast, M refers to conventional melt blending, where all components are directly mixed in the internal mixer without prior latex dispersion.

Table 1 Formulation of TW/ENR/ZnO-SiO_2 with and without NR prepared using melt and latex (hybrid) processes.

Ingredients	Content (phr)
ENR	50
NR	0 and 10
TW	50
Stearic acid	1
ZnO-SiO_2	10
MBTS	1
Sulfur	2.5

Note: The formulation is expressed in phr based on the total virgin rubber matrix (ENR and NR). TW was used as a filler-like recycled rubber component and was not included in the 100 phr rubber basis.

2.3 Characterizations

2.3.1 Cure characteristics

Rubber compounds were evaluated using a moving die rheometer (MDR) in accordance with ASTM D5289. Measurements were performed at 160 °C to determine the scorch time (T_{s2}), optimum cure time (T_{c90}), minimum torque (M_L), maximum torque (M_H), and torque difference ($M_H - M_L$). These parameters were used to assess the vulcanization rate and crosslinking behavior of the composites.

2.3.2 Mechanical properties

Tensile testing of the samples was carried out using a universal testing machine (Zwick Z 1545, Zwick GmbH & Co. KG, Ulm, Germany) at room temperature to determine the tensile properties from the stress–strain curves. Dumbbell-shaped specimens were prepared according to ISO 37 (Type 2). The tests were performed at a crosshead speed of 500 mm/min using a 500 N load cell.

2.3.3 Antibacterial properties

Antibacterial activity was evaluated against *Escherichia coli (E. coli)* and *Staphylococcus aureus (S. aureus)* following the ISO 22196–2011 standard. Bacterial suspensions in nutrient broth (NB) were adjusted to an initial concentration of 10^6 colony-forming unit per milliliter (CFU/ml). A 0.4 mL aliquot of the bacterial suspension was dropped onto a 5 × 5 cm^2 sample surface in a sterile petri dish and covered with a polyethylene film to prevent drying. The specimens were incubated at 35 °C for 8 h. Subsequently, the surviving bacteria were recovered, serially diluted tenfold, dropped on nutrient agar, and incubated again at 37°C for 24 h. The antibacterial activity was expressed as the percentage reduction of bacteria (R) calculated according to Eq. (1):

$$R = (A–B)/B \times 100 \quad (1)$$

where A and B represent the CFU values of viable bacteria before and after 8 h of incubation (linear values), respectively.

2.3.4 Morphological analysis

Morphology and elemental composition of the TW/ENR/NR/ZnO-SiO_2 blends were examined using optical microscope (OM) and scanning electron microscopy coupled with energy-dispersive X-ray spectroscopy (SEM–EDX) (Phenom ProX, Thermo Fisher Scientific, Brno, Czech Republic). Micrographs were obtained at an accelerating voltage of 30 kV.

3. Results and Discussion

3.1 Cure characteristics

The vulcanization behavior of rubber blends prepared by melt blending and latex blending exhibited a decreasing torque with time, as shown in Figure 1. The observed reversion behavior is attributed to the thermal degradation of polysulfidic crosslinks, leading to a reduction in torque at prolonged curing times. The melt-blended samples showed lower torque values than those prepared by latex blending, suggesting a higher proportion

of polysulfidic linkages, which have lower bond energy and are more prone to thermal scission [8]. In contrast, the latex-blended composites exhibited shorter scorch time (T_{s2}) and optimum cure time (T_{c90}), indicating a faster vulcanization rate. This improvement is attributed to the two-step dispersion process, in which ZnO-SiO_2 was uniformly distributed within the ENR and NR latex matrices, providing a larger reactive surface area for interaction with sulfur and accelerators.

In addition, the presence of NR in the latex-blended process enhanced compatibility with TW, improving filler dispersion and crosslink uniformity. The slight acidity of ENR latex may also promote accelerator activity, thereby enhancing cure kinetics in the rubber blends. The higher M_L, M_H, and M_H - M_L values observed for the latex-blended samples (Table 2) confirm stronger filler-rubber interactions and greater crosslink density compared with the melt-blended process. Conversely, the lower vulcanization rate observed in the melt-blended samples is attributed to their higher compound viscosity, which limits molecular mobility and reduces the diffusion of curatives during the crosslinking reaction.

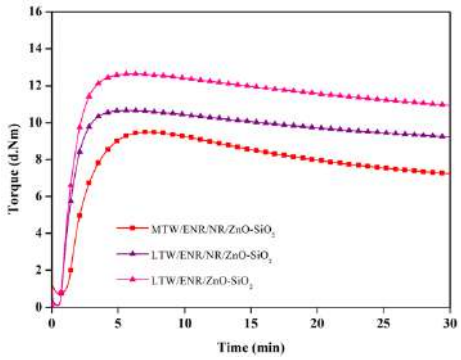

Figure 1 Cure characteristic curves of the TW/ENR/ZnO-SiO_2 with and without NR prepared using melt and latex processes at 160 °C.

Formulations	T_{s2} (min)	T_{c90} (min)	M_L (d.Nm)	M_H (d.Nm)	M_H-M_L (d.Nm)
MTW/ENR/ NR/ZnO-SiO_2	1.53 ± 0.06	4.28 ± 0.03	0.73 ± 0.01	9.55 ± 0.06	8.82 ± 0.06
LTW/ENR/ NR/ZnO-SiO_2	0.87 ± 0.06	2.67 ± 0.06	0.13 ± 0.06	10.66 ± 0.06	10.53 ± 0.06
LTW/ENR/ ZnO-SiO_2	0.84 ± 0.06	5.74 ± 0.06	0.09 ± 0.06	12.64 ± 0.06	12.55 ± 0.06

Table 2 Cure characteristics of the TW/ENR/ZnO-SiO_2 with and without NR prepared using melt and latex processes.

3.2 Mechanical properties

Mechanical properoties by means of tensile testing performances of the rubber blends prepared by melt blending and latex blending were evaluated in terms of 100 and 300% moduli, tensile strength and also elongation at break, as presented in Figure 2 and Table 3. From the stress-strain curves, the latex-blended composites with and without NR exhibited higher 100% modulus than the melt-blended samples, indicating the reinforcing effect of ZnO-SiO_2 within the rubber matrix. This improvement is attributed to enhanced filler dispersion and stronger filler-rubber interactions, resulting in increased crosslink density, consistent with the higher M_H-M_L values observed earlier. At strain 100-400%, the latex-blended process demonstrated stronger filler- rubber interactions due to the uniform distribution of ZnO-SiO_2 and the formation of a higher density of sulfidic linkages. At strain beyond 400%, the melt-blended samples displayed higher tensile strength, attributed to strain-induced crystallization facilitated by polysulfidic crosslinks that promote chain alignment under stress [9]. In contrast, the acidity of performic acid used during ENR synthesis may induce partial chain scission [10], leading to lower tensile strength and elongation at break in the latex-blended samples. Consequently, TW/ENR/ZnO-SiO_2 formulation without NR exhibited the lowest tensile strength and elongation, due to poor interfacial compatibility. Furthermore, the latex-blended composites showed higher 100% and 300% moduli compared to the melt-blended, reflecting higher crosslink density that restricts molecular mobility and reduces flexibility [11].

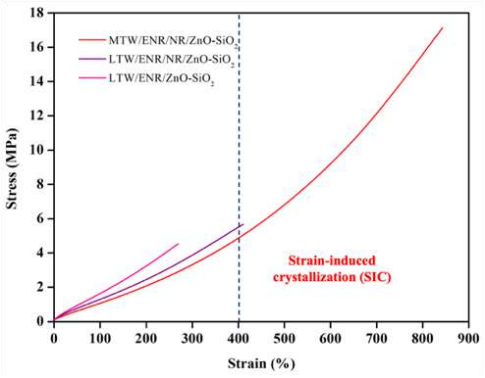

Figure 2 Stress – strain curves of the TW/ENR/ZnO-SiO_2 blend with and without NR prepared using melt and latex processes.

Table 3 Mechanical properties of the TW/ENR/ZnO-SiO_2 with and without NR prepared using melt and latex processes.

Formulations	100% Modulus (MPa)	300% Modulus (MPa)	Tensile strength (MPa)	Elongation at break (%)
MTW/ENR/ NR/ZnO-SiO_2	1.17 ± 0.03	3.65 ± 0.09	17.18 ± 0.75	847.22 ± 30.81
LTW/ENR/ NR/ZnO-SiO_2	1.30 ± 0.02	3.94 ± 0.06	5.75 ± 0.25	411.68 ± 14.17
LTW/ENR/ ZnO-SiO_2	1.63 ± 0.05	N/A	4.47 ± 0.13	271.46 ± 11.84

N/A = Not available

3.3 Antibacterial properties

Antibacterial properties of TW/ENR/ZnO-SiO_2 and TW/ENR/NR/ZnO-SiO_2 blends were evaluated over an 8-hour period, as shown in Figure 3(A). Latex-blended samples exhibited great antibacterial activity against both gram-positive *(S. aureus)* and gram-negative *(E. coli)* bacteria compared with those prepared by the melt-blending process. This enhancement is attributed to the two-step latex mixing route, which enables finer dispersion of ZnO-SiO_2 across the rubber surface and promotes the release of Zn^{2+} ions along with the generation of reactive oxygen species (ROS) through photocatalytic reactions on the surfaces of ZnO-SiO_2 and residual ZnO present in the TW phase, as illustrated in Figure 3(B). These reactive species interact with bacterial cell walls, while Zn^{2+} ions chemically react with cellular components and genetic material, ultimately leading to bacterial cell death [12]. Furthermore, the residual acidity from performic acid used during ENR synthesis contributes to bacterial inhibition by disrupting cell membranes, damaging DNA, and altering intracellular protein structures [13]. Both blending systems exhibited stronger antibacterial activity against Gram-negative bacteria than Gram-positive strains, due to the thinner and less cross-linked peptidoglycan layer in Gram-negative cell walls [14].

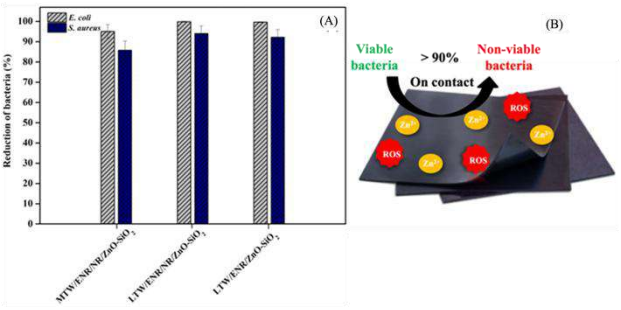

Figure 3 (A) Antibacterial activity of TW/ENR/ZnO-SiO_2 blends with and without NR prepared using melt and latex processes against *E.coli* and *S. aureus*; (B) Proposed mechanism of antibacterial action of the TW/ENR/ZnO-SiO_2 blend with and without NR, illustrating the release of Zn^{2+} ions and generation of reactive oxygen species (ROS), leading to bacterial inactivation upon contact.

3.4 Morphology

Morphological analysis using optical microscopy and SEM–EDX, as shown in Figure 4, confirmed a more homogeneous distribution of Zn and Si elements in the TW/ENR/NR/ZnO-SiO_2 blends prepared via the latex-blending process, as illustrated in Figures 4(B-C). In contrast, partial agglomeration was observed in the melt-blended samples (Figure 4A) resulting in a smaller effective surface area and slightly reduced antibacterial efficiency against *E. coli* and *S. aureus*. The enhanced dispersion of ZnO-SiO_2 achieved through the latex-blending process facilitates greater Zn^{2+} ion release and ROS generation, thereby improving crosslink density and antibacterial performance compared with the melt-blending process.

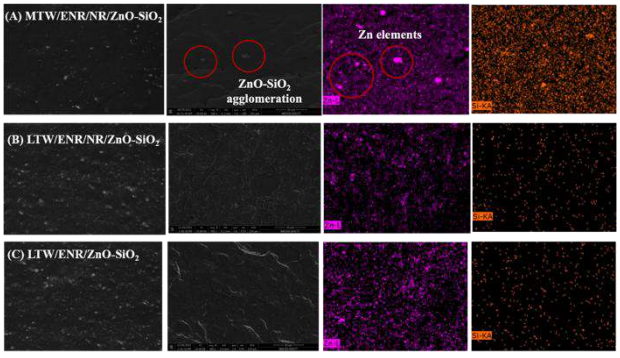

Figure 4 OM images, SEM micrographs and its EDX mapping of the TW/ENR/ZnO-SiO_2 blend with and without NR prepared using melt and latex processes.

4. Conclusion

This study highlights the critical influence of processing technique and filler dispersion on the structural, mechanical, and antibacterial properties of TW/ENR/NR/ZnO-SiO_2 blends. The latex-blending process, employing a two-step dispersion route, produced a more homogeneous distribution of ZnO-SiO_2 thereby enhancing filler–rubber interactions, crosslink density, and vulcanization efficiency compared with the melt-blending process. As a result, the latex-blended composites exhibited higher modulus and stronger antibacterial activity against *S. aureus* and *E. coli*, attributed to improved Zn^{2+} ion release and reactive oxygen species (ROS) generation. In contrast, the melt-blended composites showed greater tensile strength and elongation at break, resulting from strain-induced crystallization and flexible polysulfidic crosslinks. Morphological analysis confirmed uniform filler dispersion in the latex system and localized agglomeration in the melt process. Therefore, the findings demonstrate that processing strategy is a key factor in optimizing the balance between mechanical durability and antibacterial functionality, providing valuable guidance for the development of sustainable, multifunctional rubber materials for hygienic and industrial applications.

Acknowledgements

This work was supported by the Asahi Glass Foundation (KIRIM ID 27480). The authors also gratefully acknowledge the Petchra Pra Jom Klao Master's Degree Research Scholarship from King Mongkut's University of Technology Thonburi for additional support.

5. References

1. Whba, R.; Su'ait, M. S.; Whba, F.; Sahinbay, S.; Altin, S.; Ahmad, A. *Int. J. Biol. Macromol.* **2024**, *276*, 133796.
2. Zhao, L.; Liu, L.; Gao, J.; Zhang, L. *Polym. J.* **2024**, *311*, 127550.
3. Banoee, M.; Seif, S.; Nazari, Z.E.; Jafari-Fesharaki, P.; Shahverdi, H.R.; Moballegh, A.; Moghaddam, K.M.; Shahverdi, A.R. J. *Biomed. Mater. Res. - B Appl. Biomater.* **2010**, *93*, 557.
4. Mou, W; Li, J.; Fu, X.; Huang, C.; Chen, L.; Liu, Y. *Polym. Eng. Sci.* **2022**, *62*, 3110.
5. Hejna, A.; Zedler, Ł.; Przybysz-Romatowska, M.; Cañavate, J.; Colom, X.; Formela, K. *Polym.* **2020**, **12**, 1204.
6. Kim, D. Y.; Park, J. W.; Lee, D. Y.; Seo, K. H. *Polym.* **2020**, *12*, 2020.
7. Asaro, L.; Gratton, M.; Seghar, S.; Hocine, N.A. *Resour. Conserv. Recycl.* **2018**, *133*, 250.
8. Levin, V.Y.; Kim, S.H.; Isayev, A.I. *Rubber Chem. Technol.* **1997**, *70*, 641.
9. Mok, K.L.; Eng, A.H. *Malays. J. Chem.* **2018**, *20*, 118.
10. Bradbury, J. H.; Perera, M. C. S. *J. Appl. Polym. Sci.* **1985**, *30*, 3347.
11. Nielsen, L.E. *J. Macromol. Sci.* **1969**, *3*, 69.
12. Applerot, G.; Lipovsky, A.; Dror, R.; Perkas, N.; Nitzan, Y.; Lubart, R.; Gedanken, A. *Adv. Funct. Mater.* **2009**, *19*, 842.
13. Lou, H.; Wang, J.; Wang, Y.; Gao, Y.; Wang, W. *Poult. Sci.* **2024**, *103*, 104207.
14. Porfírio, S.; Carlson, R. W.; Azadi, P. *Trends Microbiol.* **2019**, *27*, 607.

Effect of Carbon Black and Barium Titanate Hybrid Filler on the Change of Electrical Signal in Epoxidized Natural Rubber Composite

Lyhav Boeurn[1], Sasitorn Srisawadi[3], Teeranoot Chanthasopeephan[4], Sontipee Aimmanee[4], Juthanee Phromjan[4], Yeampon Nakaramontri*[1], Frank Clemens[2]

[1]*Sustainable Polymer & Innovative Composite Materials Research Group, Department of Chemistry, Faculty of Science, King Mongkut's University of Technology Thonburi, Bangkok, Thailand.*

[2]*Empa, Swiss Federal Laboratories for Materials Testing and Research, Laboratory for High Performance Ceramics, Ueberlandstrasse 129, 8600 Duebendorf, Switzerland.*

[3]*National Metal and Materials Technology Center, 114 Thailand Science Park, Phahonyothin Road, Khlong Nueng, Khlong Luang, Pathum Thani 12120, Thailand.*

[4]*Department of Mechanical Engineering, King Mongkut's University of Technology Thonburi, 126 Prachautit Road, Bangmod, Tungkru, Bangkok, 10140, Thailand*

*E-mail: yeampon.nak@kmutt.ac.th

Abstract

Epoxidized natural rubber (ENR-25), a modified form of natural rubber with 25 mol% epoxidation, was compounded with conductive carbon black (CCB), barium titanate ($BaTiO_3$), and their hybrid fillers through melt mixing to study electrical performance. The hybrid composites were characterized for tensile properties, electrical properties, and dropping-ball testing. As a result, the CCB_{10}/BT_5 composite showed the highest dielectric constant (ε′) and moderate electrical conductivity (σ), with reduced dielectric loss (ε″), and better tensile properties. This improvement resulted from the synergistic interaction between the conductive network of CCB and the high dielectric permittivity of $BaTiO_3$, which enhances filler dispersion and interfacial polarization. Ball-dropping tests further indicated piezoelectric-like behavior due to filler network disruption. Thus, the CCB_5/BT_5 hybrid composite exhibits a piezoelectric effect, as evidenced by an increase in voltage after the ball is dropped onto the composite. This is attributed to the higher current generated after ball impact compared to the baseline condition, making it suitable for energy harvesting, sensor, and capacitor applications.

Keywords: Epoxidized natural rubber, Electrical properties, Hybrid filler.

1. Introduction

Dielectric elastomers are widely used in innovative materials for soft robotics, sensors, actuators, and energy-harvesting devices [1]. One key challenge for polymer or elastomer dielectric materials is producing films that simultaneously exhibit high dielectric permittivity and low loss. Recently, three-phase nanocomposites that integrate inorganic ceramic and conductive fillers into a polymer matrix have gained significant attention. These composites can be fabricated either by directly blending the fillers into the polymer or by first creating ceramic–conductive hybrid fillers through chemical methods and then incorporating them. The hybrid strategy helps conductive fillers disperse ceramics more effectively, while the ceramics prevent excessive contact between conductive fillers, resulting in enhanced dielectric permittivity and reduced loss [2]. Conductive fillers such as carbon nanotube (CNT) [3–5], and carbon black (CB)/barium titanate (BT) hybrid [6] have been reported in various matrices to improve dielectric and mechanical properties.

Epoxidized natural rubber (ENR) is a chemically modified form of natural rubber (NR) in which epoxide groups are introduced along the polymer backbone. This structural modification imparts enhanced oil resistance, reduced resilience and air permeability, and an increase in the glass transition temperature [7, 8]. The epoxide groups also improve interactions between the rubber matrix and inorganic fillers, promoting uniform dispersion and stronger interfacial adhesion [9]. Previous studies have shown that ENR composites filled with conductive carbon black (CCB) or CNT exhibit enhanced electrical conductivity through percolated networks [9–11]. In contrast, the incorporation of high-permittivity ceramics, such as BT, increases the dielectric constant via interfacial polarization [12]. More recent work demonstrates that combining conductive and ceramic fillers as hybrid systems synergistically improves dielectric and mechanical performance in various matrices by facilitating charge transport and preventing filler agglomeration. However, the ENR-25 matrix has not been studied yet.

In this study, ENR-25 composites containing hybrid fillers of CCB and BT are systematically investigated. The filler concentrations are varied: CCB at 5 and 10 phr, and BT at 3 and 5 phr, to determine the effect of filler composition on the electrical and mechanical properties of the composites. All hybrid composites are characterized by electrical conductivity, dielectric constant, and dielectric loss. Additionally, a dropping-ball test is used to evaluate changes in current response under mechanical impact, providing insight into the piezoelectric-like behavior and energy-harvesting potential of the composites. By optimizing the hybrid filler content, this study aims to develop ENR-based dielectric composites with enhanced electrical performance, low energy loss, and improved mechanical properties, paving the way for their application in advanced sensors, actuators, and energy-harvesting devices.

2. Experimental

2.1 Material

Conductive carbon black (CCB) was manufactured by Cabot Corporation (Texas, USA). Barium titanate (BT) powder with particle size less than 3 μm was purchased from Sigma-Aldrich (Shanghai, China), and epoxidized natural rubber (ENR-25%) was manufactured by Muang Mai Guthrie Co., Ltd., located in Surat Thani, Thailand. 2,2'-Dibenzothiazyl disulfide (MBTS) was used as an accelerator, supplied by Flexsys Inc., Termoli, Italy. Sulfur and stearic acid were provided by Imperial Chemical Co., Ltd., in Pathum Thani, Thailand. Zinc Oxide, a cure activator, was purchased from Global Chemical Co., Ltd. (Samutprakarn, Thailand).

2.2 Fabrication of rubber composites

This study utilized melt mixing to masticate the rubber with fillers and various chemicals, including an activator, an accelerator, and a crosslinking agent. Mixing was performed using an internal mixer (MX75, Chareon Tut Co., Ltd., Thailand) at 60 °C and 60 rpm. Initially, the rubber was masticated for 2 minutes, followed by the addition of fillers for 6 minutes. The hybrid filler compositions were varied with CCB at 5 and 10 phr, and BT at 3 and 5 phr. Subsequently, ZnO and stearic acid were incorporated for 2 minutes, after which mixing continued with the addition of MBTS for 1 minute. Finally, sulfur was added and mixed for 2 minutes. Once blending was complete, the compounds were passed through a two-roll mill to ensure uniform chemical dispersion throughout the matrix. The compounds were then sheeted via compression molding at 160 °C (dimensions: 150 × 150 × 2 mm^3). The compression time was determined based on the T_{c90} values obtained from a rubber processing analyzer (RPA Flex, DKSH Technology Limited, Thailand).

2.3 Characterization

The rubber composites were tested by a universal tensile machine (UTM, Zwick Z 1545, Zwick

GmbH and Co. KG, Ulm, Germany) with a loading cell of 500 N and a crosshead speed of 200 mm/min, and dumbbell-shaped specimens were prepared according to ISO 37 (type II). Electrical conductivity (σ), dielectric constant (ε'), and dielectric loss (ε") were investigated by Electrochemical Impedance Spectroscopy (E4990A, Keysight Technologies, Inc., Malaysia) to find capacitance (Cp), resistance (Rp), and dissipative factor (tan δ). The σ is calculated by following the Equation:

$$\sigma = \frac{1}{\rho} = \frac{d}{R_p \times A} \quad (1)$$

Where ρ is the volume resistivity, d is the composite thickness, A is the area of an electrode, and Rp is the resistance. Moreover, ε', and ε" are calculated by

$$A = \frac{C_p \times d}{A \times \varepsilon_0} \quad (2)$$

$$\varepsilon'' = \varepsilon' \tan\delta \quad (3)$$

where d is the thickness of the composites, Cp is the capacitance, tan δ is the loss factor, and ε_0 is the free space permittivity ($\varepsilon_o = 8.85\times10^{-12}$F/m).

The electrical deviation of the rubber composites was measured by dropping a ball 50 times through a polyvinyl chloride (PVC) pipe (Thai Pipe Industry Co., Ltd., Thailand) with a height of 30 cm, allowing it to impact the rubber composites, as shown in Figure 1a. Eventually, the rubber composite was placed in a dielectric fixture electrode, and the resistance was recorded as shown in Figure 1b. The current was computed following Equation [13]:

$$I = \frac{V}{R} \quad (4)$$

Where I, V, and R are current, voltage, and resistance, respectively.

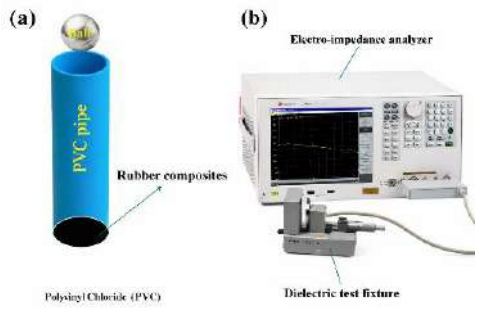

Figure 1 a) Experimental setup of the ball dropping test, and b) Instrument of electrical measurement.

3. Results and discussion

3.1 Electrical properties of ENR-25 composites

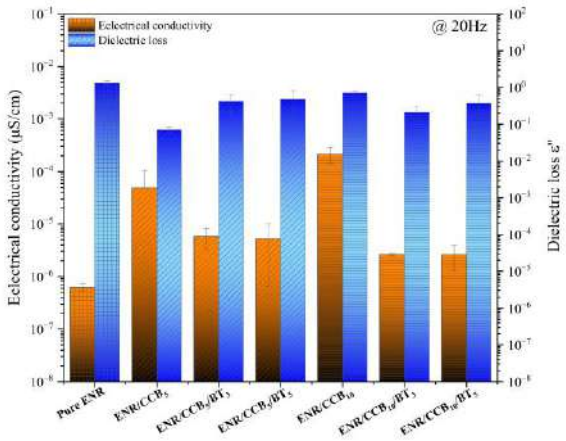

Figure 2 Electrical conductivity and dielectric loss of pure ENR, ENR/CCB and ENR/CCB/BT hybrid composites.

Electrical conductivity in rubber composites is controlled by filler particle size, shape, fabrication method, and matrix type, with strong rubber-filler interactions providing positive consequences. Figure 2 indicates the electrical conductivity and dielectric loss of ENR composites at various concentrations of CCB and BT. The electrical conductivity decreased when BT was present in the rubber matrix; it may be that BT is a dielectric material that can trap electrons from the CCB as they move between CCB particles [3]. Consequently, the electrical conductivity decreased with increasing BT content. Regarding dielectric loss, a slight decrease was observed when 3phr of BT was added, and the ε" increase occurred when 5phr of BT was added; however, the difference was not significant. This behavior may be due to the low content of BT, which is insufficient to effectively control the dielectric loss [12].

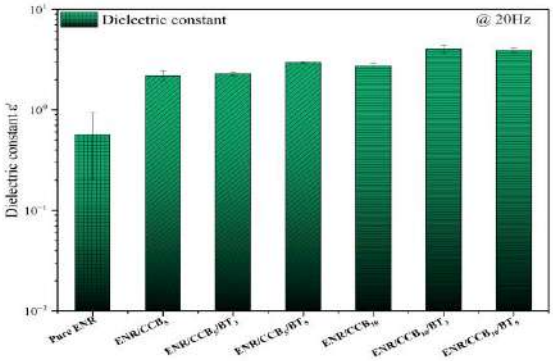

Figure 3 Dielectric constant of pure ENR, ENR/CCB and ENR/CCB/BT hybrid composites.

Figure 3 shows how the dielectric constant (ε′) changes for different ENR-25 composites measured at 20 Hz. The pure ENR-25 sample has the lowest dielectric constant, indicating limited ability to store electrical energy. When CCB is added, the dielectric constant increases slightly compared to pure ENR-25. It might be that CCB reduces interfacial polarization at the rubber-rubber interface [10], and it is also relevant that the functional group on the CCB molecule can also polarize in an electric field that has been applied [14]. However, when BT is combined with CCB, the dielectric constant increases in all hybrid composites. This improvement suggests that the combination of conductive and dielectric fillers enhances polarization within the material [6]. The highest dielectric constant is observed in the ENR-25/CCB_{10}/BT_3, indicating that increasing the BT content improves the micro-capacitor network in the rubber matrix, thereby enhancing dielectric performance [12].

3.2 Tensile properties

Table 1 Tensile properties of ENR-25 hybrid rubber composites.

Sample	M100 (MPa)	M300 (MPa)	Ts (MPa)	Eb (%)
Pure ENR	0.6±0.1	1.7±0.1	9.7±1.9	719±71
CCB_5	0.6±0.1	1.7±0.1	27.2±0.5	1177±42
CC_5/BT_3	0.7±0.1	1.9±0.1	25.2±0.7	1122±52
CCB_5/BT_5	0.7±0.1	1.9±0.1	27.2±0.8	1221±18
CCB_{10}	0.8±0.0	2.4±0.0	22.9±1.7	1025±50
CCB_{10}/BT_3	0.8±0.1	2.3±0.1	26.2±0.4	1043±43
CCB_{10}/BT_5	0.7±0.1	2.2±0.1	26.6±0.5	1057±23

M100 = Modulus at 100% strain, M300 = Modulus at 300% strain, Ts = tensile strength, Eb = elongation at break.

The ENR-25 composites show significant improvement in mechanical properties when modified with CCB and BT compared to the unfilled ENR-25. The unfilled ENR exhibits a tensile strength of 9.7 MPa and an elongation at break of 719%, serving as the baseline. Incorporating CCB increases tensile strength compared to pure ENR-25 indicating enhanced flexibility and durability. Similarly, CCB/BT hybrid composites exhibit tensile strengths of 17-26 MPa and elongations above 1000%, confirming that these additives significantly enhance both strength and stretchability. Modulus values (M100 and M300) also increase moderately across the modified samples, which may be due to increased bound rubber in the composites, resulting in slightly increased stiffness without compromising stretchability [15]. Overall, the data highlights that combining CCB and BT components effectively enhances the mechanical performance of ENR-based materials.

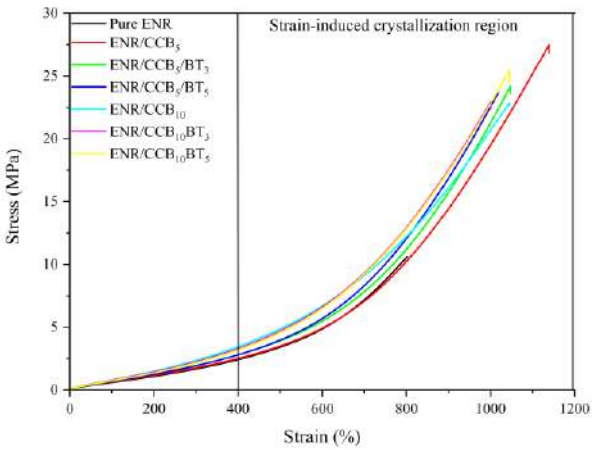

Figure 4 Stress-strain curves of ENR hybrid rubber composites.

Figure 4 shows the stress–strain curves for various ENR-25 composites, illustrating how the materials respond to tensile deformation. Incorporating barium titanate (BT) with conductive carbon black results in further changes: the ENR-25/CCB_5/BT_5 and ENR-25/CCB_{10}/BT_5 exhibit higher stress values at given strains, indicating improved load transfer and filler–matrix interaction [16]. However, excessive filler

loading slightly reduces stretchability by restricting polymer chain mobility, or it may reduce strain-induced crystallization (SIC) [1]. Overall, the addition of CCB and BT enhances the mechanical strength of the ENR composites while maintaining good stretchability, with the hybrid fillers providing a balance between stiffness and flexibility.

3.3 Electrical changes as a function of force

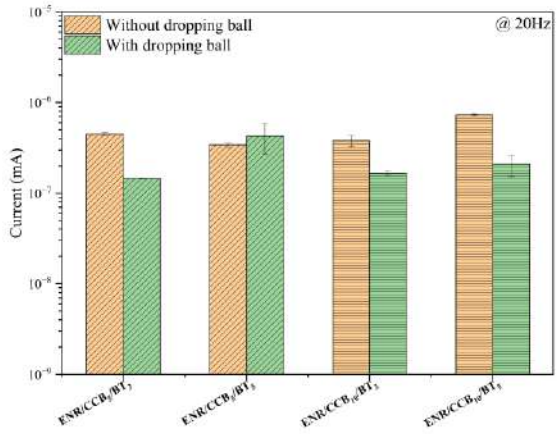

Figure 5 Comparison of the electrical current of ENR/CCB/BT composites measured at 20 Hz under two conditions: with and without the dropping-ball impact.

Figure 5 shows the currents of different ENR-25 composites, measured at 20 Hz, both with and without the dropping-ball condition. In all hybrid composites, the current (I) without the dropping ball is higher than that with the dropping ball, indicating that mechanical impact reduces the electrical current flow through the composites. This reduction may be caused by the temporary disruption of conductive pathways within the material due to deformation or compression during impact. Among the hybrid filler composites, the ENR-25/CCB_5/BT_5 composite exhibits the highest current after a ball was dropped on it, compared to other composites, indicating an optimal balance between the conductive carbon black and the dielectric barium titanate, enabling efficient charge transport [3]. Furthermore, in Equation 4, if the current increases, the composite voltage also increases. This phenomenon is also related to the piezoelectric effect that may occur in these composites. In other hybrid composites, the current decreased after the ball touches the composites, which might be due to the breaking of the CCB network, making it difficult for electrons to move along the pathways, or due to the BT polarization. This phenomenon is established as a piezoresistive effect. The overall trend indicates that mechanical stress affects the electrical behavior of these rubber composites, and the filler ratio plays a crucial role in determining their electrical stability under dynamic conditions.

4. Conclusion

The electrical properties of ENR-25 composites were improved by adding CCB/BT as a hybrid filler, especially the dielectric constant. Furthermore, ENR/CCB_{10}/BT_5 exhibits the proper dielectric and tensile properties, and, in the dropping-ball test, composites with lower CCB content and higher BT content can act in a piezoelectric-like manner due to greater changes in current after the ball is dropped on the sample. These composites can be utilized in various applications, including energy harvesting, strain sensors, and motion sensors.

5. Acknowledgement

This research was supported by the Thailand Science Research and Innovation (TSRI) and the National Science, Research, and Innovation Fund (NSRF) under Fiscal Year 2024, Grant No. FRB670016/0164. Additional support was provided by the Swiss National Science Foundation (SNSF) through the Swiss Program for International Research by Scientific Investigation Teams (SPIRIT) under Grant Agreement No. 223840 (SPRINT Project).

6. References

1. Kumar, A., Ahmad, D., Patra, K., and Hossain, M., J. Appl. Polym. Sci. 2021, 138, pp. 12–16.
2. Guan, S., Tang, Y., Song, S., Liu, H. and Zhao, S., JMSE-B. 2021, 271, 115280.
3. Chueangchayaphan, W., Luangchuang, P. and Chueangchayaphan, N., *Chin J Polym Sci*. 2021, 39, pp725–735.

4. Alam, M.N., Kumar, V., Kim, Y., Lee, D.J. and Park, S.S., Polymers. 2025, 17, pp. 1–20.
5. Bouhamed, A., Jöhrmann, N., Naifar, S., Böhm, B., Hellwig, O., Wunderle, B. and Kanoun, O., Sensors. 2022, 22, 4181.
6. Zhao, H., Xia, Y.-J., Dang, Z.-M., Zha, J.-W. and Hu, G.-H., J. Appl. Polym. Sci. 2013, 127, pp. 4440–4445.
7. Surya, I., Maulina, S. and Ismail, H., IOP Conference Series: Materials Science and Engineering. 2018, 299, 12061.
8. Chamnanvatchakit, P., Prodpran, T., Benjakul, S. and Prasarpran, S., Indian J. Sci. Technol. 2015, 8, pp 0974–6846 .
9. Siriwas, T., Pichaiyut, S., Susoff, M., Petersen, S. and Nakason, C., J. Mater. Sci. 2023, 58, pp. 15676–15695.
10. Matchawet, S., Kaesaman, A., Bomlai, P. and Nakason, C., J. Compos. Mater. 2016, 50, pp. 2191–2202.
11. Kummerlowe, C., Vennemann, N., Pieper, S., Siebert, A. and Nakaramontri, Y., Polymers 2014, 59, pp. 811–818.
12. Luangchuang, P., Chueangchayaphan, N., Sulaiman, M.A. and Chueangchayaphan, W., Polym. Int. 2021, 70, pp. 154–161.
13. Imtiyaaza, K.A., As'ari, S., Cahyani, K., Nurbayana, F., Zahro, Z., Nagifea, F., Sudarti, S. and Baihaqi, H., Sch. Jo. Phs. Ed. 2024, 5, pp. 142–149.
14. Shankar, B.S.M. and Kulkarni, S.M., Iran. Polym. J. 2019, 28, pp. 563–573.
15. Buaksuntear, K., Kohl, P., Li, Y. and Smitthipong, W., AC Appl. Polym. Mater. 2025, 7, pp. 3576–3587.
16. Rosset, S. and Shea, H.R., Appl. Phys. A. 2013, 110, pp. 281–307.

Study on the Effect of Compatibilizer Content on Mechanical Properties of NR/BR/NBR Blends

S. Kanokporn[1], C. Natchawut [1] and K.Wirunya [1,2*]

[1]*Department of Chemistry, Faculty of Science, Kasetsart University, Bangkok 10900, Thailand*

[2]*Specialized center of Rubber and Polymer Materials in agriculture and industry (RPM), Faculty of Science, Kasetsart University, Bangkok, Thailand*

**E-mail: fsciwyk@ku.ac.th*

Abstract

At present, natural rubber (NR), butadiene rubber (BR), and acrylonitrile butadiene rubber (NBR) possess complementary mechanical and thermal properties, and their blending offers a promising strategy to enhance material performance for diverse applications. However, the large polarity difference between nonpolar NR/BR and polar NBR often causes phase incompatibility and deteriorates mechanical properties. Compatibilization is therefore essential to improve interfacial adhesion in such ternary systems. Abdelsalam et al. reported that incorporating 3 phr of UB4000 enhanced phase compatibility in NR/SBR/NBR blends. This research aims to study the effect of adding a compatibilizer (Therpol AST Peletizado) at 0, 1, 3, and 5 phr to NR/BR/NBR blends with a fixed ratio of 70/20/10. FTIR, SEM, DMA, and TGA/DTG were employed to evaluate changes in chemical interactions, morphology, mechanical properties, and thermal stability. The results show that compatibilizer addition, particularly at 3 phr, enhances phase adhesion, reduces phase separation, and improves mechanical performance and thermal resistance of the blended rubber. These findings highlight that 3 phr of compatibilizer provides the optimum balance between interfacial interaction and network structure.

Keywords: Ternary rubber blend, NR, BR, NBR, Compatibilizer

1. Introduction

The rubber industry is a globally significant sector with extensive applications, and continuous improvement of material performance remains essential [1,2]. Polymer blending is a widely used strategy to combine advantageous properties from different elastomers and tailor them for specific applications [1,2]. However blending polymers with different polarity often results in poor miscibility and phase separation [1,2], which weaken mechanical strength and durability. Compatibilizers are therefore employed to promote interfacial adhesion and improve morphology uniformity .

Natural rubber (NR), a nonpolar bio-based elastomer, exhibits excellent tensile strength and elasticity but suffers from low oil and heat resistance . Butadiene rubber (BR) also nonpolar provides high resilience and low-temperature flexibility but has limited oxidative stability [1,2]. In contrast, Acrylonitrile-butadiene rubber (NBR) is polar and offers superior oil resistance and thermal stability, although it lacks strain-induced crystallization and is more expensive. Due to their polarity mismatch, NR/BR/NBR blends often display heterogeneous morphology and suboptimal properties unless compatibilized effectively.

Several studies investigating the combination of different rubbers for improved properties have focused on enhancing compatibility by adding compatibilizers during polymer blending . One such study by Abdelsalam et al. examined NR/SBR/NBR rubber blends with 3 phr of UB4000 compatibilizer and found that this loading improved the compatibility of the blended rubber [3]. Additionally, most studies commonly use this concentration of 3 phr [4,5]. However, although a compatibilizer loading of 3 phr is widely employed, many studies have not clearly explained the mechanistic rationale or guiding principles behind selecting this specific amount. Therefore, the present study aims to investigate this issue in depth, in order to clarify the

underlying reasons for choosing an optimal compatibilizer concentration and to evaluate the effects of different loadings on the properties of the rubber blends.

Therefore, this research aims to study the effect of adding the compatibilizer (Therpol AST Peletizado) at different loadings of 0, 1, 3, and 5 phr into NR/BR/NBR blends with a fixed ratio of 70/20/10 phr. The properties of the blends were analyzed using FTIR, SEM, DMA, and TGA/DTG techniques to evaluate the effect of the compatibilizer on phase compatibility, mechanical properties, and thermal stability of the blends.

2. Experimental

2.1 Materials

Natural rubber (NR), butadiene rubber (BR), and acrylonitrile–butadiene rubber (NBR) were obtained from the Rubber Authority of Thailand (RAOT). Additives used in the compounding formulations included:

- Pigment
- Nano-zinc oxide (activator)
- Stearic acid (co-activator)
- Butylated hydroxytoluene (BHT) (antioxidant)
- Tetrabenzylthiuram disulfide (TBzTD) (secondary accelerator)
- 2,2-Dithiobis(benzothiazole) (MBTS) (primary accelerator)
- Sulfur (crosslinking agent)
- Compatibilizer: **Therpol AST Peletizado** (a chemically modified natural rubber based on cis-1,4-polyisoprene, containing grafted polar functional groups (C=O).)

2.2 Preparation of NR/BR/NBR blends

Ingredients of each ternary rubber compound are presented in **Table 1** they were prepared in an internal mixer at 50 °C and a rotor speed of 45 rpm. NR was first introduced into the internal mixer and masticated for 5 minutes. Then BR, NBR, compatibilizer, pigment, nano-zinc oxide, stearic acid, and BHT were added. The mixture was transferred to a two-roll mill (50 °C), where TBzTD, MBTS, and sulfur were incorporated during the final mixing stage.

Table 1 Compounding formulations for NR/BR/NBR blends (unit: phr).

	Sample			
	1	2	3	4
NR	70	70	70	70
BR	20	20	20	20
NBR	10	10	10	10
Compatibilizer	0	1	3	5
Pigment	5	5	5	5
Nano-ZnO	2	2	2	2
Stearic Acid	0.5	0.5	0.5	0.5
BHT	1	1	1	1
TBzTD	0.5	0.5	0.5	0.5
MBTS (Thiazole)	1	1	1	1
Sulfur	2	2	2	2

2.3 Vulcanization

Vulcanization was carried out in a heated stainless-steel mold at 160 °C according to a particular cure time (optimum cure time (t_{c90})), which was determined according to ISO 6502-3 using a Moving Die Rheometer at 160 °C under pressure of 100 bar [7].

2.4 Physical testing

2.4.1 Tensile testing

Dumbbell-shaped specimens were prepared according to ISO 37. Tensile tests were performed at a crosshead speed of 500 mm/min, and tensile strength, elongation at break, and Young's modulus were recorded [8].

2.4.2 Hardness

The rubber specimen with a minimum thickness of 6 mm and a smooth surface was tested for hardness using a Shore A durometer following ISO 48-4. Measurements were taken at five points per sample [9].

2.5 Morphological study

The tensile fracture surfaces of the rubber specimens were coated with a thin conductive layer to prevent charging and scanned using high-energy electrons. The resulting images were generated through the detection of secondary electron (SE), providing detailed information on the surface topography and morphology of the rubber [2,3].

2.6 Fourier Transform Infrared Spectroscopy (FTIR)

Fourier-transform infrared spectroscopy (FTIR) analyses samples by passing infrared radiation through them and measuring the absorbed wavelengths, reported as wavenumbers (in cm^{-1}). The resulting spectrum displayed as transmittance or absorbance versus wavenumber allows identification of functional groups due to their characteristic absorption bands. The typical analytical range spans the mid-infrared region, from approximately 4,000 to 400 cm^{-1}

2.7 Thermogravimetric analysis (TGA)

A 5 mg sample was placed in a crucible within a precisely temperature-controlled furnace. The temperature was increased at a constant rate of 10 °C/min under a continuous nitrogen (N_2) purge, spanning a range from 30 to 800 °C. The instrument continuously recorded the mass of the sample, generating a thermogravimetric (TGA) curve that plots mass (or % of initial mass) versus temperature. This method allows determination of the decomposition onset temperature, mass loss rates (via DTG), and overall thermal stability of the material.

2.8 Dynamic Mechanical Analysis (DMA)

Dynamic mechanical analysis (DMA) was performed in tensile mode over a temperature range of -100 to 100 °C at a heating rate of 5 °C /min and a fixed frequency of 1 Hz to investigate the temperature-dependent viscoelastic behavior of the material. The resulting parameters, including storage modulus, loss modulus, and tan δ, were used to evaluate mechanical transitions such as the glass transition temperature (Tg) and to assess the effects of material structure and phase compatibility in polymer or rubber blend systems.

3. Results and discussions

3.1 Physical testing

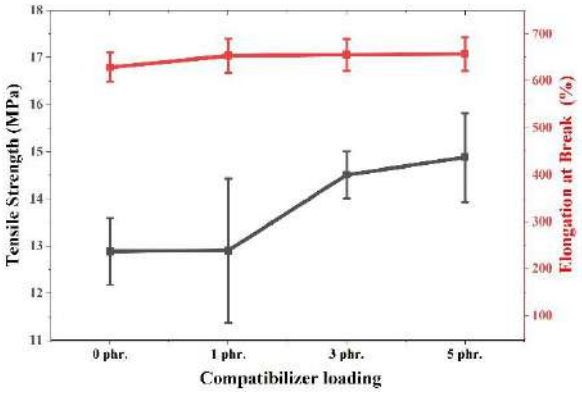

Figure 1. The tensile strength and elongation at break of NR/BR/NBR ternary blends with different compatibilizer contents.

Figure 1 shows that the addition of 1 phr of compatibilizer did not result in a noticeable change in tensile properties. However, increasing the compatibilizer content to 3 phr led to a significant improvement in tensile strength, rising from 12.9

to 14.5 MPa. Further increases in compatibilizer content beyond 3 phr did not produce any significant enhancement in tensile strength. Likewise, the elongation at break also increased initially, rising from 629% at 0 phr to 653% and 655% at 1 and 3 phr, respectively, before decreasing slightly to 635% at 5 phr. The slight improvement in elongation at break is attributed to the increased interfacial adhesion between polar and nonpolar rubber phases, reducing phase separation and stress concentration. Overall, a compatibilizer loading of 3 phr provided the most effective phase compatibility, resulting in an optimal balance between tensile strength and elongation at break in the NR/BR/NBR blends.

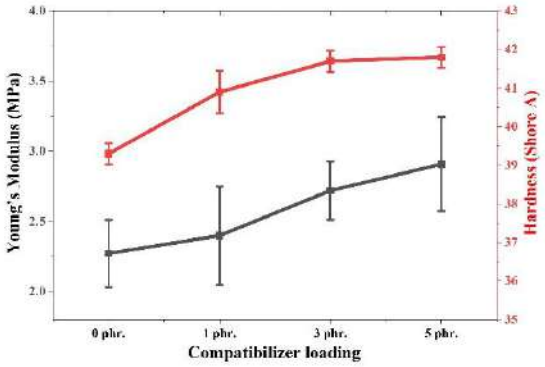

Figure 2. Young's modulus and hardness of NR/BR/NBR ternary blends with different compatibilizer contents.

Figure 2 shows that both the Young's modulus and hardness of the NR/BR/NBR blends increased systematically with higher compatibilizer loading. The Young's modulus rose from 2.27 to 2.40 and 2.72 MPa for 0, 1 and 3 phr followed by a slight decrease to 2.70 MPa at 5 phr, indicating improved interfacial adhesion and network rigidity up to 3 phr beyond which compatibilization saturation occurs. Likewise, the hardness increased from 39.3 40.9 41.7 to 41.8 Shore A for NR/BR/NBR blends with 0, 1, 3, and 5 phr of compatibilizer, respectively, indicating a rise in the effective crosslink density and the development of a more compact and structurally integrated phase morphology within the ternary blend.

3.2 Fourier Transform Infrared Spectroscopy (FTIR)

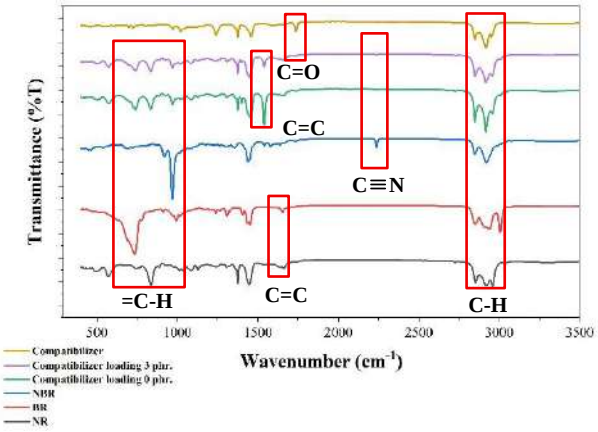

Figure 3. Fourier transform infrared spectroscopy (FTIR) of NR/BR/NBR ternary blends with different compatibilizer contents.

Figure 3 shows the FTIR spectra of NR, BR, NBR, and their NR/BR/NBR blends. It reveals that the bands at 3000-2850 cm^{-1} correspond to C-H stretching vibrations of $-CH_2$ and $-CH_3$ groups common to all rubbers. The C≡N stretching at 2235-2245 cm^{-1}, characteristic of NBR, becomes broader and slightly shifted in the NR/BR/NBR blends with compatibilizer 3 phr, suggesting interactions between the polar C≡N groups of NBR and the compatibilizer. The C=O band (1730–1780 cm^{-1}), attributed to anhydride or ester groups, appears clearly in the NR/BR/NBR blend with 3 phr compatibilizer but is absent in the 0 phr blend, confirming the existence of compatibilizer in the rubber matrix [1,10]. In the fingerprint region (1000–700 cm^{-1}), the characteristic peaks of NR at 835 cm^{-1} and BR at 966 and 915 cm^{-1} become smoother and more overlapping in the compatibilized blend, suggesting improved phase dispersion. The mechanism is based on specific physicochemical interactions between the compatibilizer and the rubber phases. The polar carbonyl (C=O) groups of the compatibilizer can interact with the nitrile (C≡N) groups of NBR through dipole‑dipole interactions, while the nonpolar backbone of the compatibilizer is compatible with NR and BR via physical entanglement and van der Waals interactions. These FTIR observations indicate enhanced interfacial interactions and improved compatibility within the NR/BR/NBR system with the addition of 3 phr compatibilizer, which is consistent with previous reports [1,2,5,7].

3.3 Thermogravimetric analysis (TGA)

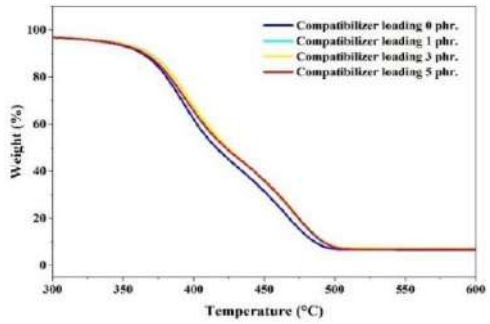

Figure 4. Thermogravimetric analysis (TGA) of NR/BR/NBR ternary blends with different compatibilizer contents.

Figure 4 shows that all rubber blends exhibited major mass loss between 350–550 °C, corresponding to the main degradation of the polymer backbone. The onset and midpoint decomposition temperatures shifted slightly to higher values with increasing compatibilizer content, indicating improved thermal stability. Specifically, the T_{50}% of the unmodified blend was around 430 °C , while those of the NR/BR/NBR blends with 1 ,3 and 5 phr compatibilizer were approximately 440 °C , 445 °C and 448 °C, respectively. This shift suggests that the compatibilizer enhances the thermal resistance of the material by stabilizing the polymer matrix [12,13]. The residual mass above 550 °C was below 5% for all samples, indicating nearly complete decomposition. Overall, the addition of the compatibilizer slightly improved the thermal stability and delayed the degradation of the NR/BR/NBR blends [1,7].

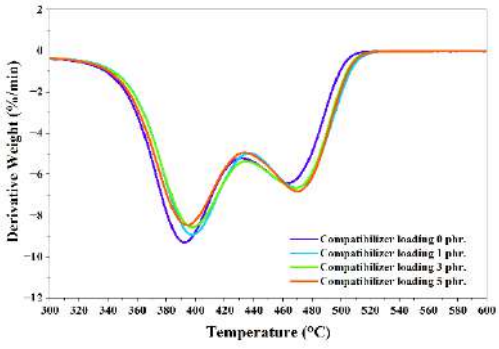

Figure 5. The derivative thermogravimetry (DTG) of NR/BR/NBR ternary blends with different compatibilizer contents.

The DTG curves show a typical two-step degradation behavior, as seen in **Figure 5**. The first peak (around 370 - 410 °C) corresponds to the decomposition of NR while the second peak (around 450 - 480 °C) is associated with the decomposition of the BR and NBR phases. With increasing compatibilizer loading, both peaks shifted toward higher temperatures, and the peak widths became narrower, suggesting more uniform degradation and greater thermal stability. The NR/BR/NBR blends with 3 phr and 5 phr compatibilizer exhibited the highest onset and peak decomposition temperatures, indicating a more stable and homogeneous network structure. These findings confirm that compatibilizer incorporation improves the thermal resistance and uniformity of the degradation process in NR/BR/NBR blends [4,11].

3.4 Dynamic Mechanical Analyzer (DMA)

DMA was conducted to investigate the miscibility of the rubber in the blends and to measure the glass transition temperatures (T_g), storage modulus, and damping behavior of the blend.

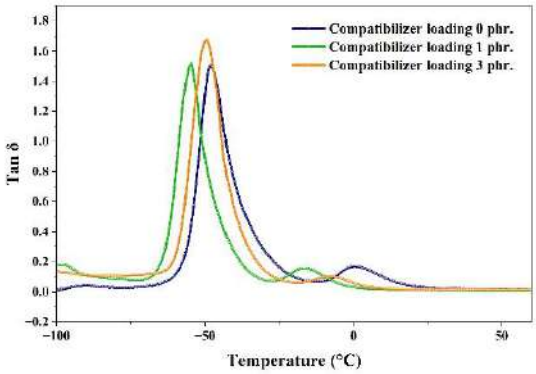

Figure 6. Tan δ as a function of temperature for NR/BR/NBR ternary blends with different compatibilizer contents.

Figure 6 shows that the addition of compatibilizer leads to a more homogeneous viscoelastic response in the NR/BR/NBR blends. NR/BR/NBR blends without compatibilizer exhibits a broad tan δ peak with a distinct high-temperature shoulder, characteristic of phase-separated systems with multiple relaxation processes. In contrast, the NR/BR/NBR blends with 1 and 3 phr compatibilizer show sharper peaks and diminished shoulder regions, indicating reduced phase heterogeneity and improved interfacial adhesion among the three rubber phases. These changes reflect a more integrated phase morphology resulting from effective compatibilization. For an incompatible system, the tan δ versus temperature curve shows two damping peaks corresponding to the glass transition temperatures of individual polymers [12,14].

However, compatibility of blend components has a single peak which is found for the combined processes. An intermediate situation arises when broadening of transition peaks occurs in the case of partially compatible systems, accompanied by a shift in the dynamic Tg to higher or lower temperatures depending on the compatibilizer content [1,2,3].

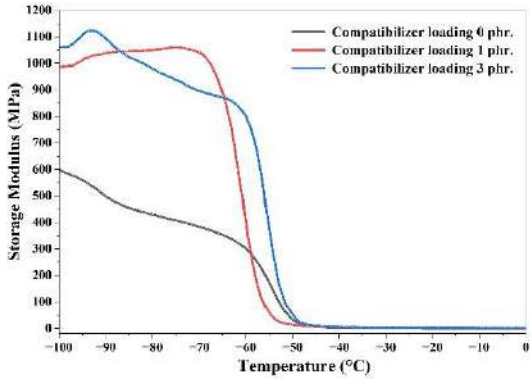

Figure 7. Storage modulus as a function of temperature of NR/BR/NBR ternary blends with different compatibilizer contents.

Figure 7 demonstrates that the incorporation of compatibilizer increases the storage modulus of the NR/BR/NBR blends in the low-temperature region and produces a sharper and more coherent glass to rubber transition. The NR/BR/NBR blends without compatibilizer exhibits a gradual modulus drop, characteristic of a system with significant phase separation and multiple relaxation processes. In contrast, the NR/BR/NBR blends with 1 and 3 phr compatibilizer show higher modulus values and a much steeper transition. The presence of the compatibilizer strengthens interfacial adhesion between the different rubber phases, leading to constrained molecular motion at the phase boundaries. As these constrained segments become partially activated with increasing temperature, the applied mechanical stress can be transferred more efficiently across the interfaces, indicating enhanced interfacial adhesion and a more unified phase morphology. Notably the NR/BR/NBR blends with 3 phr compatibilizer demonstrates the most pronounced modulus retention and the most coherent transition profile, reflecting the highest level of phase compatibilization among the examined compositions [1,2,3].

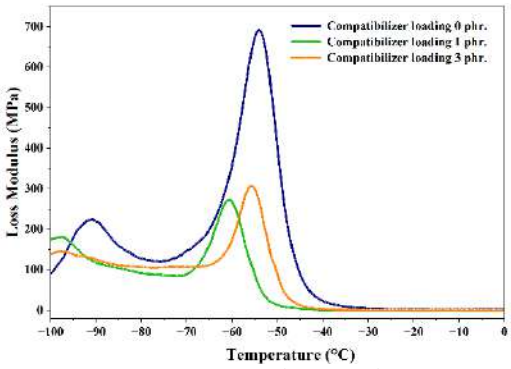

Figure 8. Loss modulus as a function of temperature of NR/BR/NBR ternary blends with different compatibilizer contents.

The loss modulus of the NR/BR/NBR blends decreases, and the relaxation behavior becomes more unified with the addition of compatibilizer. The NR/BR/NBR blends without compatibilizer exhibits a high primary loss peak together with a distinct low-temperature shoulder, indicating multiple relaxation processes associated with phase separation. In contrast, the NR/BR/NBR blends with 1 and 3 phr compatibilizer show lower peak intensities and the disappearance of the shoulder, reflecting reduced phase heterogeneity and enhanced interfacial adhesion. The more consolidated loss response in the compatibilized blends therefore suggests a more integrated phase morphology and improved overall compatibility within the ternary system.

3.5 Morphology

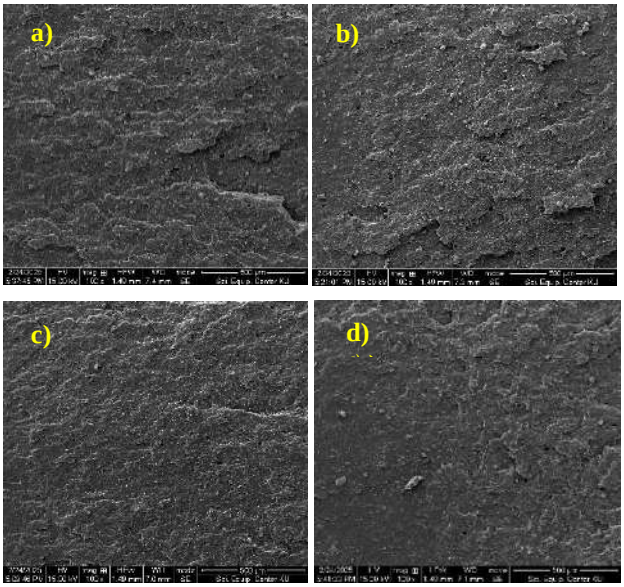

Figure 9. The tensile fractured surfaces of NR/BR/NBR ternary blends with different compatibilizer contents. a) NR/BR/NBR without compatibilizer, b) NR/BR/NBR with 1 phr compatibilizer, c) NR/BR/NBR with 3 phr compatibilizer, d) NR/BR/NBR with 5 phr compatibilizer.

The SEM images show improvement in fracture surface morphology with increasing compatibilizer content. The uncompatibilized NR/BR/NBR blend exhibits a rough and heterogeneous fracture surface due to weak interfacial adhesion, leading to interfacial debonding, microvoid formation, and localized crack propagation. The blend containing 1 phr compatibilizer shows a relatively smoother surface, although some heterogeneity remains, indicating partial improvement in interfacial interactions. At 3 phr compatibilizer, the fracture surface becomes uniform and continuous with no distinct phase boundaries, reflecting the highest level of interfacial compatibility and homogeneous stress distribution. In contrast, the 5 phr sample exhibits slight surface irregularities, likely caused by compatibilizer agglomeration due to over-addition. Overall, a compatibilizer loading of 3 phr provides the most optimal fracture morphology among all formulations [1,2,4].

4. Conclusions

The addition of the compatibilizer significantly improved the mechanical properties and viscoelastic performance of the NR/BR/NBR blends. Tensile strength, elongation at break, Young's modulus, and hardness all increased with compatibilizer loading, with 3 phr providing the most balanced enhancement. FTIR confirmed chemical interactions through broadening and shifting of the C≡N band and the appearance of the C=O band, indicating successful incorporation of the compatibilizer. DMA (tan δ, storage modulus, and loss modulus) consistently demonstrated reduced phase heterogeneity and more coherent transitions, supporting improved phase compatibility. SEM micrographs showed the most homogeneous morphology at 3 phr with distinct reduction in phase boundaries. Thermal stability (TGA/DTG) also increased slightly with higher compatibilizer loading, with the 3-5 phr compatibilizer showing the highest onset and peak degradation temperatures. Overall, NR/BR/NBR blends with compatibilizer 3 phr compatibilizer yielded the most optimal balance between interfacial adhesion, network structure, morphology, mechanical performance, and thermal resistance.

5. Acknowledgement

I would like to express sincere gratitude to all individuals and institutions who contributed to the completion of this study. Special thanks are extended to Asst. Prof. Wirunya Keawwattana, Ph.D. whose guidance, knowledge, and encouragement greatly supported the development of this research. Authors wish to thank Hub of Talents in Natural Rubber, National Research Council of Thailand for the publication support and This research is funded by Faculty of Science, Kasetsart University through the Graduate Fellowship Program.

6. References

1. Vishnu, S.; Suma, K. K.; Gireesh, V. B.; et al. Strategies to Improve Mechanical Performance of Elastomers Using Ternary Blends: A Review. *Mater. Today Sustain.* **2023**, *23*, 100443.
2. Urtekin, G.; Ullah, M. S.; Yildirim, R.; Ozkoc, G.; Kodal, M. A. A Comprehensive Review on Thermoplastic–Rubber Blends and Nanocomposites. *Polym. Compos.* **2023**, *44* (12), 8303–8329.
3. Abdelsalam, A. A.; Araby, S.; El-Sabbagh, S. H.; Abdelmoneim, A.; Hassan, M. A. A Comparative Study on Mechanical and Rheological Properties of Ternary Rubber Blends. *Polym. Polym. Compos.* **2021**, *29* (1), 15-28.
4. Abdelsalam, A. A.; Khozami, M. A. Studies on Swelling Behavior, Mechanical and Thermal Properties of Ternary Rubber Blend Composites in the Presence of Compatibilizers. *Pigment Resin Technol.* **2023**, *52* (5), 614-623.
5. Abdelsalam, A. A.; El-Sebaie, M. G.; et al. Effect of Filler Loading on the Curing Characteristics and Mechanical Properties of NR/SBR/NBR Ternary Blends. *KGK Kautsch. Gummi Kunstst.* **2020**, *73* (10), 41-47.

6. Srinivas, J.; Jagatheeshwaran, M. S.; Elayaperumal, A.; et al. Effect of Nanosilica on Mechanical and Swelling Resistance Properties of Ternary Rubber (NR/SBR/NBR) Blend Nanocomposites with and without Silane Compatibilizer. *Silicon* **2024**, *16* (4), 1669-1688.
7. International Organization for Standardization. *Rubber-Measurement of Vulcanization Characteristics Using Curemeters-Part 3: Moving-die Curemeters*; ISO 6502-3:2023; Geneva, Switzerland, 2023.
8. International Organization for Standardization. *Rubber, Vulcanized or Thermoplastic-Determination of Tensile Stress-strain Properties*; ISO 37:2017; Geneva, Switzerland, 2017.
9. International Organization for Standardization. *Rubber-Determination of Hardness-Part 4: Durometer Method (Shore Hardness)*; ISO 48-4:2018; Geneva, Switzerland, 2018.
10. Lee, S.-H.; Park, S.-Y.; Chung, K.-H.; Jang, K.-S. Phlogopite-Reinforced NR/EPDM Composites with Aminosilane Compatibilizer. *Polymers* **2021**, *13* (14), 2318.
11. Aini, N. A. M.; Othman, N.; Hussin, M. H.; Sahakaro, K.; Hayeemasae, N. Interaction Efficiency between Hybrid Fillers CB/Lignin and Rubber-Based Compatibilizer in NR/BR Composites. *Ind. Crops Prod.* **2022**, *185*, 115167.
12. Leyva-Porras, C.; Estrada-Moreno, I. A.; Piñón-Balderrama, C. I.; Flores-Gallardo, S. G.; Márquez-Lucero, A. Thermodynamic Parameters of Crosslinked Elastomers (BR, SBR, NBR) and Their Blends. *Polymers* **2024**, *16* (3), 351.
13. Shao, H.; Chen, Y.; Zhang, G.; He, A. Strategy for the NR/BR Blends with Improved Thermo-Oxidative Resistance by Using TBIR as a Reactive Compatibilizer. *Polymer* **2021**, *225*, 123761.
14. Shao, H.; Chen, Y.; Zhang, G.; He, A. Evolution of Crosslinking Network Structure and Thermo-Oxidative Aging Behavior of Unfilled NR/BR Blends with TBIR. *Polym. Degrad. Stab.* **2022**, *195*, 109771.

Rubbers and Rubber Composites Innovations for Unexplored and Sustainable Applications

IRC 2025
BANGKOK, THAILAND

International Rubber Conference 2025 (IRC 2025)

Thermoset–Rubber 2K Composite Systems: Material Combinations and Interfacial Reactions in a One-Step Injection Molding Process

Florian Löhr*[1], Elmar Moritzer[1], Benjamin Klie[2], Ulrich Giese[2]

[1]*Paderborn University, Warburger Straße 100, 33100 Paderborn, Germany*

[2]*German Institute of Rubber Technology (DIK e.V.), 30519 Hannover, Germany*

*E-mail: florian.loehr@ktp.uni-paderborn.de

Abstract

Thermoset–elastomer composite systems enable functionally integrated polymer components with high thermal, chemical, and creep resistance. In contrast to conventional thermoplastic–elastomer combinations, these composites offer advantages in applications exposed to high temperatures, aggressive media, or mechanical stress. This study investigates the development of thermoset–elastomer composites produced in a one-step two-component (2K) injection molding process without additional external adhesion promoters, focusing on the resulting interfacial reactions and adhesion mechanisms.

The experiments were conducted to analyse the influence of material pairing and processing parameters. On the thermoset side, phenolic molding compounds (PF), epoxy compounds (EP), and bulk molding compounds (BMC) were processed, while the elastomer side comprised natural rubber (NR) and hydrogenated nitrile butadiene rubber (HNBR) based rubber compounds. Adhesion behaviour was characterised by peel testing and visual analysis of failure modes.

The results demonstrate a pronounced dependence of interfacial adhesion on the material combination and curing kinetics. PF–elastomer systems showed the highest adhesion with cohesive failures, while EP systems exhibited almost no bonding. BMC–elastomer combinations achieved moderate adhesion, with HNBR displaying more than twice the peel strength compared to NR. These findings provide guidance for designing thermoset–elastomer composites with improved bonding and reduced process complexity.

Keywords: thermoset–elastomer, 2K injection molding, interfacial adhesion, bulk molding compound, peel strength

1. Introduction

Multicomponent composites consisting of hard and soft components are an essential part of modern product development. The production of hard–soft components by two-component (2K) injection molding is an established method for integrating functions into polymer components [1]. While thermoplastic–elastomer systems are widely established, thermoset–elastomer composites provide additional potential where particularly high resistance to temperature, media and creep is required [2,3]. Examples include components with integrated sealing or bearing functions in media-carrying systems or vibration-loaded applications.

Two-component injection molding with direct interfacial adhesion increases process reliability and reduces the need for additional processing steps or external additives such as applied adhesion promoters [4]. Traditionally, such adhesion has been achieved via primers or intermediary bonding agents, which require additional coating or surface activation steps, resulting in increased process complexity, cost, and environmental impact [4,5].

Therefore, the aim of this work is the development of thermoset–elastomer composites produced in the 2K injection molding process without additional externally applied adhesion-promoting layers or coatings. The investigated material pairings have so far been insufficiently studied, particularly in the context of a one-step process with chemically active interfacial reactions [5,6]. Previous research has mainly addressed thermoplastic–elastomer combinations, whereas

systematic data for thermoset–rubber systems — especially regarding kinetic matching and reactive bonding mechanisms — remain sparse. Initial studies by Heyne et al. [7,8] demonstrated that direct bonding between thermosets and elastomers is feasible when the curing reactions of both components temporally overlap and reactive species at the interface enable covalent coupling. However, their investigations also underlined that the achievable adhesion strongly depends on the formulation and the thermal process window.

An additional advantage of this approach lies in sustainability: direct adhesion in a one-step 2K injection molding process replaces adhesives, mechanical joining methods and additional processing steps. This integration shortens the process chain, reduces material and energy consumption [4], and supports future circular-economy strategies by eliminating solvent-based adhesive coatings.

2. Experimental methods

The experimental work was conducted to evaluate interfacial adhesion in thermoset–elastomer composites produced without additional external adhesion promoters using a one-step 2K injection molding process. The investigation comprised material selection, process parameter definition, and peel-test characterisation to identify correlations between material pairing, curing conditions, and resulting bond strength.

2.1 Materials and Processing

On the thermoset side, four reinforced phenolic molding compounds (Supraplast PK 3300, Süd-West Chemie GmbH and PF6507/6680/2736, Bakelite GmbH), one epoxy molding compound (Epoxidur EP 3585H, Raschig GmbH), and two bulk molding compounds (BMC) from Menzolit GmbH and Tetra-Dur Kunststoff Produktion GmbH were used. The thermoset materials used in this study were commercially available molding compounds.

On the elastomer side, two rubber compounds with significantly different polarity were examined.The non-polar compound was based on a standard Malaysian natural rubber (NR) grade (SMR 10, Weber & Schaer) without a specified Mooney viscosity. The highly polar compound was based on a partially hydrogenated nitrile butadiene rubber (HNBR - Therban AT 3443 VP, Arlanxeo) with an acrylonitrile content of 34 %, a Mooney viscosity of 39 MU (ML (1+4) at 100 °C), and a residual double- bond content of 4 %. Both compounds were cured using a sulfur-accelerator system. For the NR-based compound, additional adhesion promoting agents were incorporated to enhance bonding to the thermoset component during injection molding. The detailed formulations are listed in Table 1 and Table 2.

Table 1: NR - Mixture composition

Raw material	[phr]
Natural rubber – SMR 10	100
Silica – Ultrasil VN3 GR	15
Carbon black – N 330	50
Plasticizer – Vivatec 200	7
Activator – ZnO	6
Activator – Stearic acid	2
Crosslinking agent - Sulphur	4
Accelerator – TBBS* 80 %	1.44
Resorcin donor – Cohedur RS	3
Methylol melamine dispenser – Cohedur A200	1.5

* TBBS: N-tert-butyl-benzothiazyl sulfenamide

Table 2: HNBR - Mixture composition

Raw material	[phr]
HNBR – Therban AT 3443 VP	100
Silica – Ultrasil 7000 GR	20
Carbon black – N 330	50
Activator – ZnO	3
Activator – Stearic acid	1
Crosslinking agent – Sulphur	1
Accelerator – TMTD*	2.5
Accelerator – CBS**	1

* TMTD: tetramethyl thiuram disulphide

** CBS: N-cyclohexyl-2-benzothiazolesulfenamide

The rubber compounds were prepared using an industrial internal mixer (Werner & Pfleiderer GK 5E) with intermeshing PES3 rotors and a fill factor of 70 % at 40 °C and 40 rpm. The resulting mixtures were cooled for 5 min on a two-roll mill, and rubber sheets were produced for further processing. The speed ratio between roll 1 and roll 2 was 1:1.2, with the nip set to 1.5 mm.

The viscosity of the rubber compounds was determined according to Mooney ML (1+4) at 100 °C using a Monsanto MV 2000 E viscometer with a large rotor, a preheating time of 1 min, and a testing time of 4 min. The NR-based compound showed a viscosity of 75 MU, and the HNBR-based compound 138 MU.

The vulcanization time (tc_{90}) was determined using a Monsanto MDR 2000 E rheometer at isothermal temperatures of 150 °C, 160 °C and 180 °C (frequency 1.667 Hz, amplitude 0.1°). The maximum torque (S_{max}), minimum torque (S_{min}), torque difference ($\Delta S = S_{max} - S_{min}$) and vulcanisation time (tc_{90}) were determined for both compounds. The corresponding values are summarised in Table 3.

Table 3: Rheometer results for HNBR and NR compounds at different isothermal temperatures

Parameter	HNBR (160 / 180 °C)	NR (150 / 160 °C)
S_{max} [dNm]	40 / 36	24 / 23
S_{min} [dNm]	3.6 / 3.2	3.4 / 3.3
ΔS [dNm]	36.4 / 32.8	20.6 / 19.7
tc_{90} [min]	9 / 3	11.5 / 6

Since the processing characteristics of free-flowing molding compounds (variant 1) and highly filled, pasty bulk molding compounds (variant 2) differ considerably, the experimental work was carried out using two different injection molding machines and dedicated molds. In both variants, a rotary-table 2K injection molding setup with L-configured injection units enabled sequential processing of thermoset and elastomer materials within the same mold.

The variant 1 composites (phenolic and epoxy systems) were produced on a two-component injection molding machine ENGEL Combimelt Victory 200H/200L/80. The produced shear test specimens consisted of a thermoset plate (70 × 58.5 × 4 mm) and an elastomer strip (140 × 25 × 6 mm) with an interfacial contact area of 45 × 25 mm. Material-specific process parameters were developed through preliminary trials using a statistical design of experiments to define a reproducible processing window for the experiments; these parameters are summarized in Table 4.

Table 4: Processing parameters for variant 1 (phenolic / epoxy molding compounds + NR / HNBR)

Parameter	Thermoset (Variant 1)	Elastomer (Variant 1)
Mold temperature [°C]	170	variable
Curing time per mm sample thickness [s]	10 – 17.5	—
Curing time [min]	—	tc_{90} + 6 min
Cylinder temperature (feeding zone / die) [°C]	70 / 85	80 / 80
Injection velocity [$cm^3\ s^{-1}$]	40	8
Maximum injection pressure [bar]	500 – 900	2000
Holding pressure [bar]	400/ 300/ 200	300
Holding pressure time [s]	3 – 6	90

The BMC composites (variant 2) were processed on a KraussMaffei KM 160-750 CX DUR injection molding machine equipped with an additional bolt-on injection unit for two-component operation. The specimens consisted of a thermoset plate (150 × 60 × 4 mm) and an elastomer strip (215 × 20 × 4 mm), resulting in a contact area of 150 × 20 mm. As for variant 1, material-specific process parameters were defined to ensure a stable and reproducible processing window. They are listed in Table 5.

Table 5: Processing parameters for variant 2 (BMC + NR/ HNBR)

Parameter	Thermoset (Variant 2)	Elastomer (Variant 2)
Mold temperature [°C]	150	variable
Curing time per mm sample thickness [s]	4.5 – 12	—
Curing time [min]	—	tc_{90} + 3 min
Cylinder temperature (feeding zone / die) [°C]	25 / 30	85 / 85
Injection velocity [$cm^3\ s^{-1}$]	45	8
Maximum injection pressure [bar]	500 – 700	2500
Holding pressure [bar]	300	350
Holding pressure time [s]	0 – 5	90

2.2 Peel Test Setup and Procedure

To evaluate the interfacial adhesion of the produced thermoset–elastomer composites, peel tests were conducted to determine the separation force under peeling stress along the defined interface. All tests were performed on a universal testing machine ZwickRoell Z010 using identical test settings (pre-load: 0.3 N, test speed: 100 mm min^{-1}, clamping length: 40 mm). Depending on the specimen variant, which differs according to the tooling concept, two distinct test setups were applied.

For the 2K specimens made of reinforced phenolic or epoxy molding compounds (variant 1), the peel test was carried out according to the configuration shown in Figure 3. The thermoset substrate was mounted in a freely movable specimen holder, while the rubber strip was clamped in the upper grip and peeled off the thermoset at an angle of approximately 90-110°.

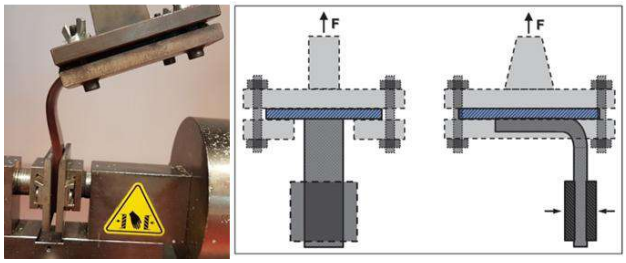

Figure 3: Peel-test device for variant 1 (left: original image, right: schematic representation) [5]

For the specimens manufactured from bulk molding compounds (variant 2), the peel test was performed in accordance with VDI Guideline 2019. As shown in Figure 4, the testing machine was equipped with a dedicated slide table. During testing, the free end of the elastomer layer (2) was pulled at a constant velocity of 100 mm min^{-1} along the tensile axis (1) under a constant peel angle of 90°, which was ensured by a guide pulley (3). The peel force was recorded continuously over the entire specimen length.

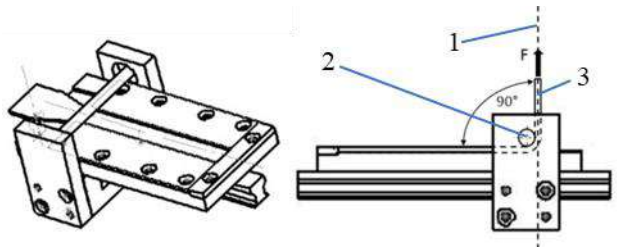

Figure 4: Schematic representation of the peel-test device for variant 2 [9]

The result of each test is a force–displacement curve that allows first conclusions about the adhesion mechanism involved and the type of failure, whether cohesive or adhesive. The peel resistance is calculated as the quotient of the peel force recorded during the test and the width of the rubber strip.

3. Results and Discussion

The following Tables 6 and 7 summarize the peel resistance values reached depending on the isothermal mold- and curing temperature set for the elastomer, several material combinations were studied. The vulcanisation of the NR-based compound was done at 150 °C and 160 °C, while the HNBR-based compound was cured at 160 °C and 180 °C tool temperature.

Table 6: 2K-parts of NR and thermoset at 150 °C and 160 °C rubber mold-/ curing temperature

Thermoset	Peel resistance F-Median [N/mm]	
	150 °C rubber curing temperature	160 °C rubber curing temperature
PF 6507	1.1 ± 0.1	1.4 ± 0.2
PF 6680	1.2 ± 0.2	1.2 ± 0.2
PF 2736	1.3 ± 0.2	1.1 ± 0.1
Supraplast PK 3300	9.8 ± 0.8	10.3 ± 0.5
Epoxidur EP 3585H	1.0 ± 0.2	0.8 ± 0.1
BMC 3102	1.1 ± 0.2	1.3 ± 0.1
BMC L4220	0.9 ± 0.2	1.1 ± 0.2

The results clearly indicate that the formation and strength of interfacial adhesion are predominantly determined by the material combination. For NR combined with the four phenolic molding compounds, distinctly different peel strength values were obtained. The

highest adhesion was measured for the material pairing of NR and Supraplast PK 3300, showing cohesive failure with a certain amount of rubber remaining on the thermoset surface after peeling, as illustrated in Figure 5.

Figure 5: Failure modes in peel tests – left: NR and Bakelite PF 6507 (adhesive failure); right: NR and Supraplast PK 3300 (cohesive failure with rubber residue)

All other tested combinations exhibited significantly lower peel resistance, resulting in adhesive failure characterized by a distinct interfacial phase separation between rubber and thermoset. This observation is consistent with findings from Heyne et al. [7,8], who attributed adhesive failure in comparable thermoset–elastomer systems to insufficient interdiffusion and limited chemical coupling at the interface when curing reactions are not synchronized. Building upon these insights, the present study extends the analysis to new thermoset–rubber material pairings and investigates the influence of process parameters and curing kinetics on interfacial adhesion within a one-step 2K injection molding process. For overlapping process windows, where the surface of the thermoset remains partly chemically reactive before the rubber compound is injected, the mold temperature has to be reduced significantly, to allow slower reaction kinetics of the thermoset.

For the HNBR-based compounds, the highest peel resistance was obtained in combination with PF 6680. Compared to PF 2736, both PF 6507 and Supraplast PK 3300 also exhibited increased bond strength at comparable curing conditions. A further increase of the mold temperature to 180 °C resulted in a general reduction of bonding strength for all investigated material combinations.

Table 7: 2K-parts of HNBR and thermoset at 160 °C and 180 °C rubber mold-/ curing temperature

Thermoset	Peel resistance F-Median [N/mm]	
	160 °C rubber curing temperature	180 °C rubber curing temperature
PF 6507	2.5 ± 0.6	1.8 ± 0.7
PF 6680	13.4 ± 1.9	7.3 ± 1.5
PF 2736	1.0 ± 0.1	1.0 ± 0.1
Supraplast PK 3300	2.7 ± 0.6	2.7 ± 0.6
Epoxidur EP 3585H	0.6 ± 0.0	No adhesion
BMC 3102	2.6 ± 0.2	3.1 ± 0.3
BMC L4220	1.2 ± 0.3	1.4 ± 0.2

In contrast, the epoxy molding compound showed only weak bonding, which completely disappeared at 180 °C mold temperature as a result of the faster epoxy curing reaction and limited interdiffusion across the interface. The overall trend indicates that excessive thermal load during vulcanization reduces adhesion for all combinations, whereas moderate curing temperatures facilitate the temporal overlap of both cross-linking reactions. Although no established threshold values for interfacial adhesion in thermoset–rubber composites exist, the observed peel strengths indicate a wide range of bonding performance. Systems exhibiting cohesive failure can therefore be regarded as indicative of technically relevant interfacial adhesion.

4. Conclusion

The study demonstrates that a wide range of thermoset–rubber material combinations are fundamentally compatible within the one-step 2K injection molding process and are capable of forming interfacial adhesion without additional external adhesion promoters. Bond strength is primarily governed by the material selection, processing conditions, and curing kinetics. The results highlight the high potential of thermoset–elastomer composite systems for technical applications requiring superior thermal and chemical resistance.

Among the investigated combinations, phenolic molding compounds in contact with NR and HNBR achieved the highest peel strengths, including cohesive

failure, whereas epoxy systems showed no measurable bonding. BMC materials exhibited basic but reproducible adhesion with HNBR providing more than twice the peel strength compared to NR. The results suggest that interfacial adhesion may originate from a partial temporal overlap of the curing reactions of both components. Further optimisation by tailored additive systems and process control is expected to enhance adhesion efficiency and facilitate durable, sustainable composite manufacturing for industrial implementation.

5. Acknowledgement

The authors would like to thank the German Aerospace Center (DLR) for the financial support of the project (01IF22604N), which is funded by the Federal Ministry of Economics and Climate Protection (BMWK). In addition, we would like to thank our cooperation partner, the German Institute of Rubber Technology, for the good collaboration.

6. References

1. Lange, C. et al.; Kunststoffe 2001, 12, 36-42.
2. Hopmann, C. et al.; Spritzgießwerkzeuge – Auslegung, Bau, Anwendung; Hanser Verlag, München, 2018, 7th ed.
3. Palik, M.; Vernetzte Präzision – Duroplaste im Automobilbau, Hanser Verlag, München, 2008
4. Diedrich, K. M.; In Proceedings of the ACS Rubber Division Meeting, Savannah, GA, April 29th to May 1st, 2002.
5. Thust, T.; Ph. D. Thesis, Martin-Luther-Universität Halle-Wittenberg, 2014
6. Technical report (IGF-Vorhaben Nr. 20553N); DKG e. V.: Frankfurt am Main, 2021.
7. Heyne, U. et al., Joining Plastics 2015, 9(2), 114-121.
8. Heyne, U. et al., Joining Plastics 2016, 10(1), 40-47.
9. Verein Deutscher Ingenieure (VDI). VDI 2019: Prüfung der Haftung von thermoplastischen Elastomeren (TPE) an Substraten; VDI: Düsseldorf, 2016.

A Mechanical property and thermal stability of natural rubber composite filled with multi-walled carbon nanotubes/carbon black or biochar

Punyarat Jantachum[1], Teeraya Khochai[1], Araya Anlakhon[1], Bualun Khumpaitool[1*]

[1] *Division of Chemistry, Faculty of Science, Udon Thani Rajabhat University, Udon Thani, Thailand.*

*E-mail: Bualan.kh@udru.ac.th

Abstract

In this work, the effects of multi-walled carbon nanotubes (MWCNT) loading, in combination with carbon black (CB) or biochar (BiO), on the swelling, crosslink density, cure characteristics, tensile properties, and thermal stability of natural rubber (NR) composites are studied. Biochar was produced from spent coffee grounds through pyrolysis at 800 °C for 2 h, yielding 29.62% moisture content, 51.40% ash, and 18.98% fixed carbon. NR/MWCNT masterbatches containing 0–3 phr of MWCNT and 20 phr of CB or BiO were prepared using latex compounding and subsequently processed by internal mixing and compression molding at 150 °C. CNT–CB composites exhibited the lowest swelling and the highest crosslink density, attributed to the homogeneous dispersion of MWCNT and CB in the NR matrix. The maximum torque during vulcanization was highest for CNT–CB composites at 3 phr MWCNT, reflecting enhanced crosslink density. Increasing MWCNT content leads to a stronger filler network and restricted rubber chain mobility, which increases the material's resistance to deformation and results in a higher 300% modulus, while the elongation at break decreases due to reduced elasticity. The tensile strength of CNT–CB composites increased by about 1.0% at 2 and 3 phr MWCNT compared to unfilled CNT–CB composites. Thermal analysis further revealed enhanced stability, as Tmax increased from 392 °C (neat NR) to 394–395 °C for CNT–CB composites. In contrast, CNT composites showed moderate improvements, while CNT–BiO composites consistently displayed the lowest performance, suggesting limited reinforcement due to weaker interfacial interactions.

Keywords: Natural rubber, Multi-walled carbon nanotubes, Carbon black, Biochar, Composite

1. Introduction

Natural Rubber (NR) is a highly adaptable elastomer that is renowned for its exceptional elasticity, flexibility, and wear resistance. It is essential in various modern industries, including automotive tires and vibration dampeners. Nevertheless, demanding engineering environments restrict the efficacy of pristine NR due to its poor thermal stability and low tensile strength. To circumvent these constraints, it has become customary to incorporate reinforcing additives into the NR matrix. Carbon-based materials are distinguished by their exceptional capacity to improve composite performance. Carbon black (CB) has been the industry standard for decades, providing robust reinforcement through high surface area and strong particle-matrix interactions [1, 2]. Recently, multi-walled carbon nanotubes (MWCNT) have become the preferred nanofillers due to their intrinsic mechanical strength and ultra-high aspect ratios. This has resulted in significant improvements in modulus and tensile properties at low loadings. However, the commercial application of MWCNT is still hindered by the high production costs and processing challenges that are linked to severe particle agglomeration [3]. Simultaneously, biochar (BiO), a byproduct of biomass pyrolysis, has been suggested as a cost-effective, renewable alternative infill in response to the increasing demand for sustainability [4]. Research suggests that biochar can partially replace CB or function as a solitary infill, offering moderate mechanical enhancement and exceptional thermal stability in comparison to pristine NR. In particular, the incorporation of spent coffee ground (SCG) biochar into polymer matrices has been shown to significantly enhance mechanical characteristics, including modulus, stiffness, and tensile strength. The

optimal performance is typically achieved at loading rates between 20% and 24% by weight [5]. This reinforcement is predominantly fueled by the abundant presence of oxygenated surface functional groups (-COOH, phenolic, -OH) and elemental carbon in SCG biochar. Nevertheless, the ultimate efficiency of biochar is extremely dependent on the processing parameters, as the vital filler-matrix interaction is significantly influenced by particle size and surface chemistry [6]. In addition, SCG biochar can inadvertently compromise the stability of certain polymers (such as PLA) by acting as a degradation catalyst, despite the fact that it generally improves the thermal stability and fire resistance of composites by restricting oxygen transport [7]. Nevertheless, a substantial research gap continues to exist in relation to the interaction between these distinct carbon replacements when they are combined, despite these insights. MWCNT, CB, and SCG biochar are well-documented for their individual benefits; however, their collective behavior in hybrid systems within an NR matrix is systematically dismissed. This study evaluates and compares two distinct hybrid filler strategies: an effective industrial system (MWCNT/CB) and a sustainable, waste-derived system (MWCNT/ biochar) to resolve this disparity. The scientific justification for selecting these particular hybrid architectures is based on a synergistic mechanism. Spherical CB particles or porous, irregular SCG biochar particles can function as physical separators to prevent the entanglement and bundling of MWCNT. In turn, the high-aspect-ratio MWCNT bridge the crevices between the larger carbon particles, establishing a continuous, hierarchical filler network that optimizes stress transfer at substantially reduced MWCNT loadings [8, 9]. This research identifies the impact of filler geometry and surface chemistry, specifically the highly functionalized, polar surface of biochar versus the relatively inert surface of traditional CB on the formation of hybrid networks and interfacial bonding with the non-polar NR matrix by directly comparing CB and biochar alongside MWCNTs. Nevertheless, there is a significant research gap in the systematic evaluation of the synergistic effects of hybrid systems that incorporate the high efficiency of MWCNT with the demonstrated performance of CB or the sustainable potential of biochar.

This research has focused on the mechanical properties and thermal stability of NR filled with MWCNT (CNT), NR filled with MWCNT and CB (CNT-CB), and NR filled with MWCNT and biochar (CNT-BiO) composites.

2. Experimental

2.1 Materials

High ammonia natural rubber (60%DRC) was purchased from GSP product Co., Ltd. (Bangkok, Thailand). The spent coffee ground (SCG), obtained from local coffee shops in Udon Thani (Thailand). Tergitol-15-S-15 was purchased from East Asiatic Company (Bangkok, Thailand). MWCNT (Diameter: 1.2 nm, Length: 5-30 μm) and CB (N330) were purchased from Thai Carbon Product Co. Ltd. (Bangkok, Thailand). Curing agents including zinc oxide (ZnO), stearic acid, N-cyclohexylbenzothiazole-2-sulfenamide (CBS), N-(1,3-Dimethylbutyl)-N-phenyl-p-phenylenediamine (6-PPD) and sulfur were purchased from GSP Products Co., Ltd. (Bangkok, Thailand).

2.2 Methods

2.2.1 Preparation of BiO from spent coffee grounds

The BiO was produced from spent coffee grounds (SCG) by drying the raw material at 80 °C for 24 hours. 50 g of SCG was prepared through slow pyrolysis in a chamber furnace. The heating rate was set to 5–10°C per minute. The BiO was produced at a pyrolysis temperature of 800 °C for 2 hours to get a BiO. The SEM image of BiO was shown in Figure 1, which showed the size of BiO about 60-120 μm.

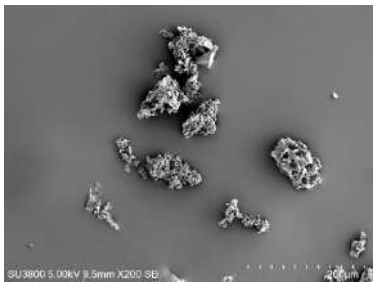

Figure 1. SEM image of biochar

2.2.2 Preparation of NR/MWCNT masterbatchs

Sufactant was added in NR latex under continuous stirr at room temperature for 1 h. Then, MWCNT at 0.5, 1, 2 and 3 parts per hundred rubber (phr) were added to NR latex (100 phr) under continuous stirr for 30 min. After that, the mixture was sonicated at 20 kHz in an ultrasonic bath at room temperature for 30 min. The mixture was poured onto a glass plate and dried at room temperature. Then, the NR/MWCNT masterbatch was dried at 60 ºC for 24 h.

2.2.3 Preparation of CNT, CNT-CB, CNT-BiO composites

Formulations of CNT, CNT-CB, CNT-BiO composites are shown in Table 1. The amounts of MWCNT were varied from 0 to 3 phr, while the content of CB or BiO was kept constant at 20 phr. The amounts of other rubber chemicals were identical for all formulations. The rubber compounds were mixed in an internal mixer at 70 ºC and a rotor speed of 15 rpm. The mixing time of all rubber compounds was kept constant at 15 min. Then, the specimens were shaped at 150 ºC by using compression molding.

Table 1. Formulation of rubber composites

Ingredients	Amount (phr)		
	CNT	CNT-CB	CNT-BiO
NR/ MWCNT	masterbatch from Section 2.2.2		
CB	-	20	-
BiO	-	-	20
ZnO	5	5	5
Stearic acid	2	2	2
6PPD	1	1	1
CBS	1	1	1
Sulfur	2	2	2

2.3 Characterizations

The moisture content of biochar was calculated by weighing approximately 1 g of biochar, transferring it to a porcelain crucible, and placing it in an oven heated to 105 ± 5 ºC for 24 hours. Volatile matter was determined by subjecting the residual material to a muffle furnace that heated to 900 ± 10 ºC for 6 minutes and weighing it. The residual material was subjected to a temperature of 750 °C in the muffle furnace for a duration of 6 hours to ascertain the ash content in accordance with ASTM D1762. The equation 1 determined the fixed carbon content:

Fixed carbon = 100-(moisture+volatile matter+ash content) (1)

Morphology of biochar were observed using scanning electron microscopy (SEM; HITACHI MODEL SU3800) at a 5 kV accelerating voltage. Before testing, the sample was coated with a thin film of gold to prevent charging on the surface.

The rubber vulcanizate for swelling and crosslink density test were cut into 10 × 10 × 2 mm^3 pieces and weighed (w_1) with an electronic balance. Then, the rubbers were submerged in 100 ml of toluene for 7 days at room temperature. After that, the swelled rubbers were taken from the solvent and excess solvent was cleaned off its surface, and weighed (w_2) with an electronic balance. The following equation was used to determine the % swelling.

$$\text{Swelling}(\%) = \left(\frac{w_2 - w_1}{w_1}\right) \times 100 \quad (2)$$

The crosslink density (V_e), was calculated by using the Flory–Rehner equation [10].

$$V_e = -\frac{\left[\ln(1 - V_r) + V_r + \chi_1 V_r^2\right]}{V_1\left[V^{1/3} - (V_r/2)\right]} \quad (3)$$

where V_1 is molecular volume of the solvent (106.2). χ is the Flory‑Huggins interaction parameter between toluene and rubber (0.397). V_r is the volume fraction of polymer in the swelling rubber in pure solvent.

Tensile properties were measured using an Instron universal tester (Instron/3366) with a crosshead speed of 500 mm/min, in accordance with ASTM D412. The results of tensile properties were revealed in terms of the 300% modulus, %elongation at break and tensile strength. The study involved testing a total of five samples.

Thermal stability of the composites was analyzed using a thermogravimetric analyzer. A 10 mg sample was placed on a platinum pan and heated from 40 to 600 ºC in a nitrogen atmosphere before switching to an oxygen atmosphere at 800 ºC at the same heating rate of 20 ºC /min.

3. Results and discussions

3.1 Proximate analysis of BiO

BiO from spent coffee ground was successfully prepared by using pyrolysis process. The moisture content, ash content and fixed carbon of BiO were 29.62%, 51.40%, and 18.98%, respectively.

3.2 Swelling and crosslink density

Figure 2 shows the % Swelling of all composites. It was found that the % swelling of CNT, CNT-CB, and CNT-BiO composites tends to increase with increasing MWCNT content up to 1 phr and then decrease with increasing MWCNT content. This may be due to solvents cannot penetrate rubber chains because they are restricted by a cross-linked network formed during vulcanization and the agglomeration of MWCNT [11]. In addition, CNT-BiO composites show the highest % swelling. This is due to the large agglomerate of BiO reducing reinforcement efficiency and may affect the swelling performance of the composite. Moreover, the addition of CB has a lower % swelling in the composites because of better dispersion and interaction with natural rubber than CNT and CNT-BiO composites [12]. Crosslink density of the composites in Fig. 3 tends to decrease with increasing MWCNT content, which is the result related to % swelling of the composites.

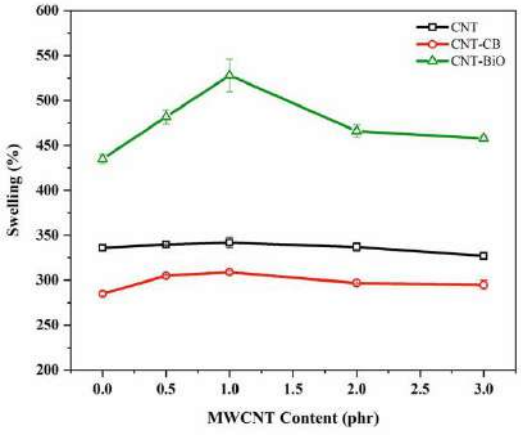

Figure 2. % Swelling of CNT, CNT-CB and CNT-BiO composites

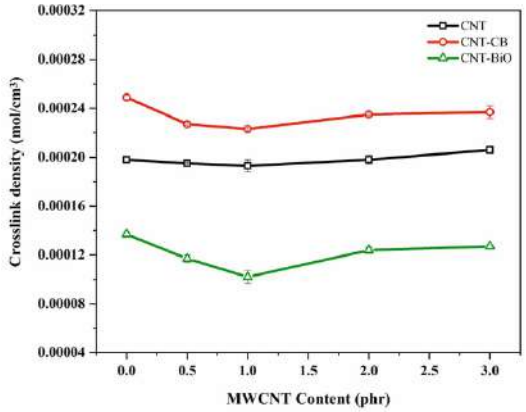

Figure 3. Crosslink density of CNT, CNT-CB and CNT-BiO composites

3.3 Cure characteristics

CNT, CNT-CB, and CNT-BiO composites are shown in Table 2. It was found that the scorch and cure times of all composites tend to increase with increasing MWCNT content. These results indicate that the adsorption of accelerators on MWCNT surfaces increased with the MWCNT content, resulting in a slower vulcanization process [13]. Moreover, delta torque values of the CNT-CB composites are higher than those of the CNT and CNT-BiO composites, respectively. A possible explanation for the increase is that CB particles help overcome the tendency of MWCNT to agglomerate, creating a more uniform and stable network [14]. In contrast, BiO particles may not provide the same level of reinforcement to MWCNT, leading to a decrease in the stiffness of the vulcanized compounds.

Table 2. Cure characteristics of rubber composites

Cure Properties	CNT				
	0 phr	0.5 phr	1 phr	2 phr	3 phr
M_H (dN.m)	7.1	6.4	6.5	6.9	7.4
M_L (dN.m)	0.7	1.4	1.5	1.5	1.5
M_H - M_L (dN.m)	6.4	4.9	4.9	5.4	5.9
T_{s2} (min)	2.2	2.3	2.7	2.6	2.5
T_{c90} (min)	5.0	5.5	5.4	5.5	5.5
	CNT-CB				
	0 phr	0.5 phr	1 phr	2 phr	3 phr
M_H (dN.m)	9.1	8.1	8.3	8.9	9.1
M_L (dN.m)	1.1	1.8	1.8	1.8	1.8
M_H - M_L (dN.m)	8.1	6.3	6.5	7.2	7.4
T_{s2} (min)	1.9	2.1	2.1	2.2	2.2
T_{c90} (min)	5.2	5.6	5.5	5.7	6.0
	CNT-BiO				
	0 phr	0.5 phr	1 phr	2 phr	3 phr
M_H (dN.m)	7.2	5.9	5.6	6.6	6.7
M_L (dN.m)	1.0	1.6	1.7	1.5	1.4
M_H - M_L (dN.m)	6.1	4.3	3.9	5.2	5.3
T_{s2} (min)	1.7	2.6	2.9	2.3	2.4
T_{c90} (min)	4.3	5.5	5.9	5.3	6.0

3.4 Tensile properties

The tensile properties of NR composites filled with MWCNT (CNT), MWCNT–CB (CNT–CB), and MWCNT–BiO (CNT–BiO) show that the CNT–CB system provides the most effective reinforcement. Figure 4 shows the 300% modulus of CNT–CB composites increases steadily with MWCNT loading, reaching about 7 MPa at 3 phr, which is higher than CNT and CNT–BiO composites. The tensile strength of CNT–CB in Fig. 5 also remains the highest, around 25–30 MPa, compared to 20–25 MPa for CNT and only 12–16 MPa for CNT–BiO, indicating a strong synergistic effect between CB and MWCNT that enhances stress transfer and network formation [15]. However, the %elongation at break of all composites in Fig. 6 shows that CNT–CB composites have the lowest elongation at break (~600%), while CNT composites have the highest (~700–750%), and CNT–BiO composites exhibit intermediate flexibility (~650–700%).

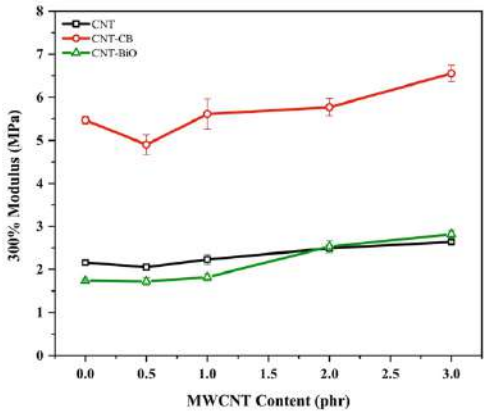

Figure 4. 300% Modulus of the composites

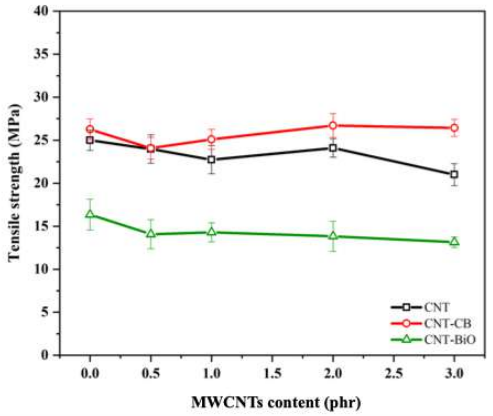

Figure 5. Tensile strength of the composites

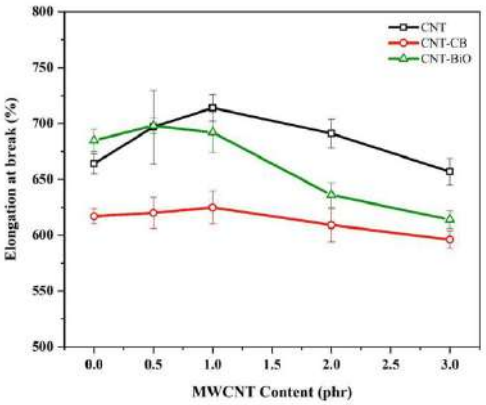

Figure 6. %Elongation at break of the composites

3.5 Thermal stability

Figure 7 shows all NR composites exhibit similar thermal degradation behavior, characterized by a single major weight-loss step between approximately 300–450 °C, which corresponds to the decomposition of the NR matrix [10]. In comparison to neat NR, the thermal stability was marginally enhanced by the incorporation of MWCNT, or when combined with CB or BiO, as demonstrated by a slight increase in the onset and maximal

degradation temperatures. From the samples, the CNT–CB composites exhibited the most improvement in thermal resistance, suggesting that the synergistic interaction between MWCNT and CB formed a more compact filler network that acted as a barrier to heat and volatile diffusion [15]. In comparison to CNT and CNT–CB systems, the CNT–BiO composites also demonstrated a small rise in stability and a slightly higher char residual at 700–800 °C. This was due to the inherently carbonaceous nature of BiO, which promotes char formation and reduces total mass loss [12]. Meanwhile, the CNT composites showed a moderate improvement in degradation temperature but had less residual mass. Thermal properties of CNT, CNT-CB, CNT-BiO composites were shown in Table 3.

Table 3. Thermal properties of CNT, CNT-CB, CNT-BiO composites

Thermal properties	CNT				
	0 phr	0.5 phr	1 phr	2 phr	3 phr
$T_{5\%}$ (°C)	262	265	265	266	266
T_{max} (°C)	390	391	392	393	393
% Residue	5.39	5.52	5.60	5.41	5.41
	CNT-CB				
	0 phr	0.5 phr	1 phr	2 phr	3 phr
$T_{5\%}$ (°C)	262	265	266	266	267
T_{max} (°C)	393	394	394	393	395
% Residue	4.18	4.58	4.50	4.60	4.47
	CNT-BiO				
	0 phr	0.5 phr	1 phr	2 phr	3 phr
$T_{5\%}$ (°C)	262	277	279	279	280
T_{max} (°C)	390	392	393	394	393
% Residue	4.07	4.48	4.52	4.61	4.62

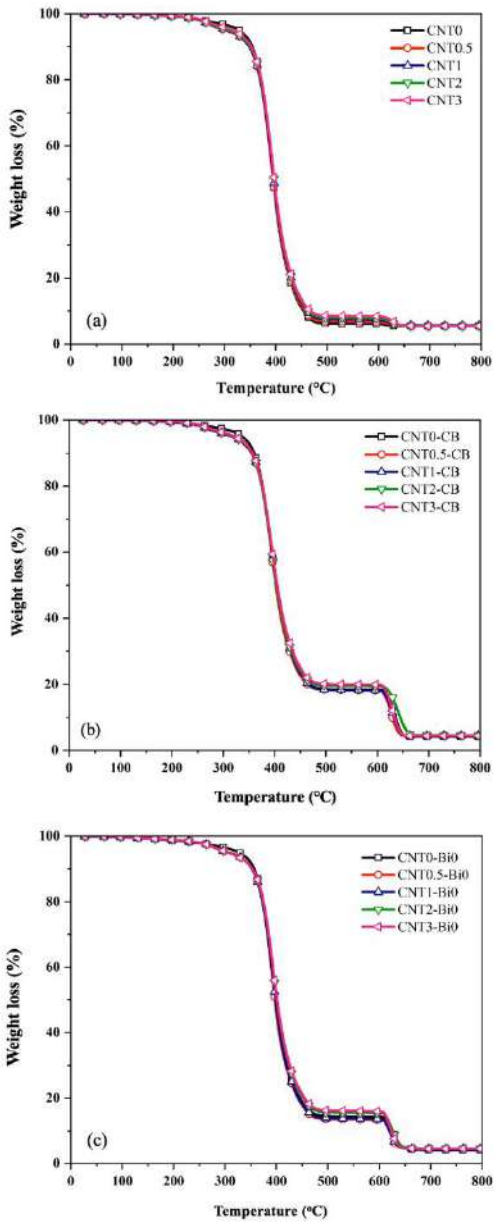

Figure 7. TGA thermograms of (a) CNT (b) CNT-CB and (c) CNT-BiO composites

4. Conclusion

In summary, incorporating 2–3 phr MWCNT into NR/CB composites enhanced tensile strength, modulus, and thermal stability, confirming a synergistic effect between MWCNT and CB. While CNT composites offered only moderate reinforcement and CNT–BiO composites exhibited limited improvements, the hybrid CNT–CB system proved most effective, demonstrating its potential for the development of advanced rubber composites.

5. Acknowledgment

The authors gratefully acknowledge the financial support from Research and development Institue of Udon Thani Rajabhat University. The instruments and facilities provided for this study from the Faculty of Science, Udon Thani Rajabhat University are very much appreciated.

6. References

1. Tong, H.; Kabeb, S. M.; Hamid, A. H.; Zulkifli, F. *Int. J. Biol. Macromol.* **2025**, 318, 144973.
2. Rattanasom, N.; Saowapark, T.; Deeprasertkul, C. *J. Appl. Polym. Sci.* **2018**, 135, 46603.
3. Guo, X.; Guo, S.; Liu, G.; Bai, L.; Liu, H.; Xu, Y.; Zhao, J.; Chai, H.; Jian, X.; Guo, L.; Liu, F. *Polymers.* **2023**, 15 (3), 477.
4. Zhang, Y.; Chen, H.; Wang, C.; Zhou, X.; Yang, H.; Wang, X.; Chen, H. *Compos. Part B Eng.* **2023**, 255, 110638.
5. Kang, J.; Li, C.; Kim, H.; Park, S. *Polymers*. **2020**, 12 (7), 1542.
6. Gomes, T. S.; Garcia, M. T.; Oliveira, A. D.; Marcondes, A. F.; Marconcini, J. M. *J. Polym. Environ.* **2023**, 31, 2288–2299.
7. Zhang, Q.; Wu, W.; Li, L.; Zhao, Y.; Wu, J.; Qiu, R.; Zhang, M. *Polym. Degrad. Stab.* **2019**, 161, 118–126.
8. Afolabi, O.A.; Ndou, N. *Polymer*. **2024**, 16, 1907.
9. Ali H.; Ali S.; Ali K.; Ullah S.; Ismail P.M. *Results Eng.* **2025**, 27, 106151.
10. nanocomposite materials—A review, Polymers 16 (2024) 1907
11. Jantachum, P.; Khumpaitool, B.; Utara, S.; *Ind. Crop. Prod.* **2023**, 195, 116407.
12. Mohamad, N.; Hassan, A.; Mohd Ishak, Z. A. *Polymers.* **2022**, 14 (3), 415.
13. Wang, Z.; Zhang, J.; Li, H.; Guo, B. *Compos. Part B Eng.* **2021**, 223, 109128.
14. Das, A.; Stöckelhuber, K. W.; Jurk, R.; Fritzsche, J.; Klüppel, M.; Heinrich, G. *Polymer*. **2016**, 98, 160–170.
15. Ibrahim, M. N.; Ismail, H.; Pasbakhsh, P.; Ahmad, Z.; Shuib, R. K. *Polym. Bull*. **2020**, 77, 6319–6332.
16. Ghosh, S.; Das, A.; Stöckelhuber, K. W.; Klüppel, M.; Heinrich, G. *Eur. Polym. J.* **2018**, 99, 262–272.
17. Das, A.; Jurk, R.; Stöckelhuber, K. W.; Wießner, S.; Heinrich, G. *Compos. Sci. Technol.* **2017**, 142, 126–134.

Multidimensional rubber composite utilizing lignin as a bio-filler

Amit Kumar Sen[*1,2], Amit Das[3], Biswanath Guria[1], Abhisek Brata Ghosh[1], Jagannath Chanda[1], Prasenjit Ghosh[1], Rabindra Mukhopadhyay[1]

[1]*Hari Shankar Singhania Elastomer and Tyre Research Institute, Mysore, India*

[3]*Leibniz-Institut für Polymerforschung Dresden e.V., Dresden, Germany*

E-mail: amit.sen@jkmail.com

Abstract

The rubber industry's reliance on petroleum-based filler materials significantly contributes to CO_2 emissions and resource depletion, posing a substantial hindrance to sustainability and the circular economy. Consequently, the industry is exploring bio-based alternatives that maintain performance while reducing environmental impact. Lignin, a renewable, aromatic polymer derived from lignocellulosic biomass, is a promising candidate. Its abundance, high carbon content, renewability, antioxidant and mechanical properties make lignin an attractive resource for rubber reinforcement. However, current lignin incorporation methods are often energy-intensive and rely on unsustainable chemicals and processes, limiting industrial adoption. Also, the incorporation of lignin into rubber poses processing challenges, primarily due to its limited compatibility with the rubber matrix. Its inherent polarity and strong self-interactions result in poor dispersion and weak interfacial adhesion, adversely affecting the performance properties of the compound. This research aims to overcome these barriers by developing a novel approach to integrate lignin nanoparticles into rubber composites. A controlled liquid phase mixing technology enables us to seamlessly incorporate 20-30 phr of lignin without sacrificing major mechanical properties. With an 11% higher bio-material content, a 17% higher elongation at break, and a 12% benefit at tanδ@70 °C, a significant improvement in lignin dispersion was achieved. The effective interaction of lignin-rubber alleviates the potential issues related to lignin utilization in terms of volume and application areas, thereby promoting lignin on a multidimensional scale and guiding the industry toward sustainability and an environmentally conscious model.

Keywords: Sustainability and Circular economy, scalable lignin-rubber production, eco-friendly material

1. Introduction

The growing concern for environmental sustainability has driven industries to seek alternatives to non-renewable materials. The research into bio-based composites and their potential applications is also accelerating due to their economic and environmental benefits. One such material is lignin, a natural polymer derived from the lignocellulosic biomass of plants, which has gained attention as a potential filler in rubber composites, including tyre manufacturing. Traditionally, carbon black and silica are the primary fillers used in tyre compounds due to their reinforcing properties. However, both these materials are derived from non-renewable resources, and their production processes have significant environmental impacts. Thus, the use of lignin as a filler offers a renewable and potentially cost-effective alternative, aligning with the increasing demand for sustainable materials in the

automotive industry. Lignin exhibits several unique characteristics, including excellent mechanical, physicochemical, and biodegradable properties, as well as antioxidant capabilities and superior thermal stability. However, incorporating lignin into a rubber matrix is challenging due to its molecular polarity, which leads to strong self-interactions; consequently, the lack of compatibility between lignin and rubber poses difficulties in achieving optimal composite properties. Several studies [1-4] have been published to improve the performance of lignin-based rubber composites. The integration of lignin into rubber composites has attracted significant interest in both academia and industry, leading to a growing number of patents that cover various aspects of lignin-rubber composite development. Patents (US8664305B2[5], and WO2023089508A1[6]) filed by a leading tyre manufacturer revealed that the lignin-based rubber composites reduce the environmental impact of tyre production as well as enhance the fuel efficiency of vehicles due to the lower rolling resistance of the lignin-filled tyres.

Despite significant advancements, challenges persist in effectively utilizing lignin as a filler in rubber composites. Poor dispersion within the rubber matrix and inherent incompatibility with hydrophobic rubber remain key obstacles. The incorporation of lignin into rubber poses processing challenges, primarily due to its limited compatibility with the rubber matrix. Its inherent polarity and strong self-interactions result in poor dispersion and weak interfacial adhesion, adversely affecting the viscosity and flow behaviour of the compound. Lignin, being hydrophilic due to its abundant hydroxyl groups, tends to form agglomerates when mixed with hydrophobic rubbers, resulting in poor dispersion and weak interfacial adhesion. This study focuses on enhancing the dispersion of lignin nanoparticles through latex-phase mixing, which not only leads to appreciable improvement in composite properties but also enables rubber compound designers to substantially elevate the sustainability quotient without compromising performance-related attributes.

2. Experimental

2.1 Materials

All the mixing ingredients were used as obtained. Natural rubber [NR] (SMR 20; from JK Industries Ltd., India), Nd-BR with 96 % cis content was supplied by Reliance Industries Ltd., India. Other ingredients used for compound preparation were N660 carbon black (Birla Carbon, India), zinc oxide (RK Industries, India), stearic acid (Godrej Soap Ltd., India), polymerised 2,2,4-trimethyl-1,2-dihydroquinoline (TMQ; Nocil, India), N-phenyl-N'-(1,3-dimethylbutyl) p-phenylene-diamine (6PPD; Nocil, India), microcrystalline wax (Raj Petro, India), oil of low polycyclic aromatic (PCA) grade (Raj Petro, India), soluble sulphur (Jain Chemicals Ltd., India), N-tert-butyl-2-benzothiazole sulfenamide (TBBS; Merchem, India) and N-(cyclohexylthio) phthalimide (CTP; Nocil, India). Lignin powder and lignin liquor were supplied by JK Paper, India.

2.2 Masterbatch preparation

Method 1: A pre-weighted amount of lignin powder is dissolved in Sodium hydroxide (NaOH) solution, and the resultant is added to the NR latex. The mixture is coagulated with 1% Formic acid (HCOOH), dried in a hot air oven, reducing the final moisture content to less than 6.5% [designated as Wet lignin-NR masterbatch and used in the formulation T2-Wet]. The resulting masterbatch contains 33.3% of lignin filler.

Method 2: This involves introducing 500 ml lignin liquor into 1 litre of NR latex, and subsequently adding 1% formic acid. The resulting sediment is dried in a hot air oven, reducing the final moisture content to less than 6.5% [designated as Liquor lignin-NR

masterbatch and used in the formulation T3-Liq]. The resulting masterbatch contains 33.3% of filler particles.

2.3 Formulation

Table 1: Detailed formulation of the compounds

Ingredients (phr) [a]	**REF. [b]**	**T1-Dry**	**T2-Wet**	**T3-Liq**
NR	40	→	-	-
BR	60	→	→	→
Powder lignin [c]	-	20	-	-
Wet lignin-NR masterbatch	-	-	60	-
Liquor lignin-NR masterbatch	-	-	-	60
GPF carbon black (CB)	45	25	25	25
Sulphur: Accelerator	1: 0.4	→	→	→

a - phr, parts per hundred rubber by weight; [b] REF-reference compound and [c] - with 6% moisture

All formulations contain (in phr): Activators – 4.0, AO – 5.0, Process aids – 5.0, and PVI – 0.1.

2.4 Mixing

Table 2: Mixing sequence in the non-productive and productive stages

Time (S)	Temperature (°C)	Actions
Non-productive batch (Master)		
0	60±2	Add rubbers/ masterbatch
25	65±3	Add CB + chemicals
110	115±4	Ram sweep
220	125±3	Ram sweep
330	135±2	Dump
Productive batch (Final)		
0	55±1	Master + curative package
90	75±2	Ram sweep
180	97±2	Dump

3. Results and Discussion

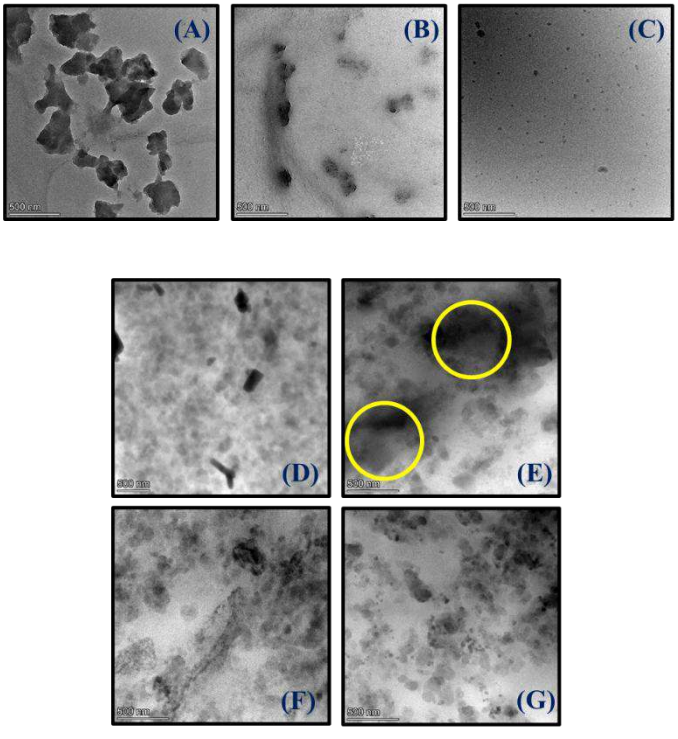

Figure 1: Transmission Electron Microscope [TEM] images of (A) powder lignin, (B) lignin powder dissolved in NaOH, (C) lignin liquor, (D) REF., (E) T1-Dry, (F) T2-Wet, and (G) T3-Liq.

The surface morphology of the raw fillers, as well as the dispersion of the same into the rubber matrix, was observed using a TEM (Talos-200S, ThermoFisher Scientific, USA). The thin specimens of the rubber composites used in TEM analysis were prepared with the aid of an ultramicrotome (Leica Ultracut UC, Leica, Germany) at (-) 70°C and a specimen thickness of 100 nm. TEM images for powder lignin show the presence of lignin chunks in a highly agglomerated stage (Figure 1A). Subsequently, improper lignin dispersion was observed in the compound T1-Dry (Figure 1E - yellow circle highlights the dark patches, which are the agglomeration of lignin). Agglomeration tendency can still be observed, as evident from Figure 1B when lignin is dissolved in NaOH, but an improved suspension of lignocellulose was observed in the liquor lignin. Overall filler dispersion of filler particles in the matrix is improved when compared to T1-Dry, but a large amount of void space (Figures 1F and 1G) indicates that much work needs to be done to obtain the optimum filler dispersion in the matrices.

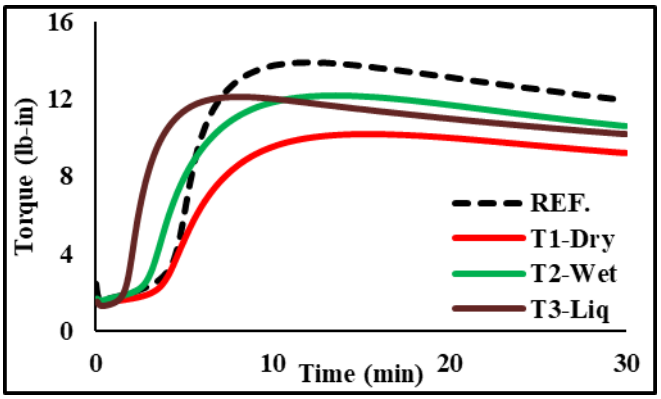

(A)

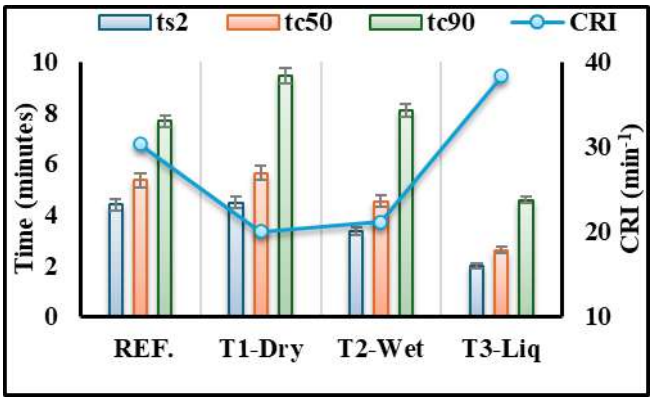

(B)

Figure 2: (A) Rheometer curve, and (B) scorch time (ts2), 50% & 90% cure (tc50 & tc90), and cure rate index (CRI) of the compounds

The curing characteristics were evaluated by utilising a Moving Die Rheometer [MDR] (Premier MDR, Alpha Technologies, USA) according to the ASTM D5289 method at 160°C for 30 minutes with a frequency of 1.67 Hz. The rheometric curve (Figure 2A) reveals that the maximum torque (M_H) is lower for all lignin compounds, although the lignin masterbatches showed higher M_H than the dry lignin compound. This could be due to the higher cross-link density, where the presence of various metal salts boosts the vulcalization reaction (7,8). Also, it is well known that a basic medium boosts the curing efficiency. The presence of alkali metal salts in untreated quantities and quality in T3-Liq may accelerate the cure rate. The same reason may also hold for the reduction of scorch time (ts2), time taken for 50% and 90% cure (tc50 and tc90, respectively). T3-Liq showed the maximum CRI among all. Presence of abundant soluble salts of potassium, chlorine, calcium, aluminium, silicon and iron could affect the rheological properties.

The tensile strength at room temperature was tested using a universal testing machine (UTM, Zwick/Roell-Z010 with a 1kN force transducer, Ulm, Germany) according to ASTM D412 standards. An optical extensometer was used as an attachment for

measuring strain. Tests were performed with a crosshead speed of 500 mm/min and a gauge length of 25 mm. Stress-strain properties of the compounds are shown in Figure 3A. Trial compounds with lignin have a lower modulus than the reference. T1-Dry compound has the lowest tensile strength among all. For lignin masterbatch compounds, an improvement over T1-Dry was observed. This indicates better load transfer between filler and polymer chain, resulting in higher modulus and especially tensile strength for them. Aged mechanical properties are much improved for T3-Liq. Liquor lignin may contain a much higher amount of hydroxyl (-OH) groups along with other metal salts,

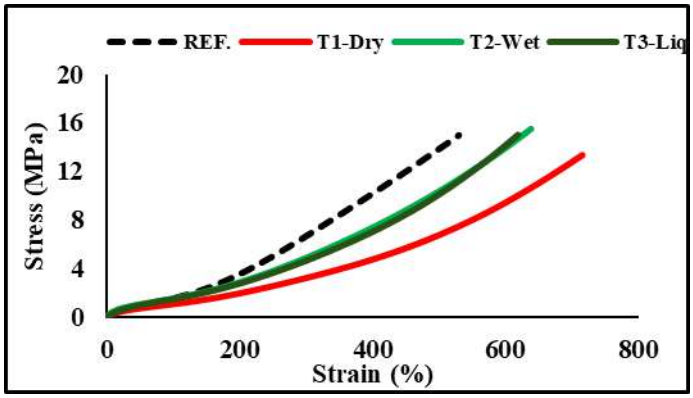

which could subsequently react readily with radical oxygen (O.) and thus exhibit better anti-oxidant properties.

(A)

(B)

Figure 3: (A) S-S curve for the compounds, and (B) changes in the unaged and aged mechanical properties

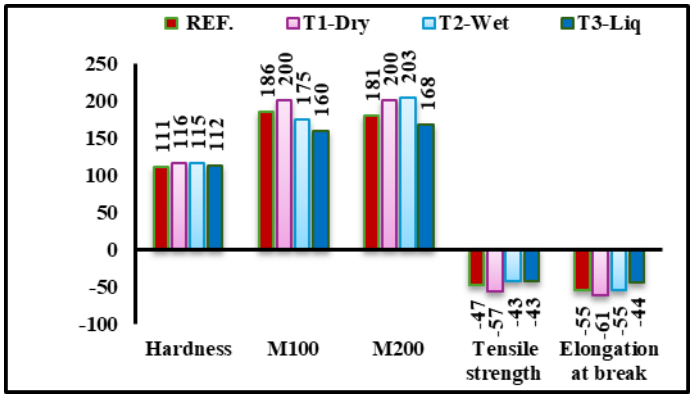

Dynamic mechanical analysis (DMA) testing was conducted with a Metravib DMA+2000, Limonest, France. The test utilised a 5% dynamic strain, 1% static strain, and an 11 Hz frequency in tension-compression

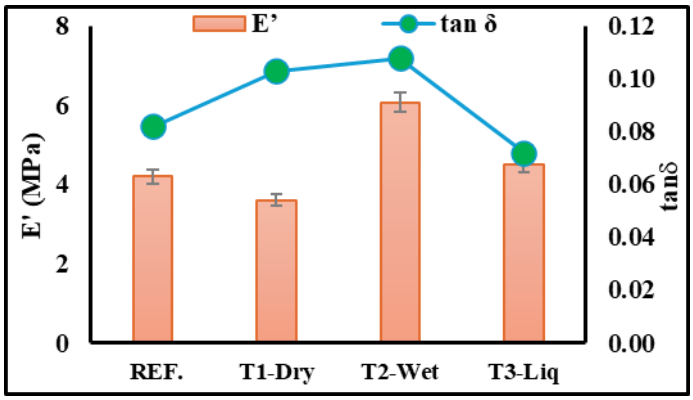

Figure 4: DMA properties of the compounds

and stabilised temperature mode with sample thicknesses of 2.5 ± 0.2 mm. Storage modulus (E'), loss modulus (E''), and tan delta (tanδ) at 70°C are recorded. The superior hysteresis (Figure 4) for T3-Liq could be due to the better dispersion of the filler particle, and also due to the better antioxidant effect of lignin liquor. An antioxidant effectively preserves the integrity and density of the crosslink network, which leads to improved hysteresis properties.

4. Conclusion

A future towards green compound development necessitates the use of bio-based fillers that can be customised as per the developer's requirement. The present work uses the common, widely available, waste & bio-based lignin liquor present in the world. The materials used in this work are cheaper without any toxic effects on humans and the environment. A better ageing resistance, along with a reduced tanδ@70°C, shows the potential to use lignin liquor in a rubber compound without any further treatment. Rheological and mechanical properties require further optimisation before implementation. Moreover, ensuring the consistent availability of high-

quality lignin liquor remains a challenge. The use of simple and conventional manufacturing procedures without requiring any modifications to existing processing techniques, and the broad availability of both materials, make the work more attractive and sustainable.

5. Acknowledgement

The authors sincerely thank Hari Shankar Singhania Elastomer and Tyre Research Institute (HASETRI), Mysore, for their technical support, research facilities, and financial support, and to the conference organizing committee for this opportunity to contribute to balancing nature and innovation for a sustainable future.

6. References

1. Luzi, F.; Torre, L.; Puglia, D. *Micro and Nanolignin in Aqueous Dispersions and Polymers.* **2022**, *1*, 293
2. Sethulekshmi, A. S.; Saritha, A.; Joseph, K. *International Journal of Biological Macromolecules.* **2022**, *194*, 819.
3. Hait, S.; Kumar, L.; Jyotirmaya Ijaradar; Anik Kumar Ghosh; De, D.; Chanda, J.; Ghosh, P.; Saikat Das Gupta; Mukhopadhyay, R.; Sven Wießner; Heinrich, G.; Das, A. *Journal of Cleaner Production.* **2024**, *1*, 143274.
4. Khan, A.; Kian, L. K.; Jawaid, M.; Khan, A. A. P.; Marwani, H. M.; Alotaibi, M. M.; Asiri, A. M. *International Journal of Biological Macromolecules* **2022**, *206*, 363–370.
5. Andrew, D.; Bruce B.; Hahn R.; Paul M.; Shawn C.; Dirk M.; Cicotte K. N.; U.S. Patent 8664305B2, January 8, 2010.
6. Tadiello, L.; Giannini,L.; Guerra S.; WO2023089508A1, November 17, 2022.
7. Chen, S.; Xu, Y.; Guo, K.; Yue, X. *Scientific Reports*, **2023,** *13(1)*, 2400.
8. Cardoso, M.; Domingos, E.; Passos, M, *Fuel*, **2009**, *88(4)*, 756

Natural Rubber, Bio-based Rubbers and Rubber Chemicals

IRC 2025
BANGKOK, THAILAND

International Rubber Conference 2025 (IRC 2025)

Degradation Trends in Plasticity and Viscosity of Selected Standard Philippine Rubber Under Prolonged Storage

Shadam Suganob, Ruben M Lim Jr, Rosemarie S. Salazar

Department of Science and Technology – Region IX, Zamboanga City, Philippines

E-mail: suganobshadam@gmail.com, rubenjr1005@gmail.com, rosemarie.salazar@ro9.dost.gov.ph

Abstract

The mechanical stability of Standard Philippine Rubber (SPR) during storage is essential for maintaining consistent processing quality. This study evaluated changes in Mooney viscosity, initial plasticity, and plasticity retention index (PRI) of three SPR grades—SPR 20, SPR 5, and SPR L—stored under ambient conditions for 40 weeks. Weekly measurements were conducted following ISO 289-1, ISO 2007, and ISO 2930 test methods.

Natural rubber typically undergoes storage hardening, reflected in increasing viscosity and plasticity due to gradual structural reorganization and slow crosslinking reactions. In contrast, PRI decreases over time as oxidative degradation progresses. These patterns were observed in all three grades.

Analysis of Covariance (ANCOVA) was applied to assess whether rates of change differed among grades. Mooney viscosity and initial plasticity showed significant increases with storage time, while PRI declined steadily. The Grade × Week interaction was not significant for Mooney viscosity ($p = 0.306$) and initial plasticity ($p = 0.068$), indicating similar hardening rates among the grades. For PRI, the interaction was borderline ($F = 3.086$, $p = 0.050$), suggesting only minimal differences in oxidative degradation slopes.

Overall, the results indicate that SPR grades exhibit broadly comparable degradation trajectories, differing primarily in initial property levels rather than in their rates of change. Future studies should examine environmental influences and stabilization strategies to refine shelf-life assessments for Standard Philippine Rubber.

Keywords: Philippine rubber, Plasticity, Viscosity, Long-term storage, Mechanical properties

1. Introduction

Natural rubber (NR) is one of the most essential polymers in modern industry, serving as a critical raw material for products such as medical gloves, pacifiers, aircraft and automotive tires, elastic components, and numerous consumer goods. Derived principally from Hevea brasiliensis latex, NR is a complex colloidal system composed of *cis*-1,4-polyisoprene, proteins, lipids, carbohydrates, and inorganic constituents [1]. Its molecular architecture and associated non-rubber components confer NR with outstanding tensile strength, elasticity, fatigue resistance, flexibility, and effective electrical insulation [2].

Despite its favorable properties, NR undergoes characteristic physical changes during storage. One of the most documented phenomena is storage hardening, in which the material progressively increases in viscosity and stiffness over time [3][5]. This transformation is attributed to an increase in the gel content of the rubber, which develops during aging, and is formed by two distinct types of crosslinking points. [4].

Storage conditions such as temperature, humidity, and aging duration further influence the rate and extent of these changes [6]. From a processing standpoint, storage-hardened rubber can require higher mastication energy, longer mixing times, and modified compounding conditions to achieve the desired processability [7].

This study aims to evaluate the changes in Mooney viscosity, initial plasticity (P_0), and plasticity retention index (PRI) of selected Standard Philippine Rubber (SPR) grades—SPR 20, SPR 5, and SPR L—during prolonged

storage under ambient conditions. By characterizing their degradation and hardening trends.

Understanding how SPR grades behave during extended storage is crucial for maintaining product uniformity, optimizing processing efficiency, and preventing unexpected variability in rubber-based manufacturing.

2. Experimental Methods

The test material was obtained from single SPR bales per grade, and no formal homogeneity study was conducted. Representative sampling was ensured by systematic slicing and quartering of each bale to obtain composite test portions, which were stored at ambient laboratory temperature and protected from direct sunlight. Samples were tested periodically, at approximately one-week intervals whenever possible, for plasticity (ISO 2007), plasticity retention index (PRI, ISO 2930), and Mooney viscosity (PNS ISO 289-1). Plasticity and PRI measurements were performed using a Wallace P14 Rapid Plastimeter and Wallace ageing chamber, respectively, while Mooney viscosity was determined with a Wallace MK III V3/4 Mooney viscometer.

To assess whether degradation rates differed among the three SPR grades, Analysis of Covariance (ANCOVA) was applied using time as the covariate and the measured property as the response variable, allowing comparison of the slopes of degradation trends while accounting for time-dependent changes. ANCOVA computations and regression visualizations were carried out using SPSS, which provided both the statistical outputs and fitted-linear models used in this study.

3. Results and Discussion

Before comparing the degradation behavior of the three SPR grades, the overall measurement characteristics of the stored bales were considered. Minor variability within each bale was regarded as inherent to the material rather than a source of analytical error, and replicate analyses from all three bales yielded relative standard deviations (%RSD) below 3%. These results indicate that the samples were sufficiently uniform for the purposes of this study; therefore, no formal homogeneity test was performed on the bales.

An initial examination of the weekly measurements for Mooney viscosity and P_0 showed generally increasing patterns over the storage period, reflecting the typical storage hardening behavior of natural rubber. In contrast, PRI exhibited a decreasing trend. For consistency and comparability, the degradation of these properties was approximated using a linear trend, providing a practical and interpretable basis for estimating and comparing degradation rates among the three SPR grades.

This linear approximation enables the use of Analysis of Covariance (ANCOVA) to evaluate whether the slopes of the degradation curves differ significantly among grades. The following subsections present the ANCOVA results for each property.

Analysis of covariance (ANCOVA) was conducted to evaluate whether the three SPR grades differed in their rates of change in Mooney viscosity during storage. Contrary to typical oxidative softening observed in some polymers, the stored rubber samples exhibited increasing Mooney viscosity over time, a behavior consistent with the well-documented phenomenon of storage hardening in natural rubber [3]. This increase is attributed due to the linkages between the active functional groups of phospholipids at the terminating end of rubber molecules [5].

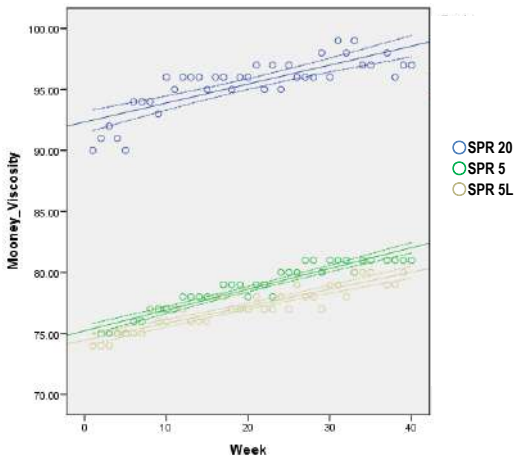

Figure 1. Linear Trends in Mooney Viscosity of SPR Grades Over Prolonged Storage

The week × grade interaction was not significant ($F = 1.198$, $p = 0.306$), indicating that the rate of storage

hardening did not differ significantly among SPR 20, SPR 5, and SPR 5L. Although the grades began with different absolute viscosity levels, their slopes were statistically parallel, showing that all three materials hardened at comparable rates during storage. This suggests a common underlying mechanism governing viscosity increase across grades under ambient conditions.

A similar trend was observed for P_0. Instead of declining, P_0 values increased gradually over the storage period, again consistent with the storage hardening behavior of natural rubber.

As with Mooney viscosity, the interaction between week and grade was not significant ($F = 2.758$, $p = 0.068$), indicating that the rates of plasticity increase (storage hardening) were similar across grades. Although the grades differed in their P_0 values, they exhibited comparable positive slopes over the storage period. This again suggests that the physical transformation processes responsible for storage hardening operate similarly across the SPR grades.

The observed increases in Mooney viscosity and P_0 over the 40-week period can be attributed to the chemical phenomenon of storage hardening. Natural rubber, primarily composed of *cis*-1,4-polyisoprene, contains minor but significant non-rubber components such as phospholipids and proteins. During prolonged storage, these components act as natural cross-linking agents. Specifically, the functional groups at the terminal ends of the polyisoprene chains interact with the fatty acid esters in phospholipids. This interaction leads to the formation of a hard gel consisting of chemical crosslinks and branching points between the rubber chains. This effectively increases the gel content of the rubber [4][5]. Physically, this results in molecular structuring where the chains become less mobile and more resistant to deformation.

Early research also indicates that storage under low-humidity conditions significantly accelerates the increase of Mooney viscosity [8]. While the present study did not continuously monitor the precise humidity levels throughout the 40-week duration, ambient humidity during storage likely contributed to the observed rate of hardening

These structural transformations occur in direct competition with oxidative degradation. Oxidative degradation attempts to break the polymer chains through chain scission [9], yet the rate of storage hardening, driven by the aforementioned cross-links, remains the dominant force influencing the physical profile of the SPR grades under ambient conditions. This imbalance explains why the "net effect" is a steady increase in viscosity and stiffness rather than the softening typical of pure oxidative degradation.

Furthermore, this dominance of storage hardening provides a critical perspective on the observed decline in the Plasticity Retention Index (PRI). Rather than indicating a significant loss of inherent thermal stability, the falling PRI is primarily a mathematical consequence of the rising P_0. Because the PRI formula is the ratio of aged plasticity (P_{30}) to P_0, the substantial increase in the denominator P_0 naturally lowers the resulting index, even when the P_{30} remains relatively stable. Thus, the declining PRI across SPR 5, SPR 20, and SPR L reflects the shared rate of molecular structuring and P_0 increase rather than a drastic acceleration of oxidative softening.

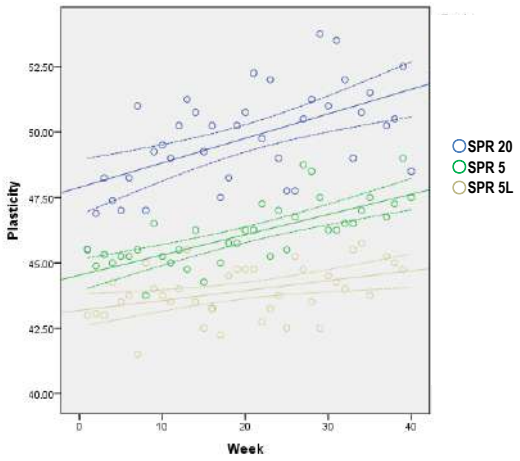

Figure 2. Linear Trends in Initial Plasticity of SPR Grades Over Prolonged Storage

The Grade × Week interaction, which tests whether the PRI degradation slopes differ among grades, yielded $F = 3.086$ with a p-value of 0.050. Positioned exactly at the conventional threshold of significance, this borderline result suggests the possibility of slightly divergent degradation rates, although the evidence is not strong enough to conclude substantial or practically meaningful

slope differences. In other words, while the statistical signal is marginal, the magnitude of the interaction effect remains small relative to the much larger differences in baseline PRI levels.

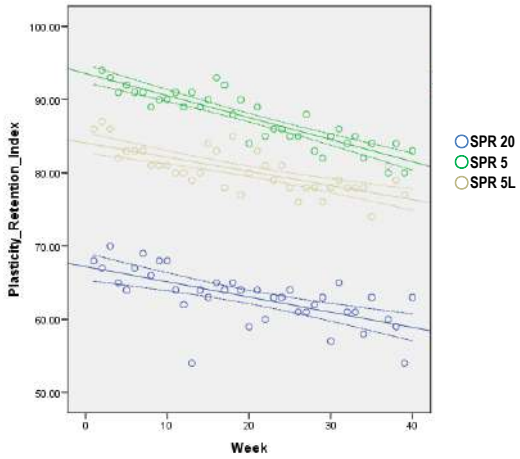

Figure 3. Linear Trends in Initial Plasticity of SPR Grades Over Prolonged Storage

4. Conclusion

Across all grades, Mooney viscosity and initial plasticity exhibited positive linear slopes, reflecting the expected storage hardening of natural rubber. This phenomenon is driven by molecular structuring and the formation of a hard gel fraction resulting from chemical crosslinks between terminal functional groups and fatty acid esters in phospholipids. In contrast, PRI showed negative linear slopes. While this trend is associated with progressive oxidative degradation, it is primarily a mathematical consequence of the significant increase in P_0 during storage.

Although the three grades differed markedly in their baseline values for all properties, ANCOVA results demonstrated that the rates of change over time were largely similar. The nonsignificant Grade × Week interactions for Mooney viscosity and initial plasticity indicate comparable hardening behavior across grades, while the borderline interaction for PRI suggests only minimal and practically limited variation in oxidative degradation rates.

Overall, the findings show that the three SPR grades follow broadly similar degradation trajectories, despite exhibiting distinct initial properties. Whereas Mooney and plasticity increased due to storage hardening, the decline in PRI was largely a function of increase in P_0. Across all three properties, the rates of change were generally comparable among grades, supporting the interpretation that storage related transformations in SPR occur through common underlying chemical mechanisms involving non rubber components regardless of grade.

Future work may expand on these findings by examining a larger number of bales and using more frequent sampling intervals to improve the resolution and accuracy of degradation trends. Longer storage durations or the use of non-linear modeling approaches may also provide deeper insight into the kinetics of hardening and oxidative decline, particularly if property changes deviate from linear behavior over extended periods. Studies that incorporate controlled environmental conditions such as temperature, humidity, and light exposure would help isolate the specific factors influencing degradation, and comparative evaluations of processing history or stabilization treatments may support the development of more robust shelf-life assessments for Standard Philippine Rubber.

5. Acknowledgement

The authors extend their sincere gratitude to the Department of Science and Technology IX (DOST-IX) for providing the facilities, resources, and institutional support that made this research possible.

6. References

1. Morton, *M. Rubber Technology*, *3rd ed.*; Springer: New York, 2013.
2. Brydson, J. A. *Rubber Materials and Their Compounds*; Elsevier Applied Science: London, 1988.
3. Gan, S. N.; Tan, C. S. *Storage Hardening of Natural Rubber*. J. Appl. Polym. Sci. 1993, 50, 1623–1630.
4. Tanaka, Y. *Structural Characterization of Natural Rubber*. Rubber Chem. Technol. 2001, 74, 355–375.

5. Yunyongwattanakorn, J.; Sakdapipanich, J.; Ho, C. C. *Storage Hardening Mechanism in Natural Rubber*. J. Appl. Polym. Sci. 2003, 90, 3308–3315.
6. Webster, C. C.; Baulkwill, W. J. *Rubber*; Longman Scientific & Technical: Essex, 1989.
7. Coran, A. Y. *Vulcanization. In Science and Technology of Rubber, 4th ed*.; Mark, J. E.; Erman, B.; Roland, C. M., Eds.; Academic Press: San Diego, 2013; pp 321–366.
8. Wood, R. I. (1952). Mooney viscosity changes in freshly prepared raw natural rubber. Rubber Chemistry and Technology, 25(4), 573–588
9. Galiani, P. D., Malmonge, J. A., Soares, B. G., & Mattoso, L. H. C. (2013). Studies on thermal-oxidative degradation behaviours of raw natural rubber: PRI and thermogravimetry analysis. Plastics, Rubber and Composites, 42(8), 334–339.

Development of Natural Rubber Insulating Gloves: Influence of Latex Centrifugation and Leaching on Mechanical and Electrical Properties

Promsak Sa-nguanthammarong*[1], Chayapha Nimsuwan[1], Chotiros Dokkhan[1], Bundit Putasaeng[1]

[1] *National Metal and Materials Technology Center, 114 Thailand Science Park, Khlongluang, Pathumthani, Thailand.*

*E-mail: promsaks@mtec.or.th

Abstract

This study develops natural rubber insulating gloves for high-voltage applications by optimizing latex grade, compounding formulation, and leaching conditions to achieve compliance with ASTM D120-14a and IEC 60903:2014. Rubber sheets were prepared from single- and double-centrifuged latex concentrates, compounded with selected additives, and subjected to water or sodium dodecyl sulfate (SDS) leaching at various temperatures and durations. Double-centrifuged latex exhibited higher dielectric strength (up to 15.4 kV/mm) due to reduced non-rubber components. Leaching further improved both mechanical and electrical performance, with SDS treatment at ambient temperature for 24 h providing the optimal balance of properties. The resulting samples met all required mechanical specifications, showed electrical performance comparable to commercial gloves, and achieved low extractable protein content (as low as 25 µg/g). Overall, the findings demonstrate that controlled latex purification combined with appropriate compounding and leaching conditions can produce natural rubber insulating gloves that satisfy international standards and support the potential for domestic manufacturing.

Keywords: Natural rubber latex, Insulating glove, Leaching, Mechanical properties, Dielectric strength

1. Introduction

Rubber insulating gloves are essential Personal Protective Equipment (PPE) for “hot line” workers, providing primary protection against electrical hazards during high-voltage operations. Ensuring their reliability is therefore critical, as glove failure can lead to severe injury or fatality. To guarantee adequate safety performance, these gloves must comply with strict international standards, including ASTM D120-14a and IEC 60903:2014, which specify requirements for mechanical integrity, dielectric strength, and overall durability.

This study follows the ASTM D120 standard, which classifies rubber insulating gloves into two types: Type I (non-ozone-resistant) and Type II (ozone-resistant). Each type is further subdivided into six classes based on their rated voltage and proof-test requirements, as summarized in Table 1.

Table 1: Classification of insulating gloves

Class	AC (V)		DC (V)		Label color
	Proof-test	Max. AC use	Proof-test	Max. DC use	
0	2,500	500	10,000	750	Beige
00	5,000	1,000	20,000	1,500	Red
1	10,000	7,500	40,000	11,250	White
2	20,000	17,000	50,000	25,500	Yellow
3	30,000	26,500	60,000	39,750	Green
4	40,000	36,000	70,000	54,000	Orange

Figure 1: Example of rubber insulating gloves
source**:** www.yotsuki.co.jp

In addition to electrical performance, rubber insulating gloves must satisfy strict mechanical requirements, as summarized in Table 2.

Table 2: Standard requirements for mechanical properties

Property	Requirement
200% modulus, max (MPa)	2.1
Tensile strength*, min (MPa)	17.2
Ultimate elongation*, min (%)	600
Tension set (at 400% elongation), max (%)	25
Tear resistance, min (kN/m)	21
Puncture resistance, min (kN/m)	18
Hardness, max (Shore A)	47

*Tensile strength and ultimate elongation after aging at 70°C for 7 days must retain at least 80% of their initial values.

Previous studies have demonstrated the potential of natural rubber as an effective electrical insulator [1-2], with dielectric performance further enhanced through material purification and nanoparticle incorporation [3-4]. Developing natural rubber for insulating gloves is therefore of significant interest, as it can add value to the material and promote greater domestic consumption. This study focuses on the development of Type I, Class 3 insulating gloves and investigates the improvement of their mechanical and electrical properties through variations in latex concentrate grades, compounding formulations, and the leaching process.

2. Methodology

2.1 Materials

Two grades of natural rubber latex concentrate were studied: Single Centrifuge (SC) and Double Centrifuge (DC). Their properties were analyzed and are summarized in Table 3.

Table 3: Properties of latex concentrates used in this study

Property	SC	DC
Total solid content (TSC), %	62.02	60.62
Dry rubber content (DRC), %	60.30	59.78
Non-rubber content (NRC), %	1.72	0.84
Alkalinity (as NH_3), %	0.64	0.61
pH value	10.74	10.57
Volatile fatty acid number (VFA)	0.024	0.025
Potassium hydroxide number (KOH)	0.534	0.295
Mechanical stability time (MST), sec	840	900
Viscosity, centipoises	73	66

2.2 Compound formulation and rubber sheet preparation

The latex was compounded using a sulfur vulcanization system, with polyvinyl methyl ether (PVME) employed as a heat-sensitizing agent for the dipping process [5]. The detailed formulation is presented in Table 4. The rubber sheets were prepared by casting 85 g of unvulcanized and compounded latex into plastic trays (13 × 20 × 3.6 cm), drying them at room temperature for 2 d, demolding, and then oven-drying at 70°C for 6 h. The resulting rubber sheets had a thickness of approximately 2 mm.

Table 4: Compound formulation

Ingredient	Parts per hundred rubber (phr)
Concentrated natural rubber latex	100
Potassium hydroxide	0.10
Zinc oxide	0.25
Zinc dibutyl dithiocarbamate	0.25
Sulphur	0.75
Antioxidant	0.75
Polyvinyl methyl ether	0.80

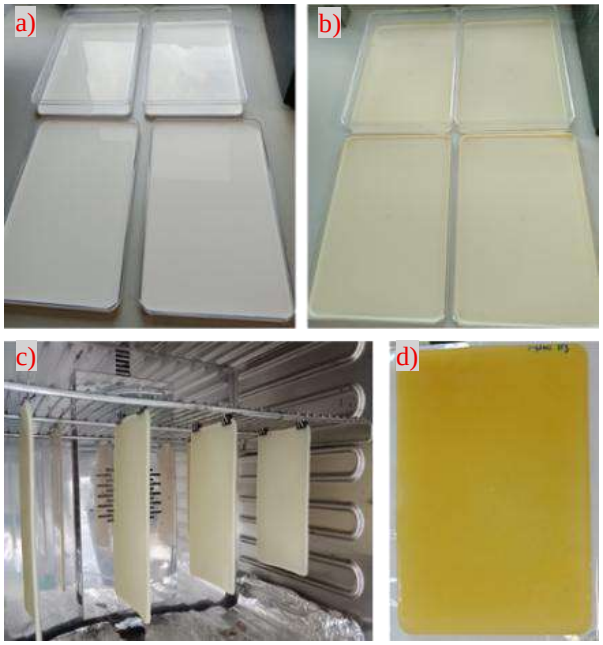

Figure 2: Rubber sheet preparation: a) casting latex into a plastic tray; b) drying at room temperature for 2 d; c) oven drying at 70 °C for 6 h; and d) driedrubber sheet.

2.3 Leaching process

The dried sheets prepared from single-centrifuged latex (SC-LCS) were subjected to leaching treatments by immersing them in either distilled water or a 1% (w/w) sodium dodecyl sulphate (SDS) solution at varied temperatures (30, 50, 70°C) for 24 h (Figure 3). After leaching, they were rinsed with distilled water at least twice, air-dried, and then oven-dried at 70°C for 6 h.

Figure 3: Leaching process: a) immersion in water or 1% SDS; b) incubation in a temperature-controlled water bath for 24 h; and c) drying at room temperature.

2.4 Property testing

Samples were tested for mechanical, electrical, and chemical properties. Mechanical tests included tensile strength, 200% modulus, elongation at break, tension set (ASTM D412), tear strength (ASTM D624, Die C), hardness (ASTM D2240), and puncture resistance (JIS T8112). Heat aging was performed according to ASTM D573. Extractable protein content was measured following ASTM D5712. Dielectric strength was evaluated using a high-voltage tester: an alternating current (AC) at 50 Hz was applied, starting from 0 V and increasing at 500 V per second until the specimen failed. The dielectric strength was calculated by dividing the breakdown voltage by the specimen thickness.

3. Results and Discussion

3.1 Effect of latex grade

The mechanical properties of the developed natural rubber latex compound sheets (SC-LCS and DC-LCS) were evaluated and compared with two commercial insulating gloves as shown in Table 5. Both SC-LCS and DC-LCS met the ASTM requirements for insulating gloves, demonstrating good potential for high-voltage applications.

The 200% modulus values of both SC-LCS and DC-LCS were well below the 2.1 MPa limit, indicating good flexibility. Tensile strength values—19.5 MPa for SC-LCS and 21.8 MPa for DC-LCS—exceeded the 17.2 MPa minimum but were slightly lower than those of commercial gloves (26.8–28.3 MPa). After aging, both developed samples retained 87% of their original tensile strength, slightly below the 95–97% retention observed in commercial gloves, yet still above the ASTM minimum requirement of 80%. For elongation at break, the SC-LCS and DC-LCS exhibited excellent extensibility, exceeding the 600% minimum requirement both before and after aging. Interestingly, the elongation values slightly increased after aging (108% and 105% retention), which suggests that some network rearrangement due to thermal oxidation may have occurred during the aging process.

The tension set values of both SC-LCS and DC-LCS were 4.0%, well below the 25% maximum, confirming excellent elastic recovery. Tear strength (42.0–43.6 kN/m) met the 21 kN/m requirement and was comparable to commercial gloves (44.8–47.9 kN/m), indicating good tear resistance. Puncture resistance exceeded the minimum requirement of 18 kN/m, demonstrating adequate resistance to mechanical penetration. Hardness values (≈37 Shore A) were lower than those of commercial gloves but within the 47 Shore A limit, indicating a softer material with greater flexibility, which can enhance user comfort during glove use.

The slightly higher tensile strength and hardness of DC-LCS compared with SC-LCS suggest that the double centrifugation process improved latex purity and network formation.

Table 5: Mechanical property requirement and comparison of commercial insulating gloves and developed samples

Property	Requirement	Commercial 1	Commercial 2	SC-LCS*	DC-LCS**
200% Modulus (MPa)	2.1 (max)	1.06 ± 0.03	0.83 ± 0.01	0.82 ± 0.05	0.84 ± 0.03
Tensile strength (MPa)					
- Before aging	17.2 (min)	26.8 ± 1.6	28.3 ± 1.3	19.5 ± 0.5	21.8 ± 0.4
- After aging 70°C, 7d	>80% of original	97%	95%	87%	87%
%Elongation at break					
- Before aging	600 (min)	817 ± 14	919 ± 12	769 ± 36	800 ± 26
- After aging 70°C, 7d	>80% of original	99%	98%	108%	105%
%Tension set at 400%	25 (max)	2.1 ± 0.2	2.6 ± 0.1	4.0 ± 0.5	4.0 ± 0.3
Tear strength (kN/m)	21 (min)	47.9 ± 3.9	44.8 ± 4.3	43.6 ± 5.7	42.0 ± 3.8
Puncture resistance, (kN/m)	18 (min)	61.2 ± 0.5	60.5 ± 0.3	51.2 ± 0.2	52.2 ± 0.6
Hardness (Shore A)	47 (max)	41.0 ± 1.0	39.0 ± 0.9	37.2 ± 0.8	37.1 ± 0.7

*single centrifuge latex compound sheet, **double centrifuge latex compound sheet

3.2 Effect of leaching

Leaching conditions significantly affected the tensile properties of SC-LCS sheet as showed in Table 6. Compared with unleached sample, all leached samples exhibited increased 200% modulus, tensile strength, and elongation at break, indicating that leaching effectively improved mechanical performance. This enhancement is attributed to the removal of water-soluble impurities and proteins during leaching, which reduced structural defects and strengthened the rubber matrix [6].

Among the conditions tested, leaching in a 1% SDS solution at 70°C produced the highest 200% modulus (1.19 MPa) and tensile strength (36.1 MPa), indicating that the combination of surfactant and elevated temperature enhanced the removal of non-rubber components and improved mechanical performance. Elongation at break, however, remained largely unchanged across all leaching conditions, suggesting that this property was not sensitive to the type or temperature of leaching. After 24 h of leaching, the extractable protein content was reduced to 25 µg/g, consistent with values observed in commercial products (13–36 µg/g). Overall, higher temperature and SDS treatment yielded cleaner rubber sheet with superior mechanical properties compared to the unleached sample.

3.3 Dielectric strength of rubber sheets

The prepared rubber sheets were evaluated for dielectric strength. According to glove standards, a breakdown voltage of 30 kV must be withstood at a maximum thickness of 2.9 mm, corresponding to a minimum dielectric strength of 10.3 kV/mm. The experimental results are presented in Table 7.

The dielectric strength results indicate that leaching significantly improves the electrical insulating performance of SC-LCS sheet. For both uncompounded and compounded SC samples, dielectric strength increased noticeably with leaching time, demonstrating that the removal of non-rubber components, water-soluble proteins, and ionic impurities plays a key role in enhancing electrical resistance. These impurities typically act as charge carriers within the rubber matrix, so their removal reduces conductivity and delays electrical breakdown.

For uncompounded SC sheets, dielectric strength increased from 8.6 kV/mm (unleached) to 13.2 kV/mm after 24 h of water leaching, and further to 14.8 kV/mm with 12 h of 1% SDS leaching. A similar trend was observed for compounded SC sheets, which initially exhibited the lowest dielectric strength (6.4 kV/mm) but improved markedly after leaching, reaching values comparable to the uncompounded sheets. The greater effectiveness of SDS leaching is attributed to the surfactant's enhanced ability to remove proteins and ionic species compared with water alone.

The DC rubber sheets, prepared from double-centrifuged latex, inherently exhibited higher dielectric strength even without leaching, with 15.4 kV/mm for the uncompounded sheet. This reflects the higher purity of DC latex, as double centrifugation removes a substantial portion of non-rubber components during latex preparation. Compounding slightly reduced dielectric strength to 12.8 kV/mm, likely due to the introduction of additives that act as polar sites or fillers. Overall, the results confirm that both leaching and latex purification are essential for maximizing dielectric performance. Extended leaching time and the use of SDS enhance electrical insulation by producing a cleaner, less conductive rubber matrix, making the sheets suitable for insulating glove applications [3, 7-8].

The results clearly show that sheets prepared from single-centrifuged latex (SC) exhibit significantly lower dielectric strength than those from double-centrifuged latex (DC), likely due to the higher non-rubber content in SC latex, which increases conductivity and reduces voltage withstand capability. Compounding further decreased dielectric strength, indicating that the added chemicals negatively affected the material's electrical performance. However, dielectric strength recovered and improved through leaching. Leaching with 1% SDS produced slightly higher values than water alone, and dielectric strength increased progressively with longer leaching times.

Table 6: Tensile properties of leached SC-LCS sheets

Leaching Agent	Temperature (°C)	200% Modulus (MPa)	Tensile strength (MPa)	Elongation at break (%)
No leaching	30	0.82 ± 0.05	19.5 ± 0.5	769 ± 36
Water	30	0.96 ± 0.07	34.5 ± 1.7	864 ± 17
	50	1.03 ± 0.03	34.5 ± 4.2	870 ± 33
	70	1.03 ± 0.05	33.3 ± 2.9	833 ± 12
1% (w/w) SDS	30	1.10 ± 0.05	32.7 ± 2.5	848 ± 17
	50	1.13 ± 0.04	34.0 ± 1.3	869 ± 12
	70	1.19 ± 0.04	36.1 ± 2.5	852 ± 25

Table 7: Dielectric strength of the sheets

Sample	Leaching	Leaching time (h)	Dielectric strength (kV/mm)
SC (Uncompounded)	No leaching	0	8.6 ± 0.3
	Water	6	11.7 ± 0.5
		12	12.9 ± 0.4
		24	13.2 ± 0.6
	1% SDS	6	12.4 ± 0.3
		12	14.8 ± 0.4
		24	14.6 ± 0.5
SC-LCS	No leaching	0	6.4 ± 0.1
	Water	6	7.8 ± 0.2
		12	8.1 ± 0.2
		24	9.0 ± 0.1
	1% SDS	6	9.0 ± 0.2
		12	10.2 ± 0.4
		24	9.7 ± 0.3
DC (Uncompounded)	No leaching	0	15.4 ± 0.2
DC-LCS	No leaching	0	12.8 ± 0.5

4. Conclusion

This study demonstrated the feasibility of developing natural rubber insulating gloves (Type I, Class 3) by optimizing latex grade, compounding formulation, and leaching conditions. Both SC-LCS and DC-LCS sheets met all ASTM mechanical property requirements. Leaching significantly enhanced mechanical performance by removing water-soluble proteins and impurities, with warm SDS leaching providing the greatest improvements in modulus, tensile strength, and elongation, while effectively reducing extractable protein levels. Dielectric strength was strongly influenced by material purity: leached SC sheets showed substantial improvement, whereas DC latex exhibited the highest dielectric strength even without leaching. Overall, the combined effects of latex purification and optimized leaching produced rubber sheets with mechanical robustness and dielectric performance that meet or exceed the minimum requirements for insulating glove applications. These findings provide a solid foundation for further development of natural rubber insulating gloves and support Thailand's efforts to add value to natural rubber through advanced rubber product manufacturing.

5. References

1. Junian S, Makmud M, and Sahari J, Natural Rubber as Electrical Insulator: A Review. Journal of Advanced Review on Scientific Research. 2015; 6: 28-42.
2. Roland CM. Electrical and Dielectric Properties of Rubber. Rubber Chemistry and Technology. 2016; 89(1): 32-53.
3. González N, Custal M, Lalaouna S, Riba J-R, Armelin E. Improvement of dielectric properties of natural rubber by adding perovskite nanoparticles. European Polymer Journal. 2016; 75: 210-22.
4. Li B, Salcedo-Galan F, Xidas PI, Manias E. Improving Electrical Breakdown Strength of Polymer Nanocomposites by Tailoring Hybrid-Filler Structure for High-Voltage Dielectric Applications. ACS Applied Nano Materials. 2018; 1(9): 4401-7.
5. Mathew S, Varghese S. Effect of Compounding Characteristics on Heat Sensitization of PVME Blended Natural Rubber Latex Compound. International Journal of Innovative Research and Development. 2015; 4(8): 232-9.
6. Ramli R, Tan K, Jefri J. Study on Morphological Structures and Mechanical Properties of Natural Rubber Latex Films Prepared at Different Prevulcanisation and Drying Temperatures. Journal of Rubber Research. 2018; 21.
7. Balpinarli M, Dai JJ, Gela G. AC and DC breakdown versus thickness characteristics for rubber gloves. IEEE Transactions on Power Delivery. 1988; 3(1): 384-91.
8. Riba J-R, González N, Canals T, Cantero R. Identification of natural rubber samples for high-voltage insulation applications. Computers & Chemical Engineering. 2019; 124: 197-205.

Acknowledgements

The authors gratefully acknowledge the support of the Provincial Electricity Authority (PEA), Thailand, for funding this research under the project "Research and Development of Natural Rubber Gloves for High Voltage Electrical Work" (Project No. C-056-62).

Sustainable NZEROSIL™ Silicas from Renewable Rice Husk

Danniel C. Liao*, Tim Yu-Ting Lin, Spencer P. Lee, Chris S. Wu, Anthony Lin, and Walter H. Waddell

ORIENTAL SILICAS CORPORATION, #99, Li-Yu Kou, Li-Yu Village, Sanyi Miaoli Taiwan

E-mail: dliao@oscsilica.com

Abstract

OSC's next generation of reinforcing precipitated silicas is the sustainable NZEROSIL™ net zero emission series made from the bio-renewable rice husk agricultural waste. Key performance properties in a model PCR tire tread were shown to be equivalent to commercial silicas (BET ~165 m^2/g) by increasing wet traction and decreasing rolling resistance. Tires for UHP, EV and LT vehicles require further increased capabilities due to the higher strains on these tires. Here, we quantify the performance of high surface area (BET ~210 m^2/g) NZEROSIL™ RH-230G granules compared to Eecosil® 230G granules, Eecosil® 230MG microgranules, and a commercial competitor Silica 1 in a 100-phr silica model tire tread. Compound cure, physical and viscoelastic properties, and silica dispersion are measured. Results show the performance of sustainable NZEROSIL™ RH-230G is equivalent within ~10% to Eecosil® 230G and 230MG silicas made from cullet (recycled glass), and is also slightly improved versus Silica 1. A 5-pass mix sequence by adding silica in three steps and a remill stage is used to maximize the M300/M100 reinforcement index when dispersing silica by reducing its %-white area.

Keywords: Precipitated Silica, BET Surface Area, Microgranule, Filler Dispersion, ImageJ Analysis, and PCR Tire Tread

1. Introduction

Michelin [1] developed a passenger car radial (PCR) tire with SSBR/BR (75/25) and highly dispersible silica (HDS) tread [2]. Tire testing showed increased wet traction, reduced rolling resistance and maintained wear life, see Figure 1. Multiple thermomechanical mixing steps were needed to disperse the silica and react with a bifunctional organosilane to optimize the M300/M100 ratio, the reinforcement index. SSBR/B/silica-filled tread with improved performance is known as the green tire.

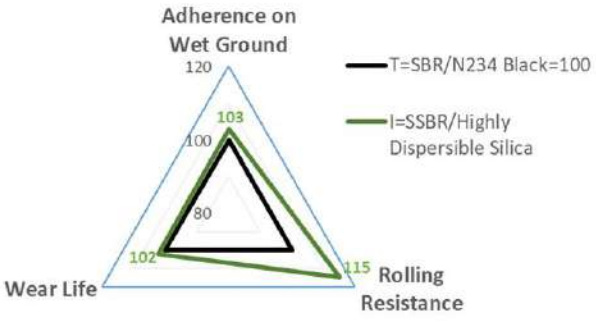

Figure 1. Radar plot of wet traction, rolling resistance and wear life performances of PCR tire Invention I relative to Control T, which is assigned a 100 value.

Oriental Silicas Corporation [3] was created in 2003 by purchasing all silica businesses in Asia from their PPG joint venture partner. OSC currently produces various amorphous precipitated silicas for different applications, including highly reinforcing silicas for tire treads. Tokusil® 255EG (BET surface area ~165 m^2/g) is an easily dispersing granule made by oven drying, milling into a powder and compacting on a textured 2-roll mill, see Figure 2. Eecosil® 350MG is a highly dispersible microgranule made by directly spray drying to the desired dust-free particle size [4]. High surface area (BET ~210 m^2/g) Eecosil® 230G granular and highly dispersible Eecosil® 230MG microgranular silicas are manufactured for ultrahigh performance (UHP), light truck (LT) and electric vehicle (EV) tire applications [5].

Figure 2. Silica powder (left), granules (center), and microgranules (right).

The most abundant mineral in the Earth's crust of continental (20-80 km) and oceanic (7-12 km) layers is igneous rock containing ~90% silicates [6]. Silicon dioxide (silica) is ~26% by weight and is found as inert, abrasive particles of crystalline quartz, cristobalite, and

tridymite. Exposure of workers to respirable crystalline silica is associated with elevated rates of lung cancer [7], so sand is not used in rubber products. Amorphous silica is made in a 2-step reaction: #1 reacts sand with soda ash (Na_2CO_3) in a furnace at <~1700°C, see Figure 3. This is essentially the same dry process used in glass making.

$$\mathbf{n\ SiO_2 + Na_2CO_3 => n\ (SiO_2)Na_2O + CO_2} \quad (1)$$

Figure 3. Dry furnace process to make sodium silicate from crystalline quartz (sand) by heating with soda ash.

Reaction #2 is the controlled acid neutralization step:

$$\mathbf{n\ (SiO_2)Na_2O + H_2SO_4 => n\ SiO_2 + Na_2SO_4 + H_2O} \quad (2)$$

Manufacturing amorphous silica takes multiple steps. Equipment, reaction conditions and processes are proprietary. Variables include reactor size, fill volume, sodium silicate concentration and add rate, acid pH and add rate, stirring rate, reaction time and temperature, and quench rate to make amorphous precipitated silicas with targeted properties for specific industrial applications.

Sodium silicate is also made from cullet, which is crushed glass recycled from any broken or discarded products. Cullet is dissolved and reacted with soda ash in solution in an autoclave at much lower temperatures than needed in a dry furnace reaction. This wet process, see Figure 4, is an environmentally friendly step using both recycled starting materials and a lower energy demand. OSC is an excellent corporate citizen and built plants in Taiwan (2013) and Malaysia (2021) to produce silicates from cullet to supply our silica manufacturing plants in Taiwan and Thailand. Controlled acid neutralization (see equation 2) is then used to precipitate the targeted amorphous silicas with the desired physical properties.

Figure 4. Wet process to produce sodium silicate from cullet.

Many tire manufacturers now desire the use of sustainable materials. Silica can be obtained from a number of eco-friendly renewable bio-sources. Rice husk (index = 20.5) and straw (12.0) have the highest yield, see Figure 5. Cornflower (11.1), sorghum (grass flowers, 10.7), and bagasse (sugar cane, 9.5) also have a high index, which is calculated by multiplying the ash content of the plant by the silica content in its ash [8]. Rice is the second most consumed food source globally after maize (corn). Corn byproducts already have commercial applications, for example as ethanol used in gasoline to form gasohol. In 2022- 2023, about 775 million metric tonnes (mmt) of rice was produced worldwide. Twelve countries each harvested >10 mmt annually. All are located in the Asia-Pacific region, except for Brazil, which is ranked #11 [9].

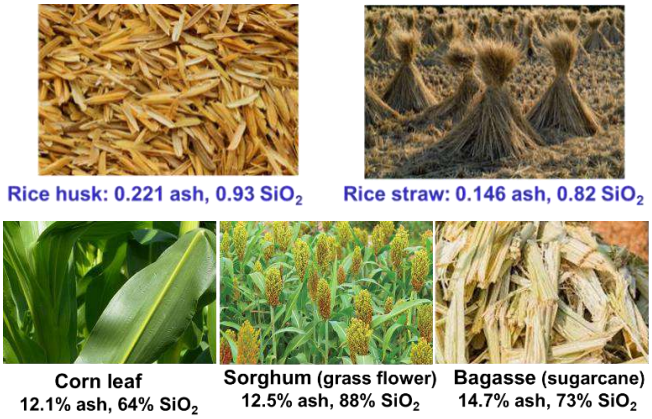

Figure 5. Rice husk, rice straw, corn leaf, sorghum and bagasse shown with their ash and silica contents.

The rice husk is the outermost layer of the rice grain. Milling yields ~70% rice, ~20% husk, 8% bran and 2% germ [10], see Figure 6. People consume white rice and brown rice, which contains the bran and germ. An agricultural waste byproduct of milling, the husk used to be simply burnt in an open-air field as a fuel or dumped into a land fill. Both actions have potentially detrimental environmental effects. Currently, rice husk ash can be used as a raw material for manufacturing industrial chemicals (various silicates, zeolites, catalysts, nanocomposites), in building material additives (for the steel industry, in concrete and cement), in lightweight construction materials (insulators, adsorbents, activated

carbon), as soil conditioners (fertilizers), and used as an alternative fuel for energy [11,12].

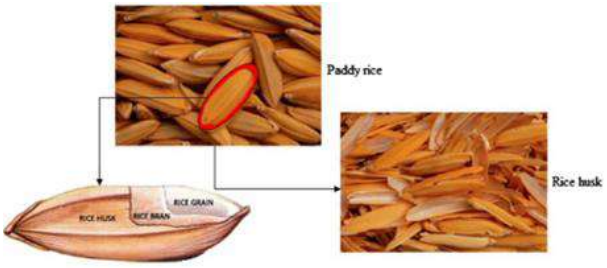

Figure 6. Components of rice: grain, bran and husk.

Sustainable NZEROSIL™ net zero emission reinforcing amorphous precipitated silicas [13] are manufactured starting from the bio-renewable rice husk. A 2-step chemical reaction is still used with the first step to produce sodium silicate, see Figure 8. It is reacted with acid to precipitate amorphous silicas, see equation 2.

Figure 7. Steps to ash the bio-renewable rice husk to be used as a starting material to produce sodium silicate, then silica.

2. Experimental

Compound mixing was performed in a Kobelco BB-2 1.5L internal mixer having 4-Wing H tangential rotors. Rubber was sheeted out after each mix stage on a 2-roll mill. Viscoelastic properties of cured compounds were measured on a Netzsch Gabometer dynamic mechanical analyzer. Tangent delta @0°C was used as a lab predictor of tire wet traction and tangent delta @60°C used as a lab predictor of tire rolling resistence, with lower values better. A Jeol JCM NeoScope scanning electron microscope (SEM) was used to measure silica dispersion at 100X magnification . NIH ImageJ software was used to quantify the %-white areas and average particle size distributions, with lower values thought more desirable for each.

3. Results and Discussion

High loadings of high surface area silica (BET ~210 m^2/g) in model tread formulations for ultrahigh performance (UHP) car, electric vehicle (EV) or light truck (LT) tires were identified from literature [14-15]. One formulation (see Table I) was developed to study different mix sequences to best incorporate and to disperse the 100-phr of high surface area, highly dispersible Eecosil® 230MG microgranule, see Figure 8.

Table I. 100-phr Silica-filled Tire Tread Formulation with a 4-Pass Mixing Sequence [16].

Mix Pass	Ingredient	phr
1st	SSBR, Trinseo 4602	75
	cis-BR, TSR 0150	25
	Silica, Eecosil 230MG	80
	TESPD Coupling Agent, Evonik Si75	10
	Carbon Black, N234	3
	Process Oil, TDAE	33.1
2nd	Silica, Eecosil 230MG	20
	Process Oil, TDAE	10
3rd	Microcrystalline Wax	1.5
	Activator, Zinc Oxide	2.5
	Accelerator, DPG	2.7
4th	Stearic acid	2
	Sulfur	1.1
	Accelerator, CBS	2.4

Mix Stage	4-Pass	5-Pass	5-Pass	6-Pass
1st	Polymers/Silica /Silane/Oil	Polymers/Silica /Silane/Oil	Polymers/Silica /Silane/Oil	Polymers/Silica /Silane/Oil
2nd	Silica/Oil	Silica/Oil	Silica/Oil	Silica/Oil
3rd	Chemicals	*REMILL*	Chemicals	*REMILL #1*
4th	Productive Mix	Chemicals	*REMILL*	Chemicals
5th		Productive Mix	Productive mix	*REMILL #2*
6th				Productive Mix

Figure 8. Mix study of 100-phr Eecosil® 230MG tread.

A 4-pass, two 5-pass by adding one remill, and a 6-pass mix with two remill steps were evaluated [16].

Compound process, physical and viscoelastic properties were comparable within ~10%. However, elongation at break values were below the target 300% needed to get M300/M100 reinforcement indices, see Table II. SEM @100X / ImageJ software analysis gave %-white area and average particle size values, see Figures 9-10.

Table II. Key Process, Physical and Viscoelastic Test Results of Four Different Mixing Sequences [16].

Mixing Sequence	4-Pass, No Remill	5-Pass, Stage 3 Remill	5-Pass, Stage 4 Remill	6-Pass, 2 Remills
MH-ML (dNm)	8.9	8.2	7.5	7.7
Ts1 (min)	2.4	2.2	2.6	2.3
T90 (min)	9.4	9.4	9.4	10
Tensile Strength (MPa)	9.1	7.9	8.5	7.7
Elongation at Break (%)	281	235	290	206
M100 (MPa)	2.7	2.8	2.2	3.2
M200 (MPa)	5.9	6.4	5.0	7.5
Reinforcement Index (M200/M100)	2.19	2.29	2.27	2.34
Wet Traction (tan δ 0°C)	0.379	0.390	0.389	0.399
Rolling Resistance (tan δ 60°C)	0.145	0.137	0.140	0.137

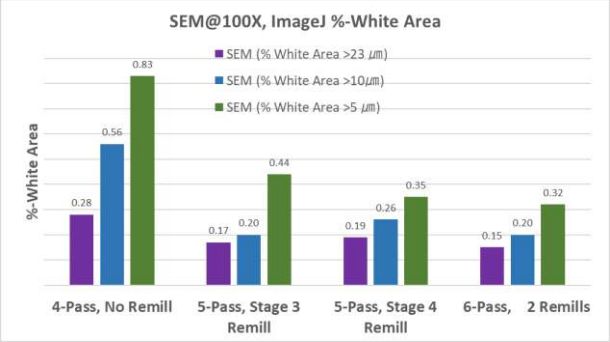

Figure 9. %-White areas from four different mixes.

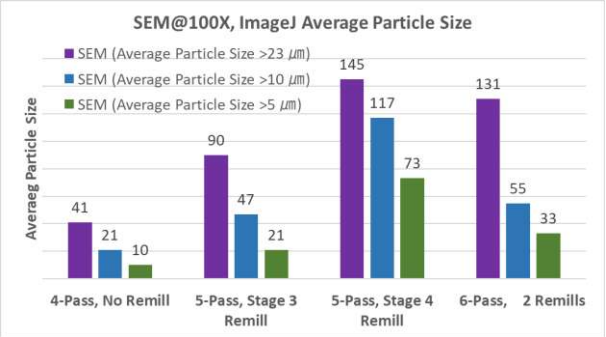

Figure 10. Average particle size distributions of four different mixes.

At most, 80-phr of highly dispersible Eecosil® 230MG microgranular silica could be incorporated into the first mix stage. The batch fill factor is also important. A 55/25-phr silica split is needed to minimize both the %-white area and average particle size values. All silane coupling agent is added with the initial 55-phr silica to promote hydrophobation to maximize the M300/M100 ratio. The remaining 25-phr of silica, carbon black and processing oil are added together later in the first stage mix, but before increasing the chamber temperature to >150°C and <160°C to promote the required silica-silane chemical hydrophobation reaction needed for tread wear.

The 4-pass mix had the highest %-white areas, and was eliminated. Smaller average particle sizes were obtained for the 5-pass mix with a stage 3 remill, and was used for follow-up studies comparing different silicas.

Using a zinc process aid [17,18] and reducing curative levels, increased elongation at break to >300%. Thus, M300/M100 reinforcement index values can now be calculated. Silica dispersion based on lower %-white areas was also improved with a zinc process aid [16].

Sustainable NZEROSIL™ RH-230G granules from rice husk, and Eecosil® 230MG microgranules and Eecosil® 230G granules made from recycled glass, and a microgranular competitor silica (Silica 1) were studied.

Table III. 100-phr Silica-filled Tire Tread Formula with a Zinc Process Aid using a 5-Pass Mixing Sequence [16]

Mix Pass	Ingredient	phr
1st	SSBR, Trinseo 4602	75
	cis-BR, TSR 0150	25
	Silica, Eecosil 230MG	80
	TESPD Coupling Agent, Evonik Si75	10
	Carbon Black, N234	3
	Process Oil, TDAE	33.1
	Process Aid, Struktol EF-44	6
2nd	Silica, Eecosil 230MG	20
	Process Oil, TDAE	10
3rd	REMILL	
4th	Microcrystalline Wax	1.5
	Activator, Zinc Oxide	2.5
	Accelerator, DPG	1.8
5th	Stearic acid	1
	Sulfur	1.1
	Accelerator, CBS	1.5

Results (see Table IV) showed NZEROSIL™ RH-230G had comparable physical performance within about 10% to Eecosil® 230MG (see Figures 11-12) and Eecosil® 230G silicas (see Figures 13-14). The Mooney viscosity is desirably lower. Ts1 scorch, tensile strength, elongation at break, and M300/M100 reinforcement index values are desirably higher. NZEROSIL™ RH-230G also had higher tensile strength and elongation at break values, and lower predicted rolling resistance

compared to Silica 1, see Figures 15-16. Sustainable NZEROSIL™ RH-230G silica is a commercial product.

Table IV. Key Properties of High Surface Area Silica Treads for UHP, EV and LT Tires [16].

Property	NZEROSIL™ RH-230G	Eecosil 230MG	Eecosil 230G	Silica 1
Mooney Viscosity (ML(1+4)@100°C)	**89.9**	**93.6**	**98.1**	**82.6**
Ts1 (min)	**5.7**	**4.2**	**4.9**	**5.7**
T90 (min)	**13.9**	**13.6**	**14.0**	**14.1**
Tensile (MPa)	**8.6**	**7.4**	**8.3**	**5.9**
Elongation at Break (%)	**376.3**	**334.4**	**344.3**	**301.0**
100% Modulus (MPa)	**1.9**	**2.1**	**2.5**	**1.8**
300% Modulus (MPa)	**6.4**	**6.5**	**7.1**	**6.1**
Reinforcement Index (M300/M100)	**3.31**	**3.04**	**2.84**	**3.29**
Wet Traction (tan δ 0℃)	**0.340**	**0.346**	**0.343**	**0.338**
Rolling Resistance (tan δ 60℃)	**0.154**	**0.160**	**0.165**	**0.172**

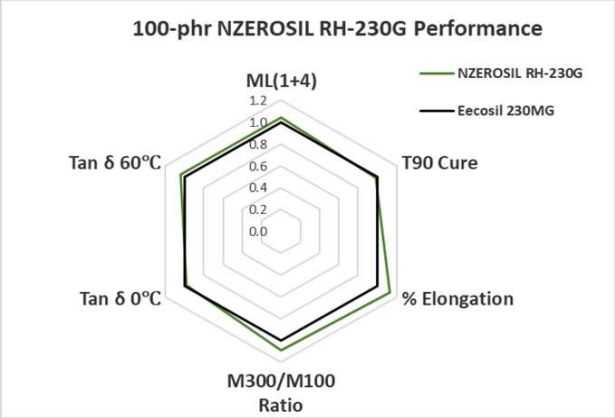

Figure 11. Radar plot of NZEROSIL™ RH-230G rice husk silica tread properties versus Eecosil® 230MG=1.0.

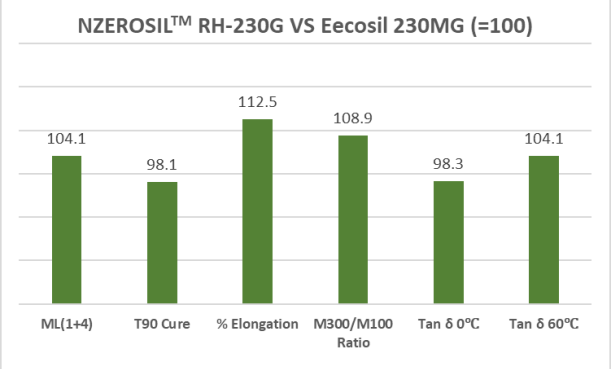

Figure 12. Bar graph of NZEROSIL™ RH-230G rice husk silica tread properties versus Eecosil® 230MG=100.

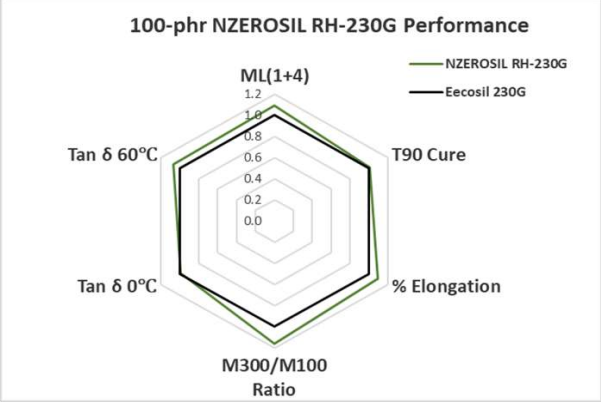

Figure 13. Radar plot of NZEROSIL™ RH-230G rice husk silica tread properties versus Eecosil® 230G=1.0.

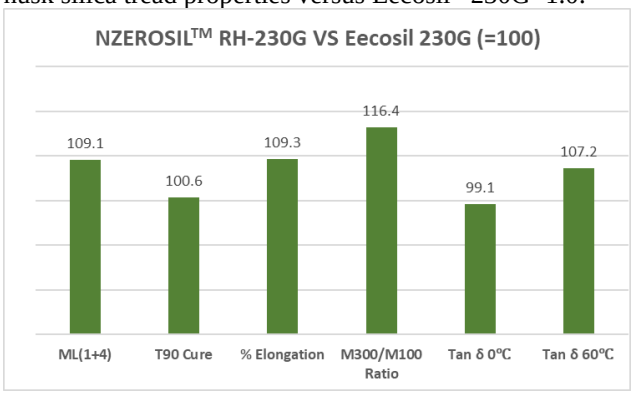

Figure 14. Bar graph of NZEROSIL™ RH-230G rice husk silica tread properties versus Eecosil® 230G=100.

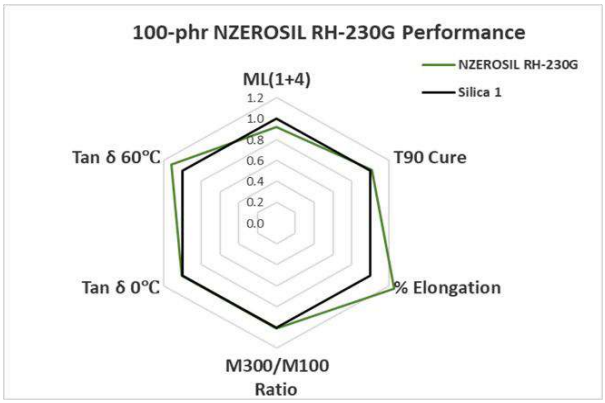

Figure 15. Radar plot of NZEROSIL™ RH-230G rice husk silica tread properties versus Silica 1=1.0.

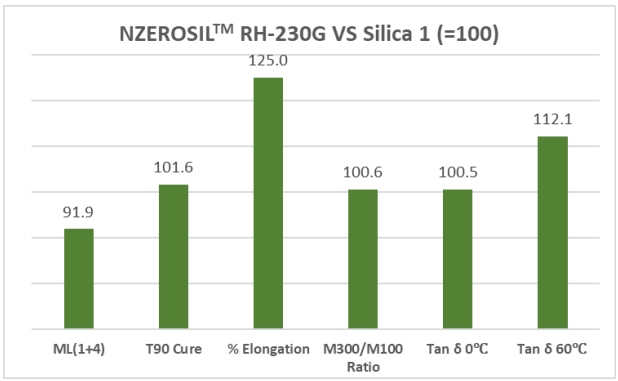

Figure 16. Bar graph of NZEROSIL™ RH-230G rice husk silica tread properties versus Silica 1=100.

SEM / ImageJ analysis shows highly dispersible Eecosil® 230MG microgranular silica gave desirably lowest %-white area values, followed by Eecosil® 230G. NZEROSIL™ RH-230G gave comparable dispersion to Silica 1, see Figure 17. Since only small differences were measured between the average particle size distributions, conclusions were not drawn, see Figure 18.

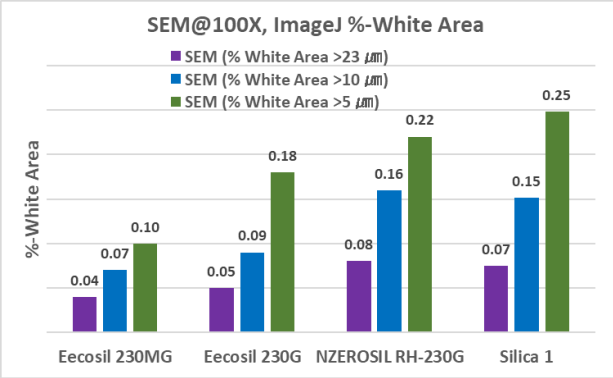

Figure 17. %-White areas of NZEROSIL™ RH-230G, Eecosil® 230MG, Eecosil® 230G and Silica 1 treads.

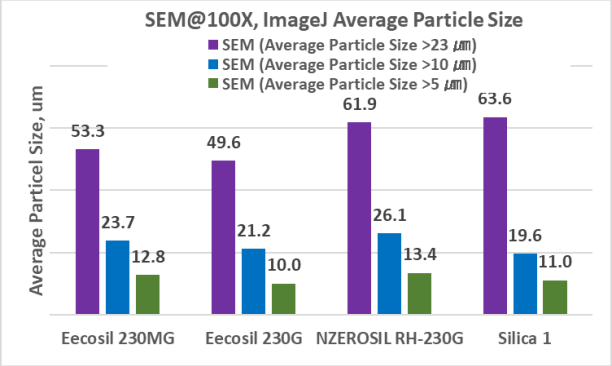

Figure 18. Average particle size distributions of NZEROSIL™ RH-230G, Eecosil® 230MG, Eecosil® 230G and Silica 1 treads.

Tread performance depends upon both material selection and efficient mixing. There are many variables. Dispersion in rubber requires: (1) Quick incorporation of silica pellets into the mix chamber. Microgranules are the desirable physical form since they are dust-free and have a more uniform pellet size. (2) Mechanical breakdown into agglomerates. (3) Breakdown into aggregates is essential for reinforcing rubber. Aggregate structures are chemically bonded during synthesis and cannot be broken down any further by more mechanical mixing. Downstream process steps after acid neutralization are important. (4) Homogenous distribution of aggregates throughout the rubber matrix. (5) Hydrophobation of silica surface silanols with the organosilane at higher temperatures. Unfortunately, these steps do not happen in series, but are convoluted occurring together. %-White areas and particle size distributions (lower is better) can be a direct quantitative measure. The M300/M100 ratio (higher is better) is the indirect test.

4. Conclusions

Results in a 100-phr silica tread modeled for UHP, EV and LT tires showed that the sustainable high surface area NZEROSIL™ 230G silica made from bio-renewable rice husk gave equivalent performance to the Eecosil® 230G granules and highly dispersible Eecosil® 230MG microgranules made from recycled broken glass. Tread performance was comparable to commercial Silica 1. A 5-pass mixing sequence with stage 3 remill better dispersed 100-phr of high surface area silicas reducing %-white area values and promoting the silica-organosilane hydrophobation reaction and optimize the M300/M100 reinforcement index. Adding silica in three steps was needed with this very high loading of high surface area silica to get better tread performance.

5. References

1. R. Rauline (to Michelin), US 5,227,425 (July 1993).
2. French application (by Rhone Poulenc) 157 703.
3. https://www.oscsilica.com/
4. L. R. Evans, S. P. Lee, W. H. Waddell, and C. S. Wu, *Rubber & Plastics News*, 25-28, Sept 4, 2017.
5. T. Y.-T. Lin, S. Lee, C. Wu, D. Liao, and W. H. Waddell, *Rubber News*, 31-34, Sept 4, 2023.
6. https://en.wikipedia.org/wiki/Silicate_mineral
7. https://www.cancer.gov/about-cancer/causes-prevention/risk/substances/crystalline-silica
8. https://www.researchgate.net/publication/342274384/figure/tbl1/AS:903762738675720@1592485236662/Ash-and-Silica-Content-of-Plants-6.png
9. https://en.wikipedia.org/wiki/List_of_countries_by_rice_production
10. S. K. S. Hossain, L. Mathur and P. K. Roy, *J. Asian Ceramic Societies*, 6(4), 299-313 (2018).
11. P. Deshmukh, J. Bhatt, D. Peshwe, and S. Pathak (Visvesvaraya National Institute of Technology), *Transactions of the Indian Institute of Metals*, 65, 63 (2012).
12. I. J. Fernandes, D. Calheiro, A. G. Kieling, C. A. M. Moraes, T. L. A. C. Rocha, F. A. Brehm, and R. C. E. Modolo (U do Vale do Rio dos Sinos-Brazil), Fuel, 165 351–359 (2016).
13. T. Y.-T. Lin, S. P. Lee, C. S. Wu, D. Liao, and W. H. Waddell, *Rubber News*, 17-22, Sept 30, 2024.
14. S. de Cayeux, L. Guy, C. Boivin, T. Chaussée, M. Gaube, A. Honoré-Gouger, A. Monton, and A. Hebbache (Solvay), Tire Technology Expo, 2017.
15. T. Chaussee (Solvay), Tyre Tech Expo 2018.
16. T. Y.-T. Lin, S. P. Lee, C. S. Wu, D. Liao, A. Lin, and W. Waddell, *Rubber News*, 24-9, Sept 1, 2025
17. C. Clarke, M. Hensel (Schill+Seilacher "Struktol"), Rubber Division, ACS, Cleveland, OH (2003).
18. J. Vander Kooi (Struktol), International Tire Conference & Exposition, Akron, OH (2006).

Development of Thermoplastic Polyurethane/Natural Rubber Blends Using Compatibilized Epoxidized Natural Rubber for 3D Printing

Torfan Srisuwanno[1], Piyawadee Luangchuang[1], Christopher Bascucci[2], Frank Clemens[2], Yeampon Nakaramontri*[1]

[1] *Sustainable Polymer & Innovative Composite Materials Research Group, Department of Chemistry, Faculty of Science, King Mongkut's University of Technology Thonburi, Bangkok 10140, Thailand.*

[2] *Department of Advanced Materials and Surfaces, Empa-Swiss Federal Laboratories for Material Science and Technology, Ueberlandstrasse 129, Dübendorf 8600, Switzerland.*

*E-mail: yeampon.nak@kmutt.ac.th

Abstract

Thermoplastic vulcanizates (TPVs) composed of thermoplastic polyurethane (TPU) and bio-based natural rubber (NR) were developed *via* material extrusion additive manufacturing (MEx-AM) for 3 D-printing applications. TPU was selected as the primary matrix polymer because of its crystalline multi-block copolymer structure consisting of alternating hard and soft segments. However, TPU alone exhibits limited elasticity, damping capability, and water resistance. To address these limitations, NR was blended with TPU, and epoxidized natural rubber (ENR) was employed as a compatibilizer. Dynamically vulcanized TPU/NR blends with varying ENR contents were prepared to examine their effects on blend performance. The addition of ENR significantly improved tensile strength, elongation at break, and toughness. The blend containing 3 phr ENR showed the highest impact strength and energy absorption, which is attributed to increased shear viscosity and improved interfacial interactions between the polar functional groups of TPU and ENR. ENR also facilitated better dispersion of rubber domains within the TPU matrix. However, excessive ENR content (>3 phr) led to agglomeration of rubber particles, resulting in reduced mechanical performance. Based on these findings, the optimal 3 phr ENR blend was selected for 3 D-printing trials. Successful printing was achieved using a nozzle temperature of 210 °C, bed temperature of 60 °C, and print speed of 7 mm/s, producing smooth surfaces and mechanically robust structures. Preliminary demonstrations confirmed the ability to fabricate complex honeycomb geometries with high flexibility and good structural integrity. Nonetheless, higher rubber contents caused nozzle clogging, indicating that further optimization of material formulation and printing parameters is required.

Keywords: Thermoplastic polyurethane, Natural rubber, Epoxidized natural rubber, Compatibilizer, 3D printing

1. Introduction

In recent years, growing environmental concerns have accelerated the development of bio-based polymers derived from renewable resources, engineered to be reprocessable, recyclable, and durable under demanding conditions. Among these approaches, blending thermoplastics (e.g., polypropylene, high-density polyethylene) with natural rubber (NR) has attracted significant attention, leading to the creation of thermoplastic vulcanizates (TPVs), a subclass of thermoplastic elastomers (TPEs). TPVs are typically produced through dynamic vulcanization of immiscible thermoplastic–elastomer blends, forming crosslinked rubber domains finely dispersed in a thermoplastic matrix that combines elasticity, melt processability, and mechanical strength [1].

Natural rubber (NR), consisting of *cis*-1,4-isoprene repeating units, is a renewable and abundant biomaterial in tropical regions such as Thailand. Its excellent elasticity and resilience make it an attractive component in bio-

based thermoplastic systems [2]. However, the inherent nonpolarity of NR often leads to incompatibility with polar thermoplastics, resulting in weak interfacial adhesion and compromised mechanical performance [1,3].

Thermoplastic polyurethane (TPU), a segmented block copolymer with alternating hard and soft segments, offers high mechanical strength, oil resistance, and excellent aging stability. Nonetheless, TPU exhibits limited elasticity and damping capability [3,4]. Blending TPU with NR can enhance flexibility, although the polarity mismatch reduces interfacial interaction. To address this challenge, epoxidized natural rubber (ENR), particularly ENR-25, has been widely employed as an effective compatibilizer. The epoxy groups introduced during NR epoxidation interact favorably with urethane linkages in TPU, improving compatibility, interfacial adhesion, and the overall mechanical behavior of the blends [3].

In this study, TPU/NR blends compatibilized with ENR were developed for material extrusion additive manufacturing (3D printing). The TPU/NR ratio was fixed at 95/5, while the ENR content was varied at 0, 3, 5, and 10 phr. The effects of ENR concentration on the blend properties were investigated through mechanical testing, impact strength, rheological analysis, morphological characterization, and 3D printing performance evaluation. This study aims to determine the optimal ENR loading that enhances interfacial adhesion, mechanical performance, and printability of TPU/NR-ENR blends. It also seeks to bridge the gap between renewable polymer utilization and the fabrication of high-performance, reprocessable elastomeric materials for flexible and sustainable 3D printed applications.

2. Experimental

2.1 Material

Thermoplastic polyurethane (TPU) with a hardness of 95 Shore A and a density of 1.14 g/cm³, supplied by BASF (Nanjing, China), was used as the matrix polymer. Epoxidized natural rubber (ENR-25) with a density of 0.97 g/cm³, obtained from Muang Mai Guthrie Co., Ltd. (Surat Thani, Thailand), was used as a compatibilizer. Natural rubber (NR, STR 5L grade) with a density of 0.92 g/cm³ was supplied by Boss Optical Ltd. (Songkhla, Thailand). Modified zinc oxide nanoparticles with nanosilica (ZnO–SiO_2) with a density of 4.00 g/cm³ was provided by Global Chemical Co., Ltd. (Samut Prakan, Thailand). Stearic acid and sulfur were purchased from Imperial Industrial Chemical Co., Ltd. (Bangkok, Thailand). Wingstay-L was obtained from Synthomer Co., Ltd. (Shanghai, China), and dibenzothiazyl disulfide (MBTS) was supplied by Flexsys (Illinois, USA).

2.2 Preparation of NR compound

Natural rubber (NR) and epoxidized natural rubber (ENR) were first masticated in an internal mixer at 60°C and 60 rpm for 3 min to reduce molecular weight and surface tension, facilitating uniform mixing and dispersion. The ENR content varied at 0, 3, 5, and 10 phr as shown in Table 1. After mastication, the compounding ingredients were added sequentially, each mixed for 1 min, followed by the addition of crosslinking agents and an extended mixing time of 2 min to ensure homogeneity, as summarized in Table 1. Mixing was performed in a 500 cm³ internal mixer (MX75, Chareon Tut Co. , Ltd. , Thailand) with a fill factor of 0.75. The resulting compound was sheeted on a two-roll mill and allowed to rest at room temperature before blending with TPU.

2.3 Preparation of dynamically cured TPU/NR-ENR blends

The rubber compound was blended with thermoplastic polyurethane (TPU) at 180 °C and 60 rpm using an internal mixer. The TPU/NR–ENR ratio was fixed at 95/5, as shown in Table 1. The mixing process began with melting of the TPU, which was identified by the initial torque peak. Once the torque stabilized (after approximately 4–5 min), the rubber compound was introduced. Mixing continued until dynamic vulcanization occurred, indicated by the appearance of a second torque peak. The blend was then mixed for an additional 4–5 min until the torque reached a steady state, confirming the formation of finely dispersed, vulcanized rubber domains within the continuous TPU matrix. The resulting TPVs

were subsequently granulated and compression-molded at 190 °C to prepare the test specimens.

Table 1 Formulation and Mixing schedule the dynamic vulcanization of TPU/NR-ENR blend.

Chemicals	**Contents (phr)**	**Time (min)**
Step 1 NR-ENR compound		
NR	100	0:00
ENR-25	0, 3, 5, and 10	0:00
Stearic acid	1	3:00
ZnO-SiO_2	5	4:00
Wingstay-L	1	5:00
MBTS	2.5	6:00
Sulfur	1	7:00
Dump		10:00
Step 2 TPU/NR-ENR Dynamic vulcanization		
TPU pellets	95	0:00
NR-ENR compound	5	8:00
Dump		14:00

2.4 Extrusion and pelletizing

The mixed TPV samples were granulated into small flakes and extruded using a modular parallel twin-screw extruder (Process 11, Thermo Fisher Scientific, Germany). A non-uniform screw configuration was employed to promote reactive blending and ensure efficient melt homogenization throughout processing. The temperature profile across the barrel zones was set to 155°C (Zone 2), 160°C (Zone 3), 170°C (Zone 4), 175°C (Zones 5–6), 180°C (Zone 7), 185°C (Zone 8), and 190°C at the die. The extruded strands were then pelletized and used as feedstock for subsequent 3D-printing applications.

2.5 Characterization

2.5.1 Tensile properties

Tensile tests were conducted on dumbbell-shaped specimens (ASTM D638-14, Type I) using a universal testing machine (Zwick Z 1545, Zwick GmbH & Co. KG, Ulm, Germany). Measurements were performed at room temperature with a 50 kN load cell and a crosshead speed of 500 mm/min.

2.5.2 Izod impact strength

Impact resistance was evaluated using the Izod impact tester (Model No. 258, Yasuda Seiki Seisakusho Co., Ltd., Japan). The specimens, notched in a V-shape with a 0.25 mm radius and 45° angle, were prepared with dimensions of 64 mm × 12.7 mm × 3.2 mm, following ASTM D256–10. The energy absorbed to fracture the specimen was recorded as the impact energy. The impact strength was calculated using Equation 1

$$\text{(Impact strength)} = \frac{\text{E } (absorbed\ energy)}{\text{A } (the\ cross\text{-}sectional\ area\ at\ the\ notch)} \quad (1)$$

2.5.3 Rheological behavior

The flow behavior of the TPV samples was evaluated using a capillary rheometer (Model RG25, Göttfert, Germany). Approximately 100 g of each sample was tested at 200°C, a temperature appropriate for complete polymer melting. A capillary die with a 1 mm diameter, 20 mm length, and 180° entry angle was used to ensure stable, accurate flow during measurement. Shear rates ranging from 10 to 2,000 s^{-1} were applied to simulate typical processing conditions. The rheological data obtained included melt viscosity, shear stress–shear rate relationships, and characteristic flow behavior such as shear-thinning response.

The morphology of the TPVs was examined using a field-emission scanning electron microscope (FE-SEM, Nova NanoSEM 450, EDS XFlash 6 Series, FEI, Australia) equipped with energy-dispersive X-ray spectroscopy (EDS). The samples were cryo-fractured in liquid nitrogen prior to imaging. To enhance contrast between phases, the TPU matrix was selectively extracted by immersing the fractured specimens in boiling xylene for 8 hours. After solvent extraction, the samples were thoroughly dried and sputter-coated with gold before SEM observation.

A selected TPU/NR–ENR blend was assessed for its 3D-printing performance using a material extrusion additive manufacturing (MEx-AM) system. Printing was conducted on a Cartesian-type 3D printer equipped with a screw-extrusion print head (The Voladora NX+, IT3D Group, Spain) fitted with a 0.4 mm nozzle as shown in Figure 1.

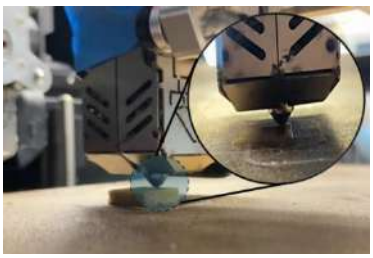

Figure 1 The Voladora NX+ 3D nozzle printer used for printing a honeycomb structure.

3. Results and discussion

3.1 Mixing torque–time behavior of TPU/NR–ENR blends

The mixing torque–time profiles of TPU/NR–ENR blends at a 95/5 ratio with varying ENR contents (0, 3, 5, and 10 phr) are shown. The initial torque increase observed between 0 and 150 s corresponds to the resistance of solid TPU pellets during the early stages of mixing. As the TPU gradually melted, the torque decreased and stabilized between approximately 250 and 530 s, indicating complete melting of the TPU matrix. Following the addition of the NR compound (540–600 s), the torque rose again due to increased rotor resistance associated with rubber crosslinking and interfacial reactions between the polar functional groups of ENR and TPU.

During this stage, the epoxide rings in ENR undergo ring-opening under high shear and elevated temperatures, generating hydroxyl (–OH) groups that can interact with the carbonyl (–C=O) groups in the urethane segments (–NH–CO–) of TPU [5,6]. The magnitude of the second torque peak increases with ENR content, reflecting the degree of interfacial bonding and the extent of dynamic crosslinking within the blend. Notably, the blend containing 3 phr ENR exhibits the highest second torque peak, suggesting optimal interfacial interactions and improved dispersion of the rubber phase within the continuous TPU matrix. The subsequent decrease in torque after approximately 625 s indicates the completion of crosslinking and the achievement of a uniformly dispersed NR phase.

The interactions among NR, ENR, and TPU can be further understood by considering the chemical reactions and intermolecular forces occurring during mixing. Previous studies have reported that [5,7], the ENR–TPU system exhibits several intermolecular interactions, including:

(1) Hydrogen bonding (–OH···O=C–NH) can occur between the hydroxyl groups (–OH) of ENR and the urethane N–H groups of TPU.

(2) Dipole–dipole interactions (–OH···O=C-) may form between hydroxyl groups (–OH) and carbonyl (–C=O) groups in urethane linkages.

(3) Dipole–induced dipole interactions (O=C–···CH_2–$C(CH_3)$–CH(OH)–CH_2–O–) the dipole of carbonyl groups in TPU induces temporary dipoles in the nonpolar hydrocarbon chains of ENR. These interactions collectively enhance interfacial compatibility. In the NR–ENR system, although NR itself lacks strongly polar functional groups, dipole–induced dipole interactions occur between the hydroxyl groups of ENR and the nonpolar NR chains [8,9], supplemented by van der Waals forces among nonpolar NR and ENR chains and hydrogen bonding among adjacent ENR molecules.

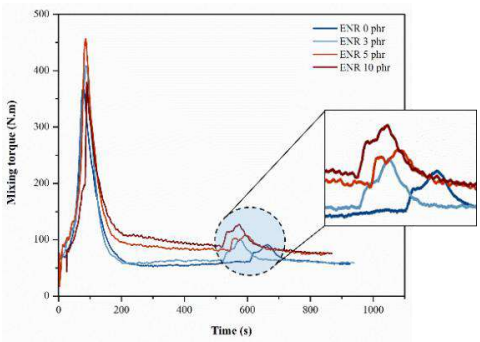

Figure 2 Relationship between mixing torque and time for dynamically vulcanized TPU/NR-ENR (95/5) blends with varying ENR content.

3.2 Mechanical properties

The stress–strain curves of thermoplastic elastomers typically show thermoplastic deformation behavior at low strains (<50%) and elastomeric characteristics at higher strains [10,11]. These materials often exhibit clear ductility with a distinct yield point. In contrast, the TPU/NR–ENR blends examined in this study displayed no observable yield point. This behavior is attributed to the chemical linkages between the hard and soft segments of TPU, which inhibit localized yielding and allow the material to deform elastically until fracture. As a result, the blends exhibit deformation behavior that differs from conventional thermoplastics.

For the TPU/NR–ENR blend with a 95/5 ratio and 3 phr ENR, the tensile properties including tensile strength, elongation at break, toughness, Young's modulus, and 100% modulus were highest, followed by a gradual decline as ENR content increased. In contrast, hardness progressively increased with higher ENR loading. The superior mechanical performance observed at 3 phr ENR is attributed to improved interfacial adhesion between the TPU and NR phases, which enhances rubber particle dispersion and enables more effective stress transfer throughout the matrix. This leads to greater resistance to deformation and improved overall mechanical integrity.

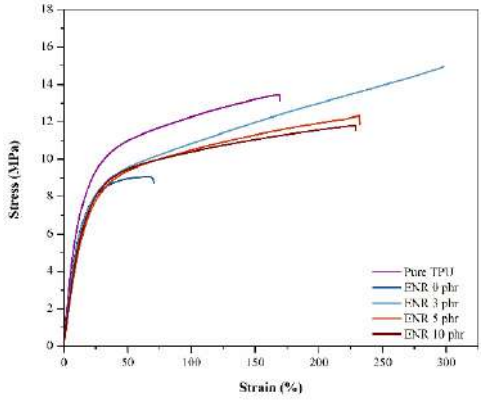

Figure 3 Relationship between stress-strain of TPU and dynamically vulcanized TPU/NR-ENR (95/5) blends with varying ENR content.

Table 2 Mechanical properties of TPU and dynamically vulcanized TPU/NR-ENR (95/5) blends with varying ENR content.

Properties	TPU/NR blend with different loadings of ENR				
	Pure TPU	0 phr	3 phr	5 phr	10 phr
Tensile strength (MPa)	13.56 ± 1.69	9.03 ± 0.26	14.28 ± 0.65	12.21 ± 0.69	11.48 ± 0.28
Elongation at break (%)	182.56 ± 19.26	70.65 ± 4.18	479.13 ± 15.31	232.21 ± 28.02	228.45 ± 23.11
Young's modulus (MPa)	82.16 ± 1.02	68.24 ± 4.23	69.52 ± 3.43	66.46 ± 4.28	66.38 ± 4.64
100% Modulus (MPa)	12.87 ± 0.27	-	10.78 ± 0.09	10.43 ± 0.11	10.42 ± 0.16
Toughness (MJ/m^3)	829.26 ± 73.71	228.59 ± 25.68	1882.91 ± 108.74	954.15 ± 119.70	847.22 ± 116.05
Hardness ShoreA	95.00 ± 0.25	90.00 ± 0.58	90.33 ± 1.00	90.33 ± 1.53	90.67 ± 0.58

3.3 Impact strength

Figure 4 presents the impact strength of TPU/NR blends at a 95/5 ratio with varying ENR contents. All TPU/NR–ENR materials exhibited excellent impact resistance, with no visible cracks or fractures observed during testing. Among all formulations, the blend containing 3 phr ENR showed the highest impact strength, which gradually decreased as ENR content increased to 10 phr. This trend indicates that an optimal ENR concentration enhances interfacial adhesion between the TPU and NR phases, thereby improving the material's ability to absorb and dissipate impact energy—consistent with the mechanical-property improvements reported earlier.

During impact loading, the dispersed rubber domains act as stress-transfer and energy-dissipating sites that deform or cavitate, effectively reducing stress concentration and suppressing crack propagation. The blend with 3 phr ENR provides the most efficient stress transfer and energy absorption due to the uniform dispersion of rubber domains and strong interfacial bonding [9,12]. In contrast, excessive ENR content leads to agglomeration of rubber particles and diminished interfacial efficiency, as NR–ENR and ENR–ENR interactions disrupt homogeneous stress distribution. Consequently, the impact strength decreases at higher ENR loadings.

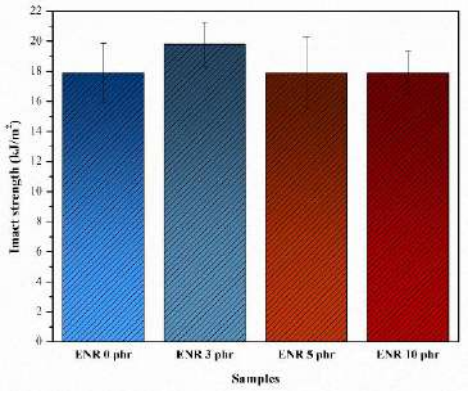

Figure 4 Impact strength for dynamically vulcanized TPU/NR-ENR (95/5) blends with varying ENR content.

3.4 Rheological behavior

As shown in Figure 5(a)–(b), the TPU/NR–ENR blend with a 95/5 ratio exhibits typical shear-thinning behavior, where the apparent viscosity decreases as the

shear rate increases. The incorporation of 3 and 5 phr ENR markedly increases both the apparent shear stress and viscosity at low shear rates, indicating stronger interfacial interactions and higher structural resistance to flow. At higher shear rates, however, the apparent shear stress and viscosity of all formulations converge. This convergence is attributed to molecular orientation and chain alignment in the direction of flow, which reduce intermolecular entanglement and minimize flow resistance, thereby diminishing the influence of interfacial interactions. The enhanced viscosity at low shear rates for the 3 and 5 phr ENR blends is attributed to optimal ENR content promoting stronger interfacial reactions between polar functional groups, such as the carbonyl groups in TPU and the epoxide groups in ENR, resulting in improved interphase bonding and interfacial adhesion. In contrast, when the ENR content reached 10 phr, this trend reversed. The reduction in apparent viscosity is likely due to agglomeration of rubber particles within the matrix, which weakens interfacial adhesion and reduces resistance to flow.

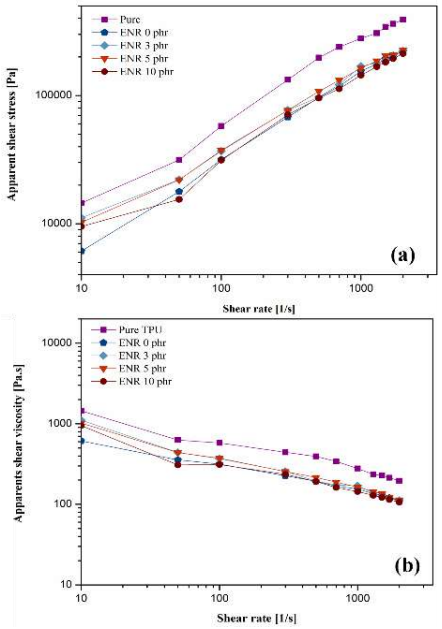

Figure 5 Rheological behavior of dynamically vulcanized TPU/NR-ENR (95/5) blends with varying ENR content at 200°C (a) Apparent shear stress as a function of apparent shear rate, and (b) Apparent shear viscosity as a function of apparent shear rate.

3.5 Morphology

At the TPU/NR blend ratio of 95/5, as shown in Figure 6(a), the blends without ENR exhibit minimal rubber-particle agglomeration and good dispersion of ZnO and sulfur. No detectable voids are observed, indicating limited interpenetration between the TPU and NR phases. With the addition of 3 phr ENR (Figure 6(b)), larger rubber domains and dense Zn/S accumulations become evident, suggesting increased crosslinking within the NR/ENR regions resulting from enhanced rubber-particle aggregation. The appearance of voids within these domains indicates partial penetration of TPU into the rubber phase [11,13], facilitated by interactions between the polar functional groups of TPU and ENR. At 5 phr ENR (Figure 6(c)), the rubber domains show further agglomeration and a reduction in internal voids, implying stronger self-association at elevated ENR contents. This observation aligns with the decline in mechanical performance at higher ENR loadings.

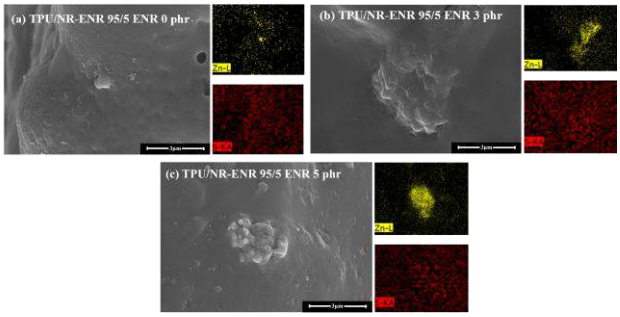

Figure 6 SEM micrographs of TPU/NR-ENR 95/5 with different content of ENR (a) 0 phr, (b) 3 phr and (c) 5 phr after extraction of TPU phase.

3.6 Printing Behavior of TPU/NR–ENR Blends

When 3D printing the TPU/NR–ENR (95/5) blend containing 3 phr ENR, the initial printing parameters were set using an infill density of 15%, a 0.4 mm nozzle, and a printing temperature of 220 °C. Due to the high shear viscosity of the material, an elevated temperature was required to sufficiently reduce viscosity and enable continuous, uniform extrusion through the nozzle. The bed temperature was maintained at 60 °C, with a layer height of 0.2 mm, an extrusion multiplier of 2.5, a printing speed of 15 mm/s, and three perimeter walls. As shown in Figure

7(a), some printed layers appeared irregular, exhibiting rounded edges and corners.

To improve print quality, the printing speed was reduced to 12 mm/s, which produced more uniform layers and eliminated unmolten residues, as illustrated in Figure 7(b). However, slight edge irregularities and gaps between top-layer filaments were still evident. To address these issues, the infill density was decreased to 7%, the specimen height to 10 mm, and the perimeter walls to two layers. The extrusion multiplier was increased to 4 to minimize discontinuities between layers. Because this adjustment substantially increased material flow, the printing speed was further reduced to 7 mm/s to ensure proper coordination between extrusion rate and nozzle movement. Without this correction, excessive extrusion would have led to filament distortion, swelling, and reduced dimensional accuracy. With the optimized parameters, the printed specimen displayed sharper corners and smooth, continuous layering, as presented in Figure 7(c).

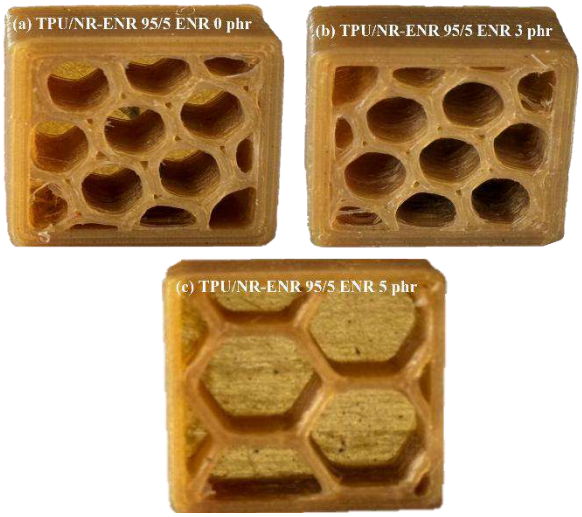

Figure 7 Printed TPU/NR-ENR (95/5 with 3 phr ENR) structures with varying parameters:(a) 15 mm/s, 3 walls; (b) 12 mm/s, 3 walls; (c) 7 mm/s, 2 walls, 7% infill.

4. Conclusion

The study demonstrates that ENR effectively acts as a compatibilizer in TPU/NR for 3D printing applications. The torque–time analysis revealed that the addition of ENR enhanced interfacial interactions TPU. Among all formulations, the blend containing 3 phr ENR exhibited the highest second torque peak, superior tensile and impact properties, and improved interfacial adhesion due to optimal phase compatibility. Rheological analysis confirmed shear-thinning behavior, with higher apparent viscosity at low shear rates for ENR-containing blends, indicating stronger interfacial resistance to flow. SEM micrographs supported these findings, showing well-dispersed rubber domains and partial phase interpenetration of TPU at 3 phr ENR. In 3D printing trials, the optimized blend (3 phr ENR) achieved uniform extrusion and smooth surface morphology under refined printing conditions, confirming its potential as a flexible, bio-based elastomer suitable for additive manufacturing applications.

Acknowledgements

This work was supported by the Petchra Pra Jom Klao Master's Degree Research Scholarship from King Mongkut's University of Technology Thonburi. The research was also funded by Thailand Science Research and Innovation (TSRI) Basic Research Fund: Fiscal year 2026 under project number FRB690020/0164 was acknowledged. The authors would like to express their gratitude to the Swiss National Science Foundation (SNSF) research and innovation programme SPIRT under grant agreement No 223,840 (SPRINT Project) for supports.

5. References

1. Pichaiyut, S.; Faibunchan, P.; Kummerlöwe, C.; Vennemann, N.; Nakason, C. *J. Polym. Environ.* **2023**, *31*, 1051.
2. Faibunchan, P.; Pichaiyut, S.; Kummerlöwe, C.; Vennemann, N.; Nakason, C. *J. Polym. Environ.* **2020**, *28*, 1050.
3. Pichaiyut, S.; Nakason, C.; Vennemann, N. *Iran. Polym. J.* **2012**, *21*, 65.
4. Kalkornsurapranee, E.; Nakason, C.; Kummerlöwe, C.; Vennemann, N. *J. Appl. Polym. Sci.* **2013**, *128*, 2358.
5. Pongdong, W.; Kummerlöwe, C.; Vennemann, N.; Thitithammawong, A.; Nakason, C. *J. Polym. Environ.* **2018**, *26*, 1145.

6. Nakaramontri, Y.; Kummerlöwe, C.; Nakason, C.; Vennemann, N. *Polym. Compos.* **2015**, *36*, 2113.
7. Srisuwanno, T.; Johns, J.; Bascucci, C.; Clemens, F.; Nakaramontri, Y. *Express Polym. Lett.* **2025**, *19*, 1053–1072.
8. Abdul Majid, R.; Ismail, H.; Mat Taib, R. *Polym.-Plast. Technol. Eng.* **2018**, *57*, 1507.
9. Kamal, M. M.; Hadithon, K. A.; Bakar, R. A. Natural rubber modified asphalt. *Proceedings of the IOP Conference Series*, Johor, Malaysia, December 19-20, 2019*;* IOP Publishing: Bristol, U.K., 2020; Vol. 498, p 012001.
10. Al Minnath, M.; Unnikrishnan, G.; Purushothaman, E. *J. Membr. Sci.* **2011**, *379*, 361.
11. Prasopdee, T.; Pannoppa, T.; Porbun, P.; Luangchuang, P.; Promoppatum, P.; Nakaramontri, Y. *Ind. Crops Prod.* **2023**, *203*, 117238.
12. Lebarbe, T. Synthesis of Novel "Green" Polyesters from Plant Oils: Application to the Rubber-Toughening of Poly(L-lactide). Ph.D. Thesis, Université Sciences et Technologies-Bordeaux I, Bordeaux, France, 2013.
13. Kalkornsurapranee, E.; Vennemann, N.; Kummerlöwe, C.; Nakason. C. *Iran. Polym. J.* **2012**, *21*, 689.

Progress in Rubber Analysis, Testing and Standards

IRC 2025
BANGKOK, THAILAND

International Rubber Conference 2025 (IRC 2025)

Development of an Integrated Design, Analysis and Evaluation System for Rubber Components

Changsu Woo[1]*, Sanghee Choi[2], Sangkyun Kim[3]

[1] *156 Gajeongbuk-ro Yuseong-gu, Daejeon, South Korea.*

[2] *157 Gongdan-dong, Gumi, Gyeongsangbuk-do, South Korea.*

[3] *7 Geumsa-dong, Geumjeong-gu,Busan, South Korea.*

*E-mail: cswoo@kimm.re.kr

Abstract

The objectives of this study are to establish test methods of rubber material and to develop a database of rubber material properties and to evaluate the performance of rubber components and to construct the prediction system of fatigue lifetime. The fatigue lifetime prediction methodology of the rubber component was proposed by incorporating finite element analysis and fatigue damage parameters from the fatigue test. Database of mechanical properties of anti-vibration rubber material, such as compound conditions, mechanical properties, degradation, and fatigue lifetime were developed. Fatigue lifetime of engine rubber mount for automobiles was nearly exactly predicted by the developed method and the validity of the fatigue lifetime estimation method was verified. Using the developed integrated design system of rubber components, the time and expense required to develop rubber components were saved and the reliability of products is expected to be enhanced.

Keywords: Rubber components, Material properties, Finite element analysis, Fatigue test, Database

1. Introduction

For products aiming to be first class, the application of rubber components for most machines including vehicles have gradually increased to achieve high quality and reliability through low vibration and noise, and enhanced operation. Therefore, an analysis and design technology for rubber components is required [1]. As much attention has been paid to the assurance of the quality and durability of vehicles, the development of technology is required to enhance the durability and reliability of anti-vibration rubber components that are the most important components of vehicles [2]. Until now, however, rubber components have been developed by trial and error as well as experiences due to the special properties of rubber. Therefore, all aspects of performance testing, including design and analysis technology, are currently very vulnerable. In particular, the mechanical data of rubber material can be obtained only by experiment as there are many rubber compounds. Therefore, it is very difficult to develop a database of mechanical properties of rubber component and there are many obstacles to overcome in the fatigue lifetime estimation and evaluation technology due to insufficient manpower and technology [3]. In this study, likewise, a database was developed that include the mechanical properties of anti-vibration rubber material for vehicles including a compound conditions, mechanical properties, deterioration, and fatigue lifetimes. And then, a fatigue analysis model of rubber components was developed by associating the results of mechanical properties on rubber components with a database. The validity of the developed model was verified with the results of the actual fatigue tests. It is, therefore, expected to save on the time and expenses that are required for developing rubber components and will help to enhance reliability of products.

2. Integrated Design System

2.1 System configuration

Manuscripts Standard mechanical properties of rubber material have not yet been established because there are various combination components and content conditions required in the manufacturing processes. Performance improvement through property estimation and securing design technology of rubber component is a

key technology that is mandatory for advancing all machines and systems. According to recent advances in large scale and super computer, it is possible to analyze the behaviors of rubber components through nonlinear analysis with finite element methods and to apply systematic and analytical methods to designing rubber components [4]. In this study, the database of the mechanical properties of rubber material including compounding conditions was developed. Design and analysis system (RubDAS; Rubber component Design & Analysis System) was developed by integrating all these items. Integrated design system of rubber component in machine was developed to perform the systematic design and analysis of rubber components. These systems are, as shown in Figure 1(a), composed of: a rubber compound program (RubCOM: Rubber Compound), mechanical property database program (RubPRO: Rubber Property), and a fatigue lifetime estimation program of rubber components (RubFAT: Rubber Fatigue). These systems are integrated design and analysis systems that include all the processes required to design rubber components: rubber compound, the determination of material constants by rubber mechanical property tests, the strength and size design of rubber components, component design through finite element analysis, and the durability estimation of rubber components.

2.2 Rubber compound program

Database of rubber compound and mechanical properties of rubber material have not yet been developed because they are possible through many experiments due to various mechanical properties required by each consumer company and the component of rubber compounds are too vast. Consumer companies of rubber products depend on the results of experiments by rubber part makers rather than selecting rubber products based on clearly standardized mechanical properties. If database of mechanical properties of rubber material are developed, it is expected to achieve standardization and the independent development of prediction software of mechanical properties. After the main factors of rubber compound were selected and the effects of interaction between factors on the mechanical properties of rubber were understood, the characteristic equations that represented various mechanical properties were derived using a rubber compound program (RubCOM) in Figure 1(b). In this study, experiments were carried out by varying the quantity of carbon black, sulfur, vulcanization accelerators, activator ZnO, and stearic acid on the natural rubber polymer base, and then the effects of these materials on the mechanical properties of rubber compound were understood, deriving a relation that could quantitatively predict changes in mechanical properties according to each factor through statistical data analysis. Mechanical properties were obtained by setting five factors (carbon black, sulfur, vulcanization accelerators, ZnO, and stearic acid) to the fifth level to derive the relation. Based on the mechanical properties, the effect of each factor and regression coefficients through statistical analysis were investigated. The validity of models was checked by obtaining characteristic regression equations. The regression equations were better as the value of the R-square drew closer to 1. Experiments were repeatedly conducted to enhance reproducibility and reliability, and their order was arbitrarily determined to exclude the effects of other factors except for main factors. The compound program was developed based on this data from the experiments and characteristic regression equations.

2.3 Database of rubber property

For the finite element analysis of a hyper-elastic model on material such as rubber, it is very important to determine its exact mechanical properties. That is why, static tests, dynamic tests, and friction tests are necessary. Static tests include simple tension, simple compression, and pure shear tests [5]. If mechanical properties of rubber are obtained with the existing simple tension tests, it is likely to create errors in finite element analysis. Because the mechanical properties of rubber change according to the environment, it is necessary to conduct tests at both high and low temperatures. When the rubber is exposed to high temperature for a long time, it increases in its hardness by aging, and that poses an important problem in material tests and mechanical environments such as the

maximum strain and cyclic load needs to be considered in experiments. Database program of rubber mechanical property (RubPRO) are made to obtain the mechanical properties of rubber in various environments before finite element analysis. In these programs, a database of results of static test, dynamic test and friction test according to changes in the mechanical environment as well as at high, low, and warm temperature were developed. Using the database, the mechanical properties of the necessary materials could be easily obtained when new rubber components are designed. Figure 3(a) shows an initial screen of rubber mechanical property database program that is composed of a database of these: static, dynamic, friction, aging, and fatigue properties. Static properties include a curve fitting program of nonlinear material constants.

(a) Integrated of design system

(b) Rubber compound program

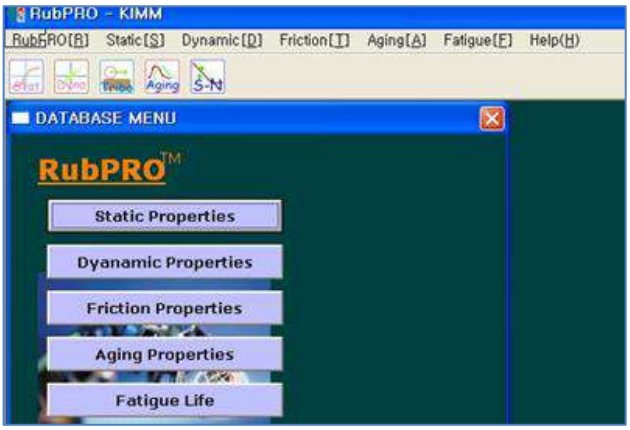

(c) Database of rubber properties

Fig. 1 Integrated of design system for rubber components

2.4 Fatigue lifetime prediction

Figure 2(a) shows the procedures to predict the fatigue lifetime of rubber components as follows: (1) using the results of material tests of rubber component to develop, finite element analysis of the component was conducted to the maximum strain in weak points; (2) fatigue tests were carried out for rubber specimens that had the same compound and mechanical properties as the components, and fatigue damage parameter was obtained from the relation of the maximum strain and fatigue lifetime; (3) the fatigue lifetime of rubber components could be predicted and evaluated using the analysis results of rubber component and the fatigue test results of rubber specimens. Fatigue lifetime curves are necessary for the same rubber materials to predict the fatigue lifetimes of rubber components. In this study, fatigue tests were conducted by manufacturing 3-dimensional fatigue specimens [6] that could reproduce the maximum tension strain by the fatigue load of rubber components as in Figure 2(b). Using the results of fatigue tests in various conditions, the correlation of fatigue lifetime with variables such as amplitude, mean displacement, and maximum tension displacement were obtained. As a result, the fatigue lifetime was similar irrespective of mean displacement and amplitude if the maximum tension displacement was fixed. the fatigue lifetime decreased as maximum tension displacement increased. The fatigue lifetime, therefore, could be represented irrespective of test conditions when the maximum tension displacement was a fatigue damage variable. Using the relation of the maximum tension

displacement and the Green-Lagrange strain that was the result of the analysis on specimens, the relation curves of Green-Lagrange strain and fatigue lifetime could be obtained as shown in Figure 2(c). The maximum tension displacement could be well represented with the maximum Green-Lagrange strain and fatigue lifetime was predicted according to the strain [7].

The database of fatigue properties, as shown in Figure2(d), includes this data: hardness, fatigue test conditions, fatigue lifetime, and aging conditions. Users could find the data after setting multiple search conditions by assigning the ranges of this data: hardness, average displacement, amplitude, the maximum displacement, and the maximum Green-Lagrange strain. The fatigue lifetime of anti-vibration rubber com-ponent used in the engine mount for automobiles was estimated to verify the validity of the fatigue lifetime prediction method of rubber component proposed in this study. Most fatigue cracks occurred at points where the strain was at a maximum value as shown in Figure 2(e) the results of the analysis were quite consistent with those of tests.

Figure 2(f) shows the relation the fatigue lifetime obtained in fatigue tests on actual rubber components and the predicted lifetime using the fatigue lifetime prediction equations of rubber specimens. Predicted fatigue lifetimes of rubber components for engine mounts as shown in Figure 9 was fairly consistent with the actual lifetime: this result verified the validity of the lifetime estimation method of rubber components proposed in this study.

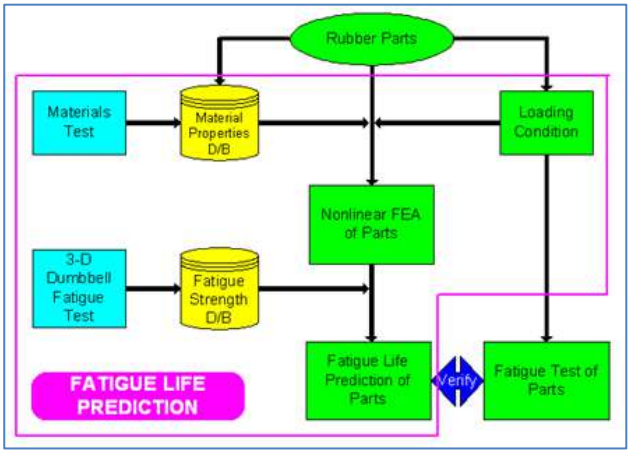

(a) Procedure to fatigue lifetime prediction

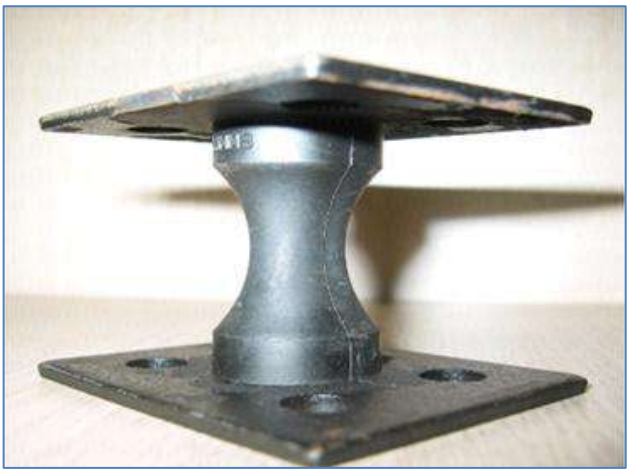

(b) 3-dimensional fatigue specimen

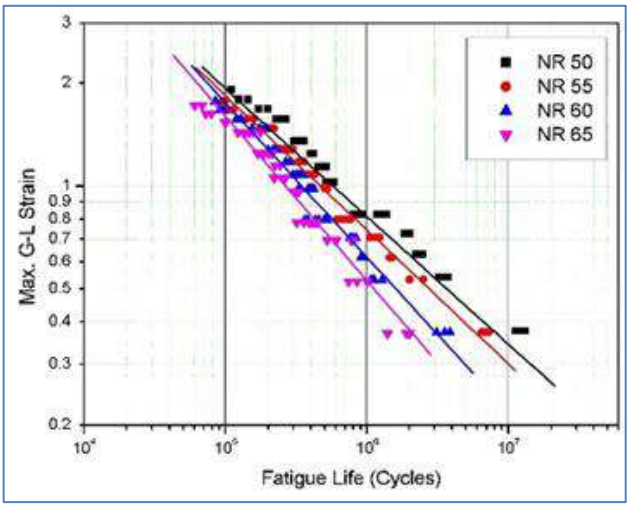

(c) Strain-fatigue life curves

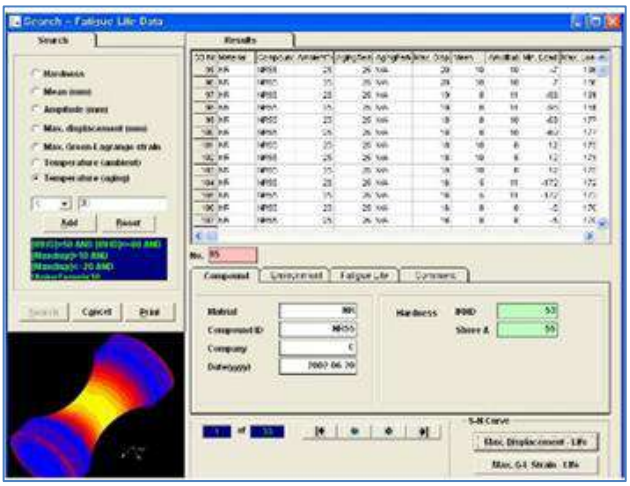

(d) Database of fatigue properties

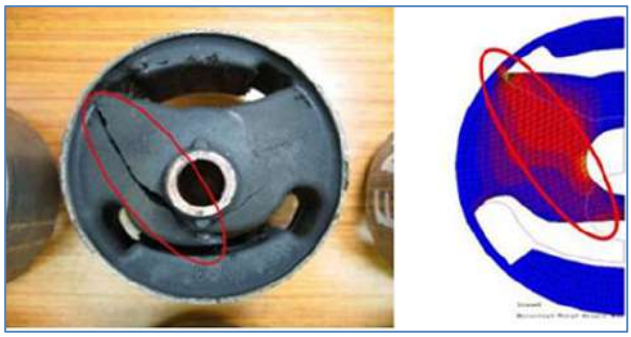

(e) Fatigue test and finite element analysis

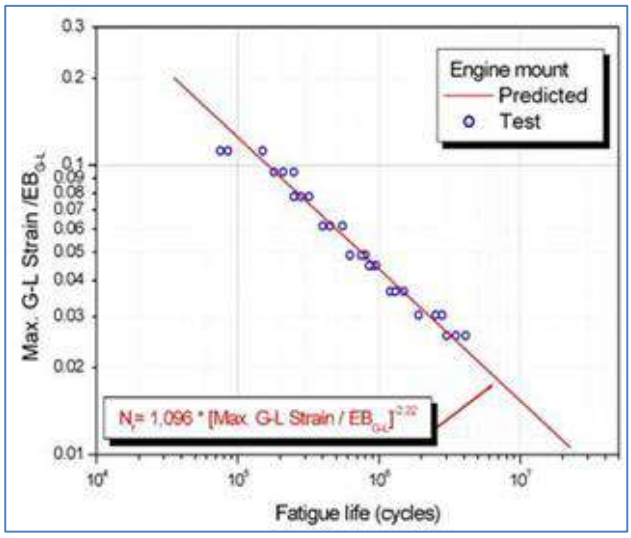

(f) Fatigue lifetime prediction

Fig. 2 Fatigue lifetime prediction of rubber components

3. Conclusions

The following conclusions were obtained through development of integrated design systems of rubber component for automobiles.

(1) To development the fatigue analysis process for rubber component, a fatigue lifetime prediction methodology was proposed by incorporating finite element analysis and fatigue damage parameter.

(2) In various test conditions, fatigue tests on three dimensional specimens were conducted to obtain fatigue lifetime according to rubber material, mean displacement, and changes in amplitude, and then the fatigue lifetime prediction equations were derived with maximum tension displacement and maximum strain as one of the fatigue damage parameters.

(3) Database of mechanical properties of anti-vibration rubber material, such as compound conditions, mechanical properties, degradation, and fatigue lifetime were developed.

(4) Fatigue lifetime of engine rubber mount for automobiles was predicted with high accuracy, which verified the validity of the developed estimation method.

(5) Using the developed integrated design system of rubber component, the time and expense required to develop rubber components were saved and the reliability of products is expected to be enhanced.

Acknowledgement

This work was supported by the materials and components technology development program (20022506) and Elastic material re-launch project in response to key strategic industries (RS-2024-00439120) funded by the Ministry of Trade, Industry and Energy of Korea.

References

1. Charlton. D. J., Yang. J., A Review of Methods to Characterize Rubber Elastic behavior for use in Finite Element Analysis, *Rubber Chemistry & Technology* 1993, 67,481-503.
2. Lake. G.J., Fatigue and Fracture of Elastomers, *Rubber Chemistry & Technology*, 1997, 68, 435-460.
3. Gent. A. N., Engineering with Rubber–How to design rubber components, Oxford University Press, NY, 1992.
4. Kim. W. D. & Kim, D. J., A study on the equi-biaxial tension test of rubber material, *KSAE*, 2003, 11, 95-104.
5. Mullin. L., *Rubber Chemistry & Technology*, 1969, 42, 339-362.
6. Takeuchi. K. & Nagakawa. M., *Int'l Polymer Sci*. 1993, 20, 64-69.
7. Fatemi. & Yang., Cumulative Fatigue Damage and Life Prediction Theories, *International J. of fatigue*, 1998, 20, 9-34.

The Role of Deformation Mode on Rubber Hysteresis and Its Dependency on Viscoelasticity

Shouliang NIE*, Junhua PANG, Yi ZHU, Wei HUANG, Xiaorong WANG
Zhongce Rubber Group Co. Ltd, Hangzhou, Zhejiang Province, 310018 China.
*E-mail: slnie@chaoyang.com

Abstract

Hysteresis, one of the fundamental characteristics of viscoelastic solids like rubber, is a long-standing source of challenges in both their production and application. Conventional wisdom has relied on simple rheological parameters such as loss factor, $tan\delta$, to access their relevance to hysteresis. However, those correlations can be unreliable as deformation modes vary significantly with real working conditions, and thus the mechanisms therein. This work elucidates the dependency of hysteresis on viscoelasticity for the three primary deformation modes, i.e., the energy-, strain-, and stress-controlled processes. We demonstrate the decisive viscoelastic parameters are $tan\delta$, E'', and $tan\delta/E'$ for each mode, respectively. This argument is experimentally validated through two case studies: the heat build-up (HBU) of rubber cylinders, and the rolling resistance (RR) of tires. Under fully strain-controlled cyclic compression, the HBU of tested samples only correlates linearly with the loss modulus, E''. While in stress-controlled mode, $tan\delta/E'$ presents the linear correlation with the temperature rise. For the examined tires with varying tread materials, an excellent correlation for RR is achieved by incorporating an exponent, *m*, on the denominator, yielding $tan\delta/E'^m$. These pracatical results robustly support our central argument that deformation mode fundamentally governs the relationship between hystersis and viscoelasticity.

Keywords: Viscoelasticity, Hysteresis, Deformation Mode, Heat Build-Up, Rolling Resistance

1. Introduction

Rubber and its composites filled with nanoparticles are extensively utilized in critical industrial applications such as tires and air springs due to their excellent mechanical properties. Those materials play a vital role in dynamic loading, cyclic mechanical fatigue, and chemical aging. As a typical viscoelastic material, their hysteresis loss characteristics [1] is of great interest for both industry and academia. This is primarily because the hysteresis determines heat generation, energy efficiency (such as tire rolling resistance), and even the safety of the product. It is important to noticed that the rubber components in the products could be loaded at quite different deformation modes. Depending on the location and operating conditions,[2] certain areas may experience constant strain amplitude deformation (i.e., strain-controlled), while other regions are under stress- or energy-controlled scenarios, as illustrated in Figure1a.

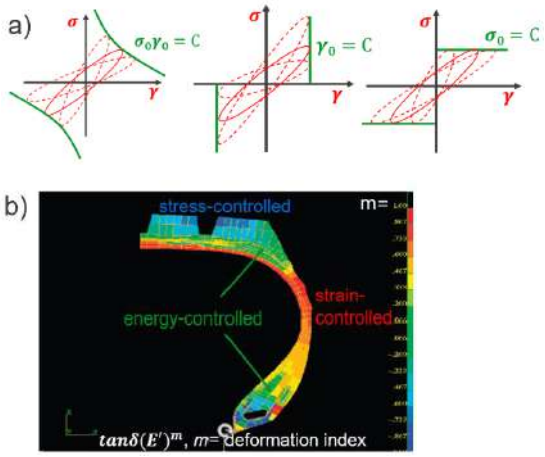

Figure 1. a) In real application, rubber products with varying stiffness practically could be deformed at constant energy, constant strain, or constant stress; b) which could result in a distribution of the deformation index in a running tire as simulated via FEA (figure is adapted from literature [2]).

In the stress-strain curve, the hysteresis loss, or the dissipated energy W_{diss}, is defined as the integral of the

loop formed by stress-strain curve.[1] This can be expressed in various formats as listed in Table 1 for each deformation mode,[3] allowing for the identification of the decisive viscoelastic parameters accordingly.

The impact of deformation mode on the relationship between hysteresis and viscoelasticity has yet to be validated through practical experiments. In present work, we aim to verified it in two common perspectives within tire industry: 1) Heat Build-Up (HBU) of rubber with moduli and crosslinking type; 2) Rolling-Resistance of tire utilizing different tread compounds.

Table 1. Three types of deformation modes and their dependency on respective viscoelastic parameters

Deformation Mode	**Expression of Hysteresis Loss**	**Decisive Viscoelastic Parameter**
Hysteresis loss	original format: $Hysteresis = W_{diss} = \oint \sigma \frac{d\varepsilon}{dt}$ $= \oint \sigma_0 sin(\omega t + \delta) \cdot \varepsilon_0 \omega cos\, \omega t dt \quad = \pi\sigma_0\varepsilon_0 sin\delta$	integral of the stress-strain loop
I) Energy-Controlled	at small δ, $sin\delta \approx tan\delta$ $W_{diss} \approx \pi\boldsymbol{\sigma_0\varepsilon_0} tan\delta$	$\boldsymbol{tan\delta}$ or $tan\delta/E'^0$
II) Strain-Controlled	with $\sigma_0 = \varepsilon_0\|E^*\|$, $\|E^*\|sin\delta = E''$ we get $W_{diss} = \pi\boldsymbol{\varepsilon_0^2} E''$	$\boldsymbol{E''}$ or $tan\delta/E'^{-1}$
III) Stress-Controlled	with $\varepsilon_0 = \sigma_0/\|E^*\|$ we get $W_{diss} = \pi\sigma_0^2\, sin\delta/\|E^*\| \approx \pi\boldsymbol{\sigma_0^2}\, tan\delta/E'$	$\boldsymbol{tan\delta/E'^{+1}}$

2. Experimental

Case 1: HBU of rubber cylinders

Two groups of carbon black filled natural rubber vulcanizates were prepared with diverse viscoelastic characteristics: 1) at the same level of stiffness but different types of crosslink networks by tunning the vulcanization package (the accelerator to sulfur ratio, A/S); 2) at the same A/S ratio but varying degree the crosslink density. More experimental details can be found in our previous article. [3]

Well-defined HBU experiments, either in strain- or stress-controlled deformation mode, were conducted on were conducted on Metravib DMA+2000 analyzer (Limonest, France) equipped with an HBU fixture for cylindrical rubber samples. Such setup allows in situ dynamic mechanical analysis (DMA) of the vulcanizates the HBU process. Rubber cylinders were submitted to the setup at room temperature and a cyclic compression frequency of 30 Hz. For strain-controlled mode, a static strain of 16% and a dynamic strain of 10% were applied. While for stress-controlled mode, a static stress of 1 MPa and a dynamic stress of 0.625 MPa was used. The testing conditions partially refers to common industrial standards, [4] which is also close to many working conditions of tires.

Case 2: Rolling resistance of tires

Five types of tread compounds, namely cpd-A to -E, were selected from our motorcycle tire production line. The rheological spectra were evaluated on a TA-RSA analyzer (TA Instruments New Castles, USA) on tension fixture for temperature sweep experiments from -70 °C~100° C at 1 Hz within the linear viscoelastic regime.

Small size 10inch motorcycle tires were produced with same tire body and tread pattern. The only difference between them is the tread materials. During the buildup process of green tire, five types of treads were laminated on tire body and then cured in the same mold. All final tires were firstly visually inspected to make sure no defects and passed the uniformity evaluation.

Rolling resistance were characterized in power consumption approach [5] via a running drum (Paul Köster GmbH, Medebach, Germany) at room temperature and

inflation pressure of 2.8 bar of tested tires. Carrying a load of 85kg, tires were running on the drum at a wheel speed of 35 km/h and record the power consumption after 30 min in steady-state.

3. Results and discussion

3.1 Rubber heat build-up (HBU)

The HBU test of rubber [4] is typically conducted as separate experiment from its characterization of viscoelastic properties, which complicates the correlation study between these two sets of results. Moreover, such correlation study often fails due to differing control modes and deformation conditions in the respective setups.

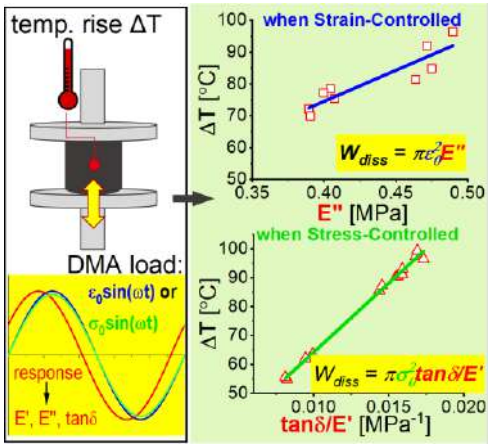

Figure 2. The rubber heat build-up amplitude ΔT due to hysteresis exhibits distinctive dependencies on viscoelastic parameters[3]: (upper plot) at strain-controlled deformation, ΔT is determined by E'' (lower plot) while in stress-controlled mode, ΔT correlates to $tan\delta/E'$.

In present work, coupled experiments were performed on an advanced dynamic mechanical analyzer (DMA), incorporating a compression HBU test fixture into the DMA apparatus. Both experiments were performed simultaneously on the same sample, facilitating effective correlation analysis. During the test, DMA precisely controlled the cyclic deformation of the sine wave on sample, either at strain-controlled mode (constant strain amplitude) or stress-controlled (constant stress amplitude). The internal temperature rise of rubber cylinder specimen, ΔT, was monitored via an inserted thermocouple in the sample core, as depicted in Figure 2 (left).

Compare the HBU results with the rheological parameters acquired from the same setup, we can do correlation analysis. As demonstrated by Figure 2 (right), the temperature rise ΔT from HBU experiments exhibits distinct dependencies on viscoelastic parameters[3] for two types of deformation modes of those examined rubber cylinders. Under strain-controlled compression, ΔT shows a good linear correlation with the loss modulus, E'' (Figure 2, right-upper), instead of other rheological parameters.[3] This is consistent with the equation expression in Table 1 for deformation at constant strain amplitude, ε_0, where the hysteresis W_{diss} only relays on the loss moduli of materials. Follow the equation expression of stress-controlled situation in Table 1, $W_{diss} = \pi\sigma_0^2\, tan\delta/E'$, the ΔT of different samples at constant stress amplitude σ_0 exhibits a best correlation to the combined rheological parameter, $tan\delta/E'$. For both examined cases, the HBU process of rubber originated from viscoelastic hysteresis does not just simply relay on $tan\delta$, which is the mostly used rheological indicator by engineers. The mechanical loss factor should be accountable when the products is under an energy-controlled deformation.

These findings have experimentally validated those decisive viscoelastic parameters for the corresponding deformation modes as summarized in Table 1.

3.2 Tire rolling resistance (RR)

The rolling resistance (RR) of tire is another key characteristic governed by the hysteresis of viscoelastic materials. In particular, the tread compound is the primary contributor to the overall RR of the whole tire. However, the dependency of tire RR on tread compound viscoelasticity remains insufficiently explored in the literature, likely due to the costly and time-consuming nature of experiments involving commercial tires. Typically, tire engineers rely on imperial viscoelastic parameters — such as such as $tan\delta$ at 60°C — as the indicator of RR.

For the first time, we employ practical experiments to investigate the correlation between tread viscoelasticity and tire RR performance. The selected five types of tread compounds maintain distinctive viscoelastic spectra as seen in Figure 3. The tire body structure and tread pattern were kept the same across all samples, ensuring the only difference between the five groups of tires was tread compound. The RR of tires was quantified by the power loss to keep the tire running on the drum, i.e., subtracting the power required to drive a bare drum from the total power consumption.

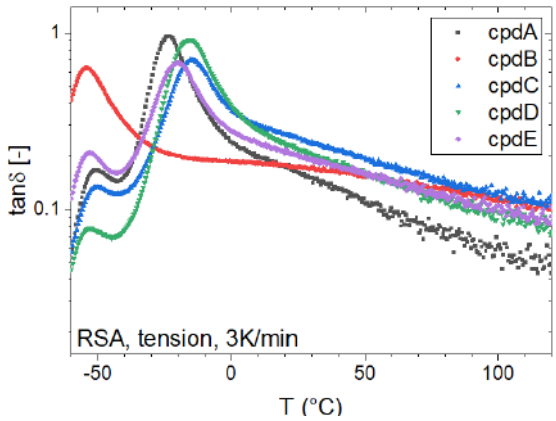

Figure 3. Temperature ramp of the five tread materials for RR study.

The RR of tire was firstly plotted against the $tan\delta$ at 60°C from DMA temperature sweeps as shown in Figure 4a. Evidently, some tread compounds does not meet the overall correlation relationship, such as cpd-B. Compared to other five compounds, cpd-B was rather stiff with higher moduli in rubbery state. To carry the same amount of loading weight, stiff tread can resist the deformation amplitude.

Referring to the concept of "deformation index" from Futamura et al., [2] an exponent *m* can be incorporated into a combined format of rheological parameter, $tan\delta/E'^{\wedge m}$ so that the contribution from materials' stiffness is considered. Then wen can get a satifactory correlation plot as Figure 4b. It suggests that the deformation mode tread under rolling conditions is predominantly stress-controlled. It falls the same trend of prior FEA simulation results reported in the literature. [2]

Another perspective should be pointed out is that those rheological parameters was obtained from linear viscoelastic regime at a fixed deformation frequency and temperature, while the real operating conditions of tire tread should be more complex. It covers a range of frequencies, temperatures, and strain amplitudes, involving the nonlinear region of viscoelasticity. Nevertheless, within the limited characterization tools and capability in academia and industry as of now, a better rheological parameter for final tire RR prediction is provided here. Last but not least, it is the deformation mode leads to different hysteresis mechanisms thus the variation of decisive rheological parameters for tire RR. Compounders should pay attention to conventional approach, which may fail your design of compound viscoelastic properties as testified in present case in Figure 4a.

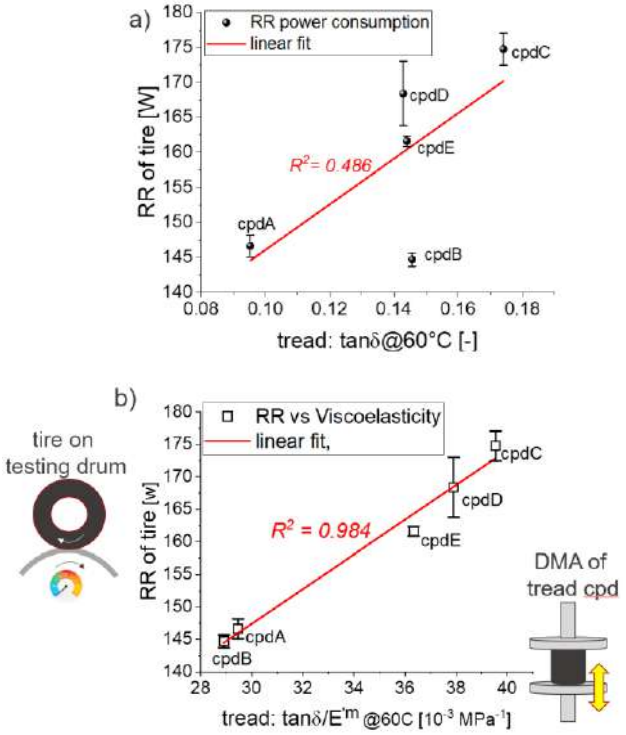

Figure 4. Based on practical experiments of real tires, it is found that tire rolling resistance well correlates to b) $tan\delta/E'^{\wedge m}$ instead of a) $tan\delta$ at 60°C for those tread compounds. This implies that the deformation of tread in such tire is under stress-controlled dominated deformation during running.

4. Conclusion

Depending on the product, area, and operating conditions, the deformation modes of rubber materials can vary. It is essential to recognize that these variations will lead to distinct impacts of viscoelastic parameters on hysteresis. Based on the corresponding expressions of dissipated work for the three types of deformation modes, the decisive parameters can be directly extracted.

Via both HBU experiments and RR study of tires, the above expressions have been verified, accordingly. Current results offer suitable parameters, or combinations thereof, to be used as material evaluation indicators in real world applications where heat generation, rolling resistance or any energy dissipation-governed phenomena are critical.

Acknowledgements

The authors expressed gratitude to Dr. C. G. Robertson for the helpful discussion. The support of tire production and indoor experiments by D. Tan, L. Gao, S. Mao, and J. Lv from Zhongce Rubber is acknowledged.

References

1. Ferry J.D., *Viscoelastic Properties of Polymers*, 3rd Ed., John Wiley & Sons, Inc, New York, 1980.
2. Futamura S., Goldstein A.A., Prediction and simulation of tire performance characteristics based on deformation index concept, *Rubber Chem. Tech.*, 2016; 89:1.
3. Nie S., Huang W., Ren P., Wang X., *Macromol. Rapid Commun.* 2025; 2400847.
4. ASTM D623-07, *ASTM International*, West Conshohocken, USA 2019.
5. Gent A. N., Walter J. D., *The Pneumatic tire*. NHTSA, Washington DC., 2006, p475.

Establishment of a library database of some compounding ingredients using a Py-GC/MS technique

P. TUMWISED[1,2*], S. WIRASATE[1], C. SIRISINHA [1]

[1]*Rubber Technology Research Centre, Faculty of Science, Mahidol University, Nakhon Pathom 73170, Thailand.*

[2]*Polymer Science and Technology Program, Department of Chemistry, Faculty of Science, Mahidol University, Nakhon Pathom 73170, Thailand.*

prin.tum@student.mahidol.ac.th

Abstract

This work investigated a powerful method for providing a library database for reverse engineering in the rubber additive industry, utilising the Pyrolysis-GC/MS (Py-GC/MS) technique. This technique offers analyses of raw rubber and additives existing in vulcanised rubber, which is crucial for product development in response to trading regulations. The results showed that pyrolysates at a temperature of 300°C in a vulcanised sample of standard Thai rubber 20 (denoted as C-STR20) detected: (i) D-limonene as a characteristic of polyisoprene from NR, and (ii) carbon disulphide resulting from sulphur reacting with the NR backbone. In addition, pyrolysates of three accelerators were determined. For the N-cyclohexyl-2-benzothiazolesulfenamide (CBS), cyclohexylamine, benzothiazole, 2-(methylmercapto)benzothiazole, and N-cyclohexyl-2-benzothiazolamine were detected. Caprolactam was found as a characteristic of Dithiocaprolactame (DTDC), a sulphur-donor accelerator. Dibenzylamine was detected as a characteristic of Tetrabenzylthiuram disulphide (TBzTD). In summary, the Py-GC/MS technique, under proper test conditions, demonstrated the potential to identify curatives in vulcanised rubber products with simple sample preparation and a short test duration.

Keywords: Natural rubber, Accelerators, Py-GC/MS, GC-MS library database, Reverse engineering

1. Introduction

Data from 2014 indicate a continuous decline in Thailand's domestic exports of rubber compounds, unlike many other countries. This trend suggests a loss in market share, which may be attributed to the relatively lower performance and cost competitiveness of locally produced compounds compared to international competitors[1]. In addition, import regulations in several countries have restricted the use of rubber compounds and rubber products that release carcinogenic substances, particularly nitrosamines, which are often generated from certain types of cure accelerators[2-5]. To enhance the competitiveness of the domestic rubber compound industry, it is essential to adopt reverse engineering approaches[6]. These methods can be applied to improve and optimise compound formulations, enhancing their performance while also making them safer for human health and more environmentally friendly. Strengthening these aspects is critical to enabling the domestic industry to compete more effectively in the global market and regain a greater share of market presence.

Pyrolysis-gas chromatography-mass spectrometry (Py-GC-MS) is a powerful analytical technique that combines thermal decomposition with chromatographic separation and mass spectrometric detection. It is particularly well-suited for the characterisation of complex, non-volatile materials such as polymers, additives, and composite matrix materials by rapidly heating a sample in an inert atmosphere, which causes it to decompose into volatile fragments thermally. These pyrolysates are then immediately introduced into a gas chromatograph, where they are separated based on their volatilities and interaction with the column stationary phase. The separated substances are subsequently analysed by mass

spectrometry and matched to library data, providing both qualitative and semi-quantitative insights into the sample chemical compositions.

The analysis of raw materials can be performed by pyrolysing raw chemicals to examine their thermal degradation mechanisms. This approach also provides quantitative data indicating which pyrolysates are produced in greater amounts at specific pyrolysis temperatures. Such information is often characteristic of individual polymers and additives[7]. Although the analysis of raw materials has been extensively studied over the years, the introduction of new additives developed to replace traditional chemicals requires continual updates to existing databases to maintain market competitiveness[8]. Moreover, analysing polymers and additives in finished rubber products is more complex than analysing them in raw materials. This is because rubber products undergo compounding through mechanical mixing, followed by vulcanisation, which involves heat and chemical reactions. These processes may alter the nature and composition of the pyrolysis products. Therefore, it is crucial to study the pyrolysates of the ingredients, both before and after vulcanisation, to characterise the materials and accurately understand their transformations during processing.

Our study aims to establish a comprehensive database for the qualification of some ingredients in vulcanised rubber using the Pyrolysis–Gas Chromatography/Mass Spectrometry (Py-GC/MS) technique. This database is intended to serve as a reference tool for identifying and differentiating accelerators based on their characteristic pyrolysis products. In addition, this work investigates the behaviour and stability of specific pyrolysates that may disappear, decompose, or transform into secondary products during the curing process. Furthermore, the study seeks to identify appropriate pyrolysate markers capable of distinguishing each accelerator present in the rubber compound, even after vulcanisation. The establishment of such markers not only enhances the analytical capabilities of Py-GC/MS for rubber compound characterisation but also advances reverse engineering and quality control processes in the rubber industry.

2. Experimental

2.1 Rubber and ingredients

Standard Thai Rubber 20 (STR20) from Thai Hua Rubber Public Co., Ltd was used as the rubber matrix in this study. Zinc oxide (White Seal, Thai-Lysaght Co., Ltd) and stearic acid (PALMAC1500, IOI Acidchem Sdn., Bhd) were used as activators. A commercial-grade sulphur as a crosslinker was supplied by The Siam Chemicals Public Co. N-Cyclohexyl-2-benzothiazolesulfenamide (CBS) from Northeast Auxiliary Chemical Industry Co., Ltd, Tetrabenzylthiuram disulphide (TBzTD) from Akrochem Corporation, and Dithiodicaprolactam or the so-called Caprolactam disulphide (DTDC) from SonQuem Limited were used as cure accelerators.

Table 1. Rubber compound recipe

Ingredients	Amount (phr)
STR20	100
Zinc oxide	5
Stearic acid	1
Sulphur	1
CBS	1.25
TBzTD	0.5
DTDC	0.7

2.2 Preparation of vulcanised rubber

The mixing was carried out using a two-roll mill (RM-150W, LABTECH) for 10 min at room temperature. The vulcanisation was carried out using a hydraulic hot press at 160°C for 10 min.

2.3 Pyrolysis gas chromatography-mass spectrometry

Raw ingredients and vulcanised rubber were characterised with a multi-shot pyrolyser (EGA/PY-3030D, Frontier Lab Ltd.) coupled to a GC/MS (5977A MSD with 7790 GC system, Agilent Technologies Inc., CA, USA). Approximately 0.5 mg samples were pyrolysed in single-shot mode at 300°C for 12 sec. The GC column is an ultra-alloy capillary with a length of 30 m, an internal diameter of 0.25 mm, and a film thickness of 0.25 μm. The GC oven was heated to 40°C and held for 2 min, then ramped to 280°C and held for 15 min. MSD conditions

were set at the MS source temperature of 230°C and MS quad temperature of 150°C. The mass scan range was 10-700 m/z with a scan speed of 3,125 (u/s). The analysis of the samples from the NIST Mass Spectral Search Program for the NIST/EPA/NIH Mass Spectral Library Version 2.2

3. Results and discussion

3.1 Identification of raw ingredients

3.1.1 Characteristics of CBS at a pyrolysis temperature of 300°C

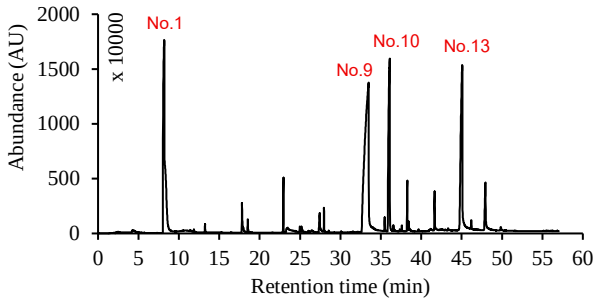

Figure 1. GC-MS chromatogram of raw CBS at 300°C

To ensure that the curatives were completely decomposed and their signals had a sufficiently high intensity, the pyrolysis temperature was set to 300°C. Figure 1 shows the pyrolysis products of the CBS accelerator, demonstrating high abundance signals of cyclohexylamine, 2-mercaptobenzothiazole, N-cyclohexyl-2-benzothiazolamine, and 2,2'-Dithiobis(benzothiazole) at retention times of 8.200, 33.481, 36.111, and 45.091 min, respectively, which are characteristic markers of CBS[9]. In addition, there are signals of a small fragment occurring during the pyrolysis process, as shown in Table 2.

Table 2. Pyrolysis products of raw CBS at 300°C

Peak No.	Retention time (min)	Pyrolysis products
1	8.200	Cyclohexylamine
2	17.804	Benzothiazole
3	18.542	Cyclohexylformamide
4	22.960	Oxalic acid, dicyclohexyl ester
5	23.422	N-cyclohexylcyclohexanimine
6	25.167	N-Phenylcyclohexylamine
7	27.488	2(3H)-Benzothiazolone
8	27.946	Methylcyclohexane
9	33.481	2-Mercaptobenzothiazole
10	36.111	N-Cyclohexyl-2-benzothiazolamine
11	38.255	Carbazole, 3-isothiocyanato-
12	41.657	2,2'-Bibenzothiazole
13	45.091	2,2'-Dithiobis(benzothiazole)

3.1.2 Characteristics of TBzTD at a pyrolysis temperature of 300°C

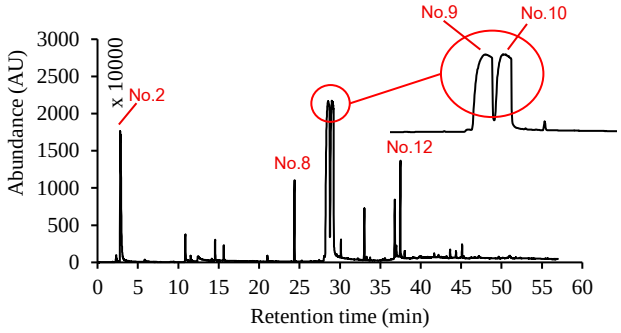

Figure 2. GC-MS chromatogram of raw TBzTD at 300°C

In Figure 2, the pyrolysis products of the TBzTD accelerator exhibit a pronounced peak corresponding to carbon disulphide at a retention time of 2.801 min. This compound arises from the thermal decomposition of thiuram disulphide, supporting the sulphur-donating function of the TBzTD accelerator[8]. Besides, bibenzyl is detected at a retention time of 24.369 min, consistent with the coupling of two benzyl radicals, suggesting that the pyrolysis mechanism involved homolytic bond cleavage[10]. The double peak splitting at retention times of 28.545 and 29.031 min arises from two pyrolysates that are close in molecular mass, the effect of the dehydrogenation of dibenzylamine to N-benzylidenebenzylamine[10]. The last characteristic peak at retention time of 37.483 is tribenzylamine, as occurred from the deamination and amination of benzylamine and dibenzylamine[10]. Another fragment of TBzTD is shown in Table 3.

Table 3. Pyrolysis products of raw TBzTD at 300°C

Peak No.	Retention time (min)	Pyrolysis products
1	2.310	Sulphur dioxide
2	2.801	Carbon disulphide
3	10.867	Benzaldehyde
4	11.532	Benzonitrile
5	12.406	Benzylamine
6	14.545	Benzene, (isocyanomethyl)-
7	15.638	Benzyl nitrile
8	24.369	Bibenzyl
9	28.545	Dibenzylamine
10	29.031	N-Benzylidenebenzylamine
11	30.115	Benzyl sulphide
12	37.483	Tribenzylamine

3.1.2 Characteristics of DTDC at a pyrolysis temperature of 300°C

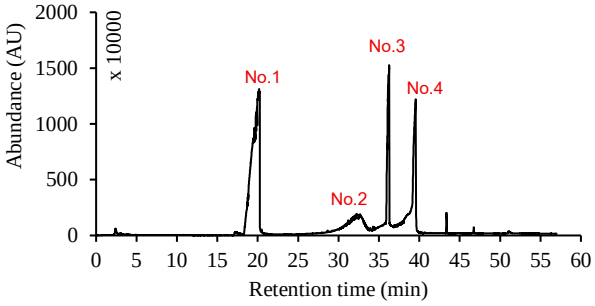

Figure 3. GC-MS chromatogram of raw DTDC at 300°C

DTDC is a secondary accelerator often used as a sulphur donor to improve heat resistance with mono- and disulphidic in EV and semi-EV cure systems[11]. In Figure 3, the pyrolysis products of DTDC at 300°C can only be matched to a pyrolysis database of caprolactam with a molecular mass of 113 m/z at a retention time of 20.162 min due to data limitations, while the chromatograms also show high peaks at 36.289 and 39.555 min. The mass spectra of both peaks of 256 m/z and 288 m/z agree with the molecular mass of caprolactam sulphide and caprolactam disulphide, as shown in Figure 4. The DTDC pyrolysates, consisting mostly of caprolactam linked to mono- and disulphides, suggest that caprolactam remains stable and does not undergo structural transformation at 300°C. Furthermore, the results also show a signal of rhombic sulphur (S_8) at a retention time of 32.649 min.

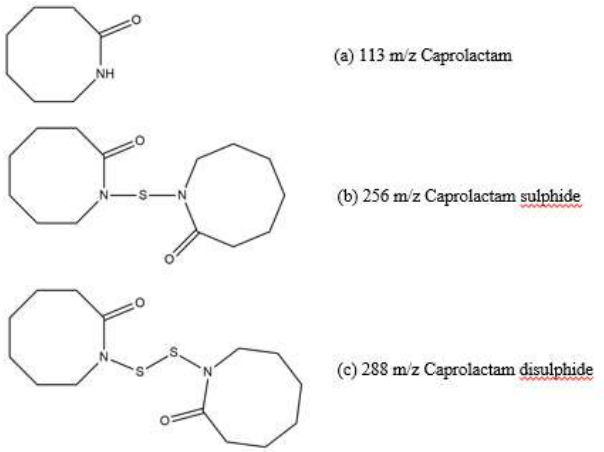

Figure 4. Suggested chemical structures of molecular mass 113 m/z, 256 m/z and 288 m/z: (a) Caprolactam, (b) Caprolactam sulphide, and (c) Caprolactam disulphide

Table 4. Pyrolysis products of raw DTDC at 300°C

Peak No.	Retention time (min)	Pyrolysis products
1	20.162	Caprolactam
2	32.649	Cyclic octaatomic sulphur
3	36.289	Caprolactam sulphide (256 m/z)
4	39.555	Caprolactam disulphide (288 m/z)

3.1 Identification of ingredients in vulcanised rubber

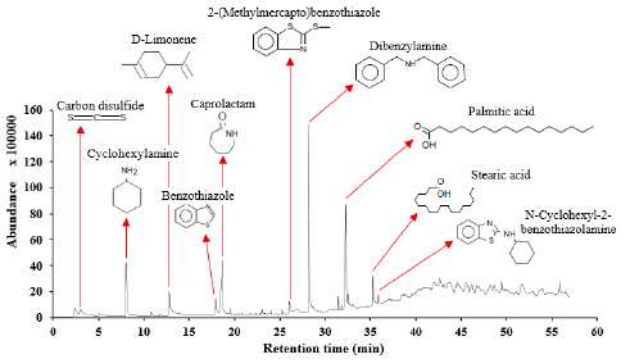

Figure 5. GC-MS chromatogram of C-STR20 at 300°C

In vulcanised rubber analysis, a temperature of 300°C was selected to avoid signal from the rubber matrix pyrolysates and to ensure complete pyrolysis of the accelerators. The GC-MS chromatogram in Figure 5 reveals only a few pyrolysates identified as ingredients in vulcanised rubber: at a retention time of 3.047 min, there is a signal for carbon disulphide, attributed to sulphur reacting with carbon in the rubber matrix after

vulcanisation. For CBS accelerator, the main characteristic signals are: cyclohexylamine, benzothiazole, 2-(methylmercapto)benzothiazole and N-cyclohexyl-2-benzothiazolamine, at retention times of 8.027, 17.913, 26.055, and 35.840 min, respectively, and are consistent with pyrolysates of the raw CBS except 2-(methylmercapto)benzothiazole, due to the unique product derived from a transformation of 2-mercaptobenzothiazole reacted with the rubber matrix during the vulcanisation process.

Table 5. Pyrolysis products of C-STR20 at 300°C

Peak No.	Retention time (min)	Pyrolysis products
1	3.047	Carbon disulfide
2	8.027	Cyclohexylamine
3	12.834	D-Limonene
4	17.913	Benzothiazole
5	18.724	Caprolactam
6	26.055	2-(Methylmercapto)benzothiazole
7	28.224	Dibenzylamine
8	32.288	Palmitic acid
9	35.242	Stearic acid
10	35.840	N-Cyclohexyl-2-benzothiazolamine

However, benzothiazole and 2-(methyl mercapto)benzothiazole are not applicable for identifying CBS, since both pyrolysates are also detected in other sulphenamide accelerators, such as MBT and MBTS[12, 13]. The chromatogram also exhibits high abundances of caprolactam and dibenzylamine at retention times of 18.724 and 28.224 min, respectively, as characteristics of DTDC and TBzTD. The results suggest that both pyrolysates exhibit high thermal stability, even during the curing process. In addition, pyrolysis at 300°C demonstrates a signal for D-limonene (aka. dipentene) at 12.834 min, a fragment derived from the thermal degradation of polyisoprene in STR20[14]. Furthermore, the chromatogram of vulcanised rubber shows peaks of palmitic acid and stearic acid, as activators in C-STR20, at retention times of 32.288 and 35.242 min, respectively. Unexpectedly, no signals of zinc stearate (as a resulting product from a reaction between ZnO and stearic acid added) were detected in the vulcanisates. It is proposed that during the vulcanising process, Zn^{2+} from zinc stearate might react with accelerators, leading to a retransformation of zinc stearate back to stearic acid[15].

4. Conclusion

The Py-GC/MS technique successfully establishes a library database of accelerators in vulcanised rubber, with potential markers at 300°C. Suitable markers for CBS in vulcanised rubber are cyclohexylamine and N-cyclohexyl-2-benzothiazolamine. The markers of TBzTD and DTDC are dibenzylamine and caprolactam, respectively. Besides, the Py-GC/MS technique is applicable for identifying other ingredients such as fatty acids and rubber matrix.

5. Acknowledgements

This study was supported by the Rubber Technology Research Centre (RTEC) for analytical instruments and facilities. The author is deeply indebted to my academic advisor, Professor Dr. Chakrit Sirisinha, for their invaluable guidance, constructive feedback, and unwavering encouragement.

6. References

1. Sowcharoensuk, C. Thailand Industry Outlook 2025-2027: Rubber Industry. Krungsri Research: 2024.
2. Spiegelhalder, B.; Preussmann, R. Nitrosamines and rubber. *IARC Sci Publ* **1982**, (41), 231-243.
3. Willoughby, B. G.; Scott, K. W. Nitrosamine formation in rubber: I. Influence of mixing history. *Rubber chemistry and technology* **1998**, *71* (2), 310-322.
4. Willoughby, B. G.; Scott, K. W. Nitrosamine formation in rubber: II. Influence of cure. *Rubber chemistry and technology* **1998**, *71* (4), 766-777.
5. Manchuri, K. M.; Kuril, A. K.; Shaik, M. A.; Gopireddy, V. S. R.; Sultana, N. An update on latest regulatory guidelines and analytical methodologies

for N-nitrosamine impurities in pharmaceutical products – 2024. *Medical Gas Research* **2025**, *15* (4), 535-543. DOI: 10.4103/mgr.MEDGASRES-D-24-00124.

6. Datta, S.; Stoček, R.; Kuřitka, I.; Sáha, P. Determination of compounding formulation of cured rubber by reverse engineering. *Polymer Engineering & Science* **2015**, *55* (6), 1450-1458.
7. Pacáková, V.; Virt, J. PLASTICS. In *Encyclopedia of Analytical Science (Second Edition)*, Worsfold, P., Townshend, A., Poole, C. Eds.; Elsevier, 2005; pp 180-187.
8. Sheth, P.; Desai, R. Replacing TMTD with Nitrosamine Free TBzTD-Accelerator in Curing of Rubber. *International Journal for Scientific Research & Development* **2013**, *1* (3).
9. Li, H.; Han, F.; Jiang, L.; Yang, T.; Du, L.; Zhu, J. Continuous Synthesis of N-Cyclohexyl-2-benzothiazole Sulfenamide with Microfluidics and Its Kinetic Study. *Industrial & Engineering Chemistry Research* **2021**, *60* (39), 14134-14142. DOI: 10.1021/acs.iecr.1c02881.
10. Robinson, K. J.; Fecteau, K. M.; Gould, I. R.; Hartnett, H. E.; Williams, L. B.; Shock, E. L. Metastable equilibrium of substitution reactions among oxygen-and nitrogen-bearing organic compounds at hydrothermal conditions. *Geochimica et Cosmochimica Acta* **2020**, *272*, 93-104.
11. Hewitt, N. *Compounding precipitated silica in elastomers: theory and practice*; William Andrew, 2007.
12. Tamási, K.; Kollár, M. S. Effect of different sulfur content in Natural Rubber mixtures on their thermo-mechanical and surface properties. *International Journal of Engineering Research & Science* **2018**, *4* (2), 28-37.
13. Samarasinghe, I.; Walpalage, S.; Edirisinghe, D.; Egodage, S. Study on sulfur vulcanised natural rubber formulated with nitrosamine safe diisopropyl xanthogen polysulfide/tertiary butyl benzothiazole sulphenamide binary accelerator system. *Progress in Rubber, Plastics and Recycling Technology* **2021**, *37* (3), 190-202.
14. Wang, H.; Fan, X.; Yu, H.; Li, J.; Cui, X.; Xu, X. Characterization of natural rubber concerning its components and molecular weight in Taraxacum kok-saghyz Rodin using pyrolysis gas chromatography-mass spectrometry. *Journal of Separation Science* **2023**, *46* (19), 2201041.
15. Ikeda, Y.; Sakaki, Y.; Yasuda, Y.; Junkong, P.; Ohashi, T.; Miyaji, K.; Kobayashi, H. Roles of dinuclear bridging bidentate zinc/stearate complexes in sulfur cross-linking of isoprene rubber. *Organometallics* **2019**, *38* (11), 2363-2380.

Performance Evaluation of Silicone-Based Isolators Under Varying Temperatures and Excitation Levels Using a Thermal Chamber Shaker

Erdem Rahmi SENOZ[1], Umut CALIK*[2]

[1] *Balıkhisar, Koca Seyit Onbaşı Sk. No:1, 06750 ASELSAN Akyurt, Ankara, Turkiye.*

[2] *Balıkhisar, Koca Seyit Onbaşı Sk. No:1, 06750 ASELSAN Akyurt, Ankara, Turkiye.*

*E-mail: ucalik@aselsan.com

Abstract

This study aims to compare the performance of silicon-based isolators with similar size and similar catalog stiffness values, which have obtained from three different manufacturers. These three isolators have tested under different variable parameters such as environmental temperatures, vibration excitation types and isolator orientations. The change in isolator transmissibility functions was compared under different ambient temperatures of -40 °C, +23°C, and +75°C, different vibration excitation types, including sine sweep, white noise, and shock inputs, and different isolator axes (radial / axial) for each product. The isolators demonstrating the most consistent transmissibility behavior will be preferred to preserve the overall stabilization performance.

Keywords: Vibration Isolator, Silicone, Frequency, Transmissibility Function, Temperature

1. Introduction

Isolators are used to decrease the defined vibration profile energies, which is defined in the standards or identified with data collected from the platform, for various air/land/sea equipment. These isolators are generally selected as silicone-based elastomers. The isolators can be exposed to wide-band temperature changes under the determined environmental conditions. Therefore, studies have been carried out to identify products with the lowest possible natural frequency and damping change by creating these extreme scenarios in tests. Thus, it is aimed to reduce the effects that disrupt system stabilization.

2. Experimental Methods

2.1 Isolator Manufacturers

The insulators used were supplied by the three companies listed below. External volume dimension information has been shared in millimeters for each product.

1. Isolator 1: Lord Corporation (60x60x26) [1]
2. Isolator 2: Hutchinson (60x60x28) [2]
3. Isolator 3: Smac (60x60x32) [3]

The specified three isolators have been positioned from left to right in the same sequence, as shown in Figure 1. All of the isolators are silicon-based isolators with high damping characteristics.

Figure 1. Tested Three Different Isolators

2.2 Test Setup Assembly

The test setup was designed by attaching four isolators to a 28-kg payload. The stiffness center of the isolators and the center of gravity of the payload was coincided by mounting two of them onto the left arm and two of them onto the right arm of the payload. In the test setup, accelerometers were placed in both isolated region and shaker table to be able to plot transmissibility function of the isolator for vibration input profiles. Also, 2 temperature sensors were integrated inside the cabin and

on the isolator to be able to read the isolator and ambient temperature simultaneously. The example test setup image is shown in Figure 2.

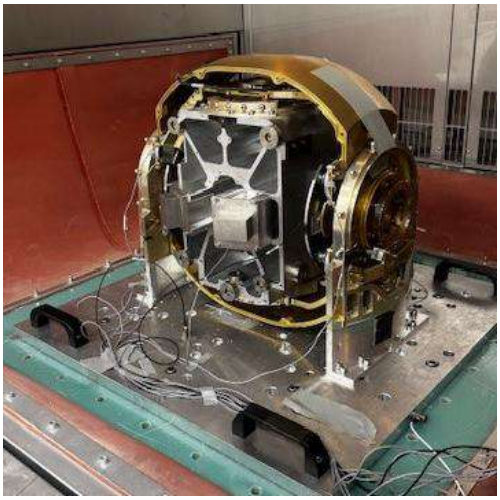

Figure 2. Assembly of the Test Setup

2.3 Combined Vibration and Temperature Chamber

LDS brand 120kN force capacity shaker was used as a vibration exciter. A thermal chamber integrated with the exciter, capable of heating and cooling at a rate of 10 degrees/minute, was used.

Figure 3. Shaker and Thermal Chamber

2.4 Test Profiles

Test profiles are divided into 3 test scenarios as sine sweep, white noise, and shock. Test scenario details are specified below.

1. Sine Sweep: Sweep Up, 5-30Hz, 0.5mm peak to peak, 2 minutes logarithmic sweep
2. White Noise: 5-2000Hz, $0.001 g^2/Hz$, 1.4gRMS, 1-minute data collect
3. Shock: Sawtooth, 20g-11ms, 20% compensated

All these test scenarios were applied at -40°C / +23°C / +75°C for all different type isolators. Also, tests were repeated for the radial and axial axis of isolators. Thus, a total of 54 different test scenarios (2 (axis) x 3 (temperature) x 3 (input profile) x 3 (isolators)) have been obtained.

Under shock input, natural frequency and damping calculations are obtained by performing an analytical solution of a single degree of freedom system. In Figure 4, blue curve represents input measurement of 20g-11ms with 20% compensation, yellow curve represents time domain data of the measured shock output and orange curve represents single degree of freedom system analytical calculated isolator output. It can be seen yellow and orange curves have great fit.

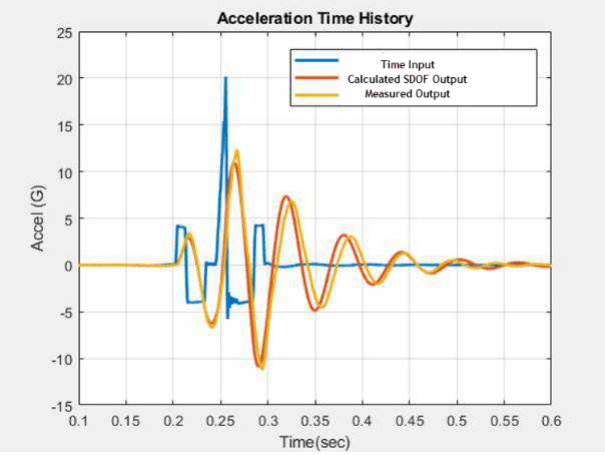

Figure 4. Calculated and Measured Time Domain Response of An Isolator

3. Results and Discussion

A preliminary examination of the results shows that the effect of temperature on the natural frequency and damping ratio can be clearly observed from transmissibility plots. All isolator exhibits a similar trend as shown in Figure 5; however, when the plot of Isolator 1 is taken as a representative example, the natural frequency increases by approximately 5-6 Hz from the coldest to the hottest temperature. In addition, the transmission ratio at the resonance frequency decreases from 4.0 to 3.2, indicating that the isolator provides better vibration attenuation at higher temperatures.

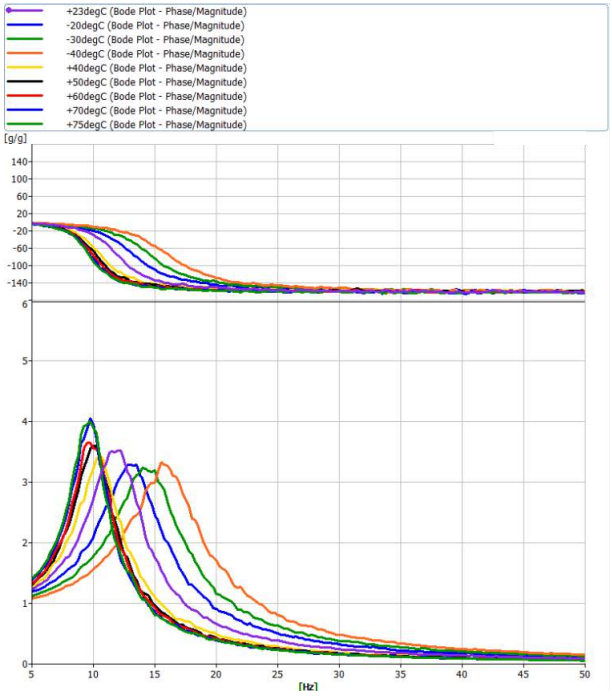

Figure 5. Transfer Function Change with Temperature Effect

The 54 different test results obtained for all isolator have been shared in Table 1. Natural frequency values for these tests have been shared in the table. The damping ratio obtained in these tests is approximately between 0.10 and 0.15.

The static creep of isolators due to the effect of gravity is also taken into consideration. Approximately 4 mm, 3 mm and 2 mm of static creep under load was observed respectively in the Isolator 1, 2 and 3, which were measured after being held for one day under room conditions.

The maximum relative displacement observed in the Isolator 1, 2 and 3 during the shock was measured as approximately 12 mm, 10 mm and 10 mm under +75°C environmental conditions, respectively.

The results show significant variations depending on the type of the vibration input applied. First, the sine sweep natural frequency results of Isolator 1 is between 10-11 Hz at room and high temperature scenarios, for low temperature scenarios it is between 15-16 Hz. Isolator 2 is between 11-13 Hz at room and high temperature scenarios, for low temperature scenarios it is between 15-16 Hz. Isolator 3 similarly is between 11-13 Hz at room and high temperature scenarios, for low temperature scenarios it is between 15-16 Hz. Second, in the white noise tests, it was observed that the natural frequency results of Isolator 1 varied in between 10-12 Hz at room and high temperature scenarios, for low temperature scenarios it is 16 Hz. Isolator 2 varied in between 12-14 Hz at room and high temperature scenarios, for low temperature scenarios in between 17-19 Hz. Isolator 3 varied in between 12-15 Hz at room and high temperature scenarios, for low temperature scenarios in between 17-20 Hz. Finally, in the shock tests, the natural frequency results of Isolator 1 in between 9-10 Hz at room and high temperature scenarios, for low temperature scenarios it is 12 Hz. Isolator 2 is between 11-12 Hz at room and high temperature scenarios, for low temperature scenarios it is 13 Hz. Isolator 3 similarly is between 11-12 Hz at room and high temperature scenarios, for low temperature scenarios in between 13-14 Hz.

Table 1. Isolator 1 Test Results

Test Parameter			**Isolator 1 Lord**	**Isolator 2 Hutchinson**	**Isolator 3 Smac**
Axis	**Test Input**	**Temp [°C]**	**Natural Frequency [Hz]**		
Axial	Sine Sweep	+23	11	13	12
	White Noise		12	14	12
	Shock		10	12	12
Radial	Sine Sweep		11	13	13
	White Noise		12	14	15
	Shock		9	12	12
Axial	Sine Sweep	+75	11	11	11
	White Noise		11	12	12
	Shock		10	11	11
Radial	Sine Sweep		10	11	12
	White Noise		10	12	13
	Shock		9	11	12
Axial	Sine Sweep	-40	15	15	15
	White Noise		16	17	17
	Shock		12	13	13
Radial	Sine Sweep		16	16	16
	White Noise		16	19	20
	Shock		12	13	14

While changes in isolator performance are at minimal levels under room conditions relative to +75°C temperature, it has been observed that the change is greater in all isolators under -40°C environmental conditions. Therefore, it is important to examine the properties of elastomer materials that need to work in cold environments.

It has been observed that the ratio of axial and radial natural frequencies is very close to 1:1 in all used isolators. This situation is taken into consideration to prevent differences in the axis during the selection.

The natural frequency and damping values depending on vibration input and environmental temperature are of great importance in the designs to be made.

4. Conclusion

As a result of the tests performed, similar values can be observed between the isolators. It can be said that isolators number 2 and 3 are stiffer compared to isolator number 1. When the effect of temperature is considered with reference to room temperature conditions (+23°C), the effect on frequency change is more obvious at -40°C.

Considering the ambient temperature as a reference according to sine sweep tests, it should be kept in mind that the transmissibility functions of isolators can shift approximately 3 Hz under temperature requirements of -40°C to +75°C. However, this change should be evaluated together with performance tests carried out with the vibration profile where isolators will be exposed to in the usage area, not by referencing sine sweep tests.

All performed tests were carried out for performance tests. It is also necessary to evaluate if there any permanent deformations that will occur under fatigue with long-term endurance tests.

With the obtained test results nonlinear finite element analysis models can be created. Test results and analysis validation studies will be carried out as a future work.

5. Acknowledgment

I would like to thank to ASELSAN for providing test equipment support in the studies.

6. References.

1. Parker Corporation. Aerospace & Defense Isolator Catalog. LORD Vibration, Shock & Motion Control Products, Parker Corporation, Cleveland, OH, 2021.
2. Barry Controls. Hutchinson Mounting Products 2011, Barry Controls, Brighton, MA, USA, 2011.
3. SMAC SAS. Standard & Adapted Isolators Catalogue, SMAC SAS, Toulon Cedex 09, France, 2022.
4. Department of Defense. MIL-STD-810H: Environmental Engineering Considerations and Laboratory Tests; MIL-STD-810H, 31 January 2019, Washington, DC, USA.
5. NATO Standardization Office. AECTP-400: Mechanical Environmental Tests, Edition D Version 1; North Atlantic Treaty Organization: Brussels, Belgium, 28 Nov 2019.

Recycling and Circular Economy in the Rubber Industry

IRC 2025
BANGKOK, THAILAND

International Rubber Conference 2025 (IRC 2025)

Flame-Retardant Performance of Epichlorohydrin-Modified Reclaimed Rubber

Selly Mitra Mailanda[1,2], Rathanawan Magaraphan*[1,2]

[1]*Polymer Processing and Polymer Nanomaterials Research Unit, Petroleum and Petrochemical College, Chulalongkorn University, Bangkok 10330, Thailand.*

[2]*Center of Excellence in Green Materials for Industrial Application, Chulalongkorn University, Bangkok 10330, Thailand.*

*Corresponding author at Polymer Processing and Polymer Nanomaterials Research Unit, Petroleum and Petrochemical College, Chulalongkorn University, Bangkok 10330, Thailand.

*E-mail addresses: Rathanawan.K@chula.ac.th (R. Magaraphan)

Abstract

Waste tire rubber is highly flammable (LOI: 17–18%), which limits its safe use and motivates both recycling and flame-retardant modification. In this work, ground tire rubber (GTR) was devulcanized using caprolactam and subsequently functionalized with p-coumaric acid (PCA) and modified with epichlorohydrin (ECH) to introduce chlorine-containing groups into the reclaimed rubber. Swelling measurements showed a strong increase in sol fraction and swelling index and a reduction in crosslink density from 18.1×10^{-5} to about 5×10^{-5} mol/cm³, corresponding to devulcanization degrees of 72–78%. At the same time, torque rheometry revealed a marked decrease in torque and its flattening compared with raw GTR, confirming efficient cleavage of sulfur crosslinks and the formation of a re-processable rubber phase. ATR-FTIR and DSC indicated epoxide ring opening and changes in the fingerprint region after modification, and FE-SEM/EDX detected a stepwise increase in chlorine content from 0 to 0.56 and 1.28 wt% for FD-GTRECH4 and FD-GTRECH9, respectively, evidencing successful grafting of PCA/ECH onto the devulcanized rubber. Flame-retardant testing showed that the limiting oxygen index increased from 18.4% for the reference rubber to 19.0% for the highest ECH loading, while all formulations maintained a UL-94 V-2 rating without dripping. These results demonstrate that ECH-modified, caprolactam-devulcanized GTR is a promising recycled matrix with improved, though still modest, flame-retardant performance and potential for further optimization.

Keywords: Ground Tire Rubber, Devulcanization, Revulcanization, Flame-retardant

1. Introduction

Tires are made from vulcanized rubber using sulfur, which improves mechanical properties such as durability, weather resistance, and flexibility. However, the rapid growth of the automotive industry has led to increased tire and waste tire production, creating disposal challenges [1]. Mechanical forces combined with specific chemical agents can selectively break S–S cross-links in waste tire rubber. This reduces energy consumption and preserves the mechanical properties by avoiding main-chain scission. Devulcanization agents are crucial for cleaving crosslink bonds and preventing reattachment, thereby enhancing both the devulcanization degree and efficiency. Amine-based devulcanizing agents, such as hexadecyl amine under microwave irradiation, have been used by Molanorouzi and Mohaved [2], who proposed an ionic devulcanization mechanism involving amines.

The action of flame-retardants (FRs) in the combustion process involves a gas-phase reaction between fuel and oxygen that proceeds through preheating, volatilization/decomposition, ignition, combustion, and flame propagation. FRs act by disrupting one or more of these stages via chemical and/or physical mechanisms, operating in the solid, liquid, or gas phase. A common mechanism is gas-phase radical quenching, halogenated FRs scavenge reactive radicals that sustain the flame,

thereby suppressing propagation [3]. Organo-halogen compounds can store and release halogens within polymers, but not all are effective flame retardants. Consequently, organochlorine and organobromine compounds are the most suitable halogen-based FRs [4]. This study uses ECH, a chlorine-containing epoxy compound, to graft modified reclaimed rubber, thereby improving reclaimed rubber's flame-retardant performance. The epoxy group reacts with the acid/alcohol groups of PCA on the reclaimed rubber, while the devulcanizing agent also acts as a catalyst, opening the epoxide ring [5]. Re-vulcanization of modified reclaimed rubber is achieved using dicumyl peroxide (DCP) as a curing agent. DCP effectively generates free radicals, forming a more stable crosslinked network than sulfur curing. Unlike sulfur, it does not produce by-products such as sulfur dioxide, thereby reducing odors, harmful emissions, and environmental impact. Furthermore, devulcanization may generate the residual reactive sulfur species and radicals from cleavage of original S-S bonds [17]. These unstable sulfur fragments can reduce the efficiency of peroxides by scavenging radicals. The zinc stearic activator system converts these residues into stable, short-chain sulfidic crosslinks, thereby preventing thermal or oxidative degradation. This allows peroxide to effectively form C-C bonds while simultaneously stabilizing the sulfur debris into a reinforcing network [6, 21]. This study introduces ECH, containing a Cl group, as a potential additive to enhance fire resistance in reclaimed rubber. ZnO is an effective synergist with ECH in reclaimed rubber systems. It reacts with retained chlorine to form zinc chloride ($ZnCl_2$), a strong Lewis acid that catalyzes dehydrochlorination and early crosslinking of rubber chains. Additionally, the aromatic structure of the PCA facilitates the formation of a stable char layer that effectively blocks heat and oxygen. Moreover, ZnO serves as an essential smoke suppressant by trapping corrosive HCl gas, though careful loading control is necessary to prevent zinc burning [18-20].

Modified and revulcanized reclaimed rubber was characterized using a moving die rheometer (MDR), scanning electron microscopy with energy-dispersive X-ray spectroscopy (SEM-EDX), and attenuated total reflectance fourier transform infrared spectroscopy (ATR-FTIR), and its flame properties were measured using the limiting oxygen index (LOI) and UL-94. This research focuses on simple methods that use environmental sources and low-energy chemicals.

2. Experimental

2.1 Materials

The ground tire rubber (GTR) with a 20-mesh particle size was manufactured by Union Commercial Development Co., Ltd. Processing oil (alpha-terpineol) was purchased from beScents. The devulcanizing agent used was caprolactam (99%, Sigma-Aldrich). p-Coumaric acid (PCA) was purchased from MySkinRecipes. Bio-based ECH was obtained from AGC Vinuthai Public Company Limited (AVT). Revulcanizing agents (dicumyl peroxide (DCP) was purchased from Sigma Aldrich, zinc oxide (ZnO) was obtained from Krungthepchemi.com, and stearic acid 98% was obtained from Loba Chemie Pvt. Ltd).

Table 1. Formulations of devulcanization, modification, and revulcanization compounds.

Formula no.	Sample Codes	GTR (phr)	Alpha-terpineol (phr)	Capro (phr)	PCA (phr)	ECH (phr)	Revulcanization				
							GTR (phr)		ZnO (phr)	Stearic acid (phr)	DCP (phr)
							D-GTR	FD-GTR			
(1-5) Devulcanization and modifying reclaimed rubber (D-GTR and FD-GTRs)											
1	D-0	100									
2	D-GTR	100	10	5							
3	FD-GTR	100	10	5	10						
4	FD-GTRECH4	100	10	5	10	4					
5	FD-GTRECH9	100	10	5	10	9					
(6-9) Revulcanization (RF-GTRs)											
6	R-GTR						100		5	2	2
7	RF-GTR							100	5	2	2
8	RF-GTRECH4							100	5	2	2
9	RF-GTRECH9							100	5	2	2

2.2 Devulcanization and functionalization process

To produce FD-GTR, 100 phr of GTR was first swollen with 10 phr of alpha-terpineol for 30 min. Then, 5 phr of devulcanizing agent (caprolactam) was added. The modified rubber was further treated with 10 phr of PCA, using an internal mixer (MX105-D40L50) equipped with a Cam-type rotor. The mixing process was conducted at 180°C for 75 min at 70 rpm, and torque and temperature were monitored using Chareon Tut software. In this study, D-0 denotes the devulcanized rubber obtained via only thermal devulcanization. In contrast, D-GTR refers to devulcanized rubber produced solely with a chemical devulcanization agent, as shown in Table 1.

2.3 Modifying reclaimed rubber with ECH

100 phr of FD-GTR was added with 4 and 9 phr of ECH at 80 °C for 30 min at 15 rpm in an internal mixer, as formulated in Table 1, known as FD-GTRECHs.

2.4 Revulcanization process

The FD-GTRECHs (100 phr) were compounded on a two-roll mill (Labtech LRM 110, 0.8 mm gap) with 5 phr of zinc oxide, 2 phr of stearic acid, and 2 phr of dicumyl peroxide for 10 min. D-0 is a sample used to control the process that undergoes only thermal devulcanization, and it becomes R-0 after revulcanization. The sample was then placed in a mold, and the curing time (t_{90}) was determined using a moving die rheometer (MDR) (Techpro A022S-rheoTECH MD+) at 160 °C for 60 min. According to ISO 3417:1991, the time that can be used for compression will be measured by this equation:

$$\text{Optimum cure time } (t_{90}) = 0.9\,(M_H - M_L) + M_L \quad (1)$$

where M_H is the maximum torque, and M_L is the minimum torque.

After compounding, the samples were cured using compression molding (LABTECH LP 20) at 13 MPa and 160 °C for approximately 10 min, based on the t_{90} torque from the MDR, followed by 5 min of cooling. The resulting sheets were 2 mm thick, with dimensions adjusted according to the test requirements [9].

2.5 Measurements

Following ASTM D 6814-02, the swelling test assessed devulcanization in devulcanized, modified, and revulcanized rubber. A 2 g rubber sample was extracted in 250 mL acetone for 12 h, dried at 80 °C to a constant weight (m_1), extracted into toluene for 16 h, and vacuum-dried at 80 °C to a constant weight (m_2) [8]. The sol and gel fractions are calculated by:

$$\%\text{Sol} = \frac{m_1 - m_2}{m_1} \times 100 \quad (2)$$

$$\%\text{Gel} = 100 - \%\text{Sol} \quad (3)$$

The sample with a certain mass (~2 g) was Soxhlet-extracted in 250 mL of acetone for 12 h, subsequently dried at 80 °C to constant weight (m_i), and then swelled in 250 mL of toluene for 72 h at room temperature. Following removal from toluene, the sample was weighed (m_t) and then dried at 80 °C to a constant weight (m_d). The crosslink density is calculated using the Flory-Rehner equation:

$$v_e = \frac{-[\ln(1-V_r+xV_r^2)]}{\left[V_1\left(V_r^{\frac{1}{3}}-\frac{V_r}{2}\right)\right]} \quad (4)$$

Where V_r represents the volume fraction, χ denotes the rubber-solvent interaction (0.43) [8]. The molar volume of toluene, V_1, is 106.13 cm^3 mol^{-1}. The rubber volume fraction is determined by:

$$V_r = \frac{m_d/\rho_d}{m_d/\rho_d + m_s/\rho_s} \quad (5)$$

Where m_d and ρ_d are the mass and density of the rubber after extraction and drying, respectively. The density of rubber was determined from mass and dimensional measurements using a Sartorious model QUINTIX224-1S. ρ_s denotes the density of the toluene. m_s refers to the mass of toluene absorbed by the sample, which is calculated as follows:

$$m_s = m_t - m_d \quad (6)$$

Devulcanization degree is calculated as follows:

$$R_d\,(\%) = \left(\frac{v_{e1} - v_{e2}}{v_{e1}}\right) \times 100 \quad (7)$$

Where R_d represents the devulcanization degree. Parameters v_{e1} and v_{e2} are the crosslink density of the vulcanized rubber and the reclaimed rubber, respectively.

The swelling percentage (%Swelling) was calculated as:

$$\%\text{Swelling} = \frac{m_t - m_d}{m_d} \times 100\% \quad (8)$$

Differential Scanning Calorimetry (DSC 3+ STARe System, Mettler-Toledo (Thailand) Ltd.) was performed under a nitrogen atmosphere. FD-GTRECHs sample was

heated from 25 to 150 °C at 10 °C/min. The isothermal experiments were conducted with the STARe Default DB V16.40 program at 150 °C for 5 min, followed by cooling to 25 °C at 10 °C/min [7].

Fourier Transform Infrared Spectroscopy (FTIR, Thermo Scientific Nicolet iS5 with iD7 ATR) was used to analyze the structural changes in devulcanized and modified rubber [3].

The sample was prepared post-compression for surface and elemental analysis (C, O, S, and Cl) using a Hitachi S-4800 scanning electron microscope (SEM) operated at 20 kV and equipped with energy-dispersive X-ray spectroscopy (EDX) in EMAX mode [7].

The Limiting Oxygen Index (LOI) was measured using a Stanton Redcroft FTA, following ASTM D-2863-06A. Revulcanized reclaimed rubber with PCA and ECH was prepared in dimensions of 110 × 6.5 × 3 mm [10].

Flame-retardant properties were evaluated using the FTT UL-94 (Model UL-94) test method, as specified in ASTM D 3801. Samples were prepared in dimensions of 125 × 13 × 3 mm and tested vertically [10].

3. Results and Discussion

3.1 Characterization of modified reclaimed rubber with ECH

Rubber typically exhibits poor fire resistance, limiting use under stringent safety standards. Grafting PCA and ECH introduces chlorine-containing groups into the rubber. During combustion, these C–Cl groups can release halogen species that quench flame radicals in the gas phase, thereby interrupting combustion chain reactions and reducing the material's flammability [11]. Figure 1 shows that PCA provides a COOH site to react with ECH without losing Cl, and PCA is functionalized on reclaimed rubber via thiol-ene reaction [5].

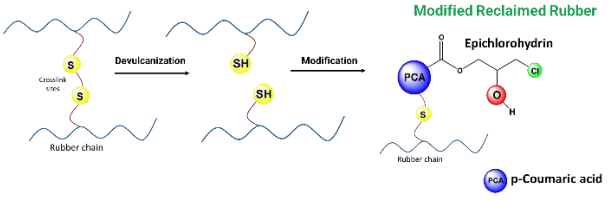

Figure 1. Proposed reaction scheme for devulcanized rubber modified with PCA and ECH.

Differential scanning calorimetry (DSC) was used to assess the thermal behavior of FD-GTR with varying ECH concentrations, as shown in Figure 2. The epoxy groups react with the carboxylic acid groups of PCA, while caprolactam helps open the epoxy rings, and the chlorine groups remain intact. To preserve chlorine in the modified rubber, the reaction was conducted at 70–120 °C, within the epoxide ring-opening temperature range, while maintaining Cl retention. The DSC of FD-GTR shows a smooth baseline from 70–120 °C, indicating no notable endothermic or exothermic events. By contrast, the downward peaks observed at 70–90 °C for FD-GTRECH4 and FD-GTRECH9 correspond to exothermic epoxide ring-opening reactions between ECH and the carboxylic acid group on FD-GTR [12].

The exothermic peak is assigned to epoxide ring-opening of ECH activated at this temperature. In FD-GTRECH9, the peak is more pronounced at 70–90 °C, indicating a greater extent of ring-opening due to the higher ECH content.

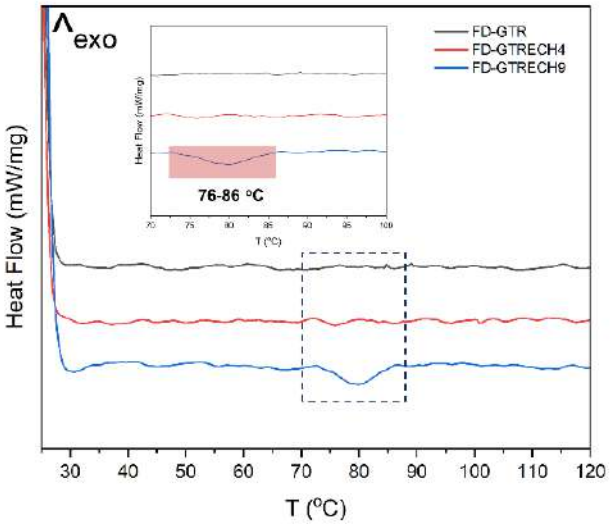

Figure 2. DSC thermograms of FD-GTRs.

Accordingly, conducting the reaction at 80 °C provides sufficient thermal energy for effective ring opening while limiting chlorine loss and secondary reactions. This moderate condition preserves Cl in the network and supports the targeted improvements in flame retardancy.

In Figure 3, PCA shows a strong –OH band at 3357 cm^{-1}, a sharp C=O stretch near 1670 cm^{-1}, and a C=C

stretch at 1591 cm^{-1} (cinnamate side chain) [13]. ATR-FTIR also confirms the incorporation of ECH into FD-GTR in the Figure. 3, the epoxide bands of neat ECH at 917 and 1268 cm^{-1} diminish in FD-GTRECHs, consistent with ring-opening, while a C–Cl band at 724 cm^{-1} persists for both 4 and 9 phr, evidencing chlorine retention relevant to flame retardancy.

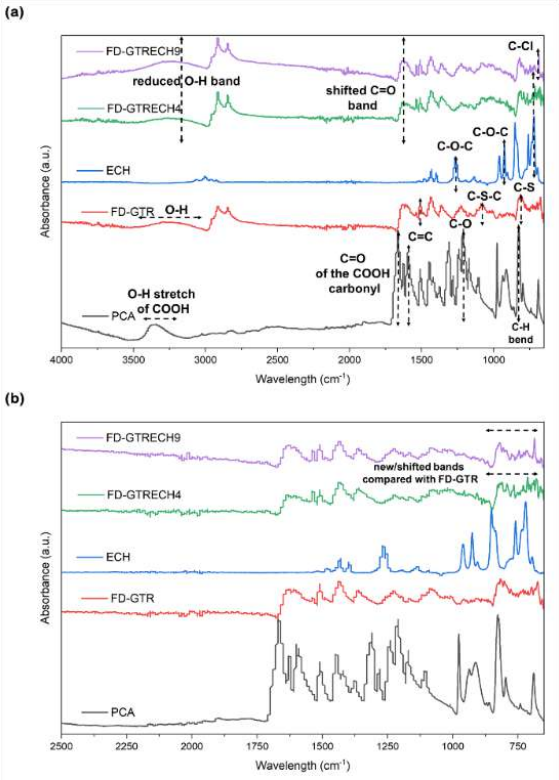

Figure 3. ATR-FTIR spectra of (a) FD-GTRs and (b) Fingerprint regions of FD-GTRs.

FE-SEM images show that the surface of FD-GTR shows rubber particle morphology, while FD-GTRECH4 and FD-GTRECH9 exhibit a slightly rougher surface with more heterogeneous texture after ECH grafting.

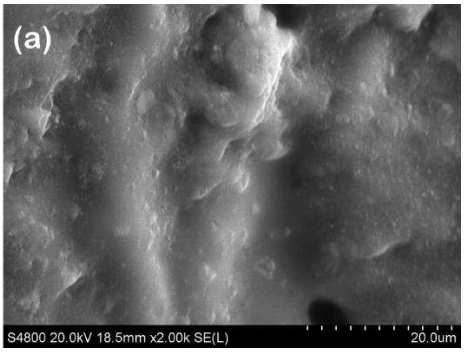

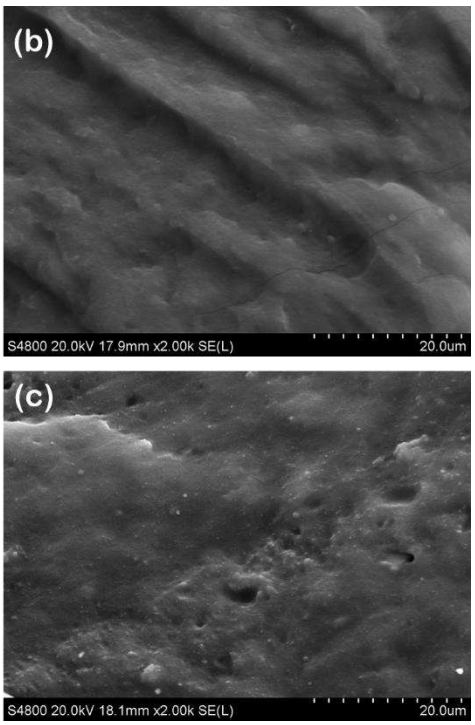

Figure 5. SEM results of (a) FD-GTR, (b) FD-GTRECH4, and (c) FD-GTRECH9.

In Table 2, EDX analysis confirms this chemical change, FD-GTR contains only C, O, S, and N with no detectable chlorine. In contrast, FD-GTRECH4 and FD-GTRECH9 show increasing Cl contents of 0.56 and 1.28 wt%, respectively, while C, O, S, and N remain at similar levels. This stepwise increase in chlorine clearly demonstrates the successful incorporation of ECH-derived Cl into the reclaimed rubber structure. It provides a basis for the expected halogen-based flame-retardant effect.

Table 2. The EDX results after ECH modification.

Sample Code	wt%				
	C	O	S	N	Cl
FD-GTR	63.29	26.45	1.98	8.30	0.00
FD-GTRECH4	61.86	27.95	1.76	7.88	0.56
FD-GTRECH9	63.24	26.28	1.49	7.72	1.28

The rheometer torque curves show that devulcanization and subsequent modification considerably soften the original tire rubber. Untreated GTR exhibits the highest torque and a gradual increase with time, characteristic of a stiff, densely crosslinked network. In contrast, all devulcanized samples (D-0, D-GTR, FD-GTR, and FD-GTRECH4/9) display much lower, nearly constant torque values, indicating that the sulfur crosslinks

have mainly been broken and that the modified reclaimed rubbers remain processable even after modification with PCA and ECH.

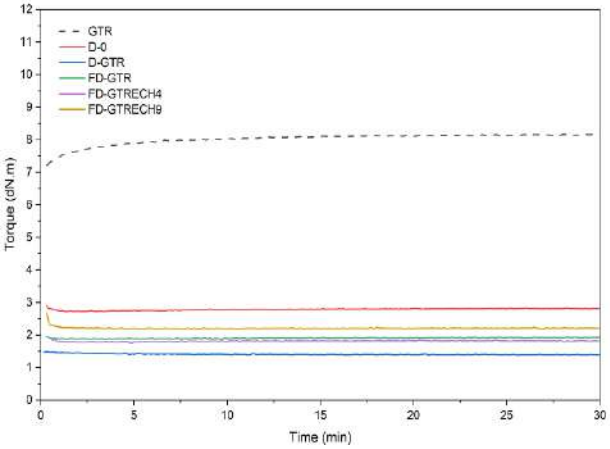

Figure 4. Torque profiles of (a) FD-GTRs.

The swelling data, crosslink density, and degree of devulcanization collectively support the conclusion that devulcanization occurred. Compared with GTR, D-0, D-GTR, and FD-GTR show a substantial increase in sol fraction and swelling, accompanied by a drastic drop in crosslink density from 18.12×10^{-5} to about $4–5\times10^{-5}$ mol/cm³, yielding high devulcanization degrees of roughly 72–78%. These changes indicate that many sulfur crosslinks were cleaved, resulting in a much looser network, as expected for effective devulcanization.

Table 3. Sol-gel fraction, swelling degree, crosslinking density (CLD), and devulcanization degree (DD).

Sample Code	Density (g/cm^3)	Sol (%)	Gel (%)	Swelling (%)	CLD (10^{-5} mol/cm³)	DD (%)
GTR	1.148	4.42 ± 0.3	95.58 ± 0.3	242.12 ± 5.7	18.12 ± 4.4	-
D-0	1.200	7.42 ± 0.8	92.58 ± 0.8	273.52 ± 2.0	12.87 ± 1.2	28.94 ± 6.8
D-GTR	1.132	14.78 ± 0.1	85.22 ± 0.1	471.76 ± 6.1	5.08 ± 1.1	71.95 ± 6.0
FD-GTR	1.120	29.35 ± 4.8	70.65 ± 4.8	521.25 ± 4.4	4.22 ± 0.4	76.74 ± 2.0
FD-GTRECH4	1.162	31.19 ± 3.4	68.81 ± 3.34	525.07 ± 2.4	4.04 ± 1.4	77.68 ± 7.7
FD-GTRECH9	1.145	22.57 ± 6.2	77.43 ± 6.2	496.45± 10.2	4.48 ± 0.8	75.26 ± 4.3

3.2 Flame-retardancy

Natural rubber and tire rubbers burn easily because their LOI is only about 17–18%, which is below the 21% oxygen content of air. This intrinsic flammability limits their safe use in applications where fire risk is important. To address this limitation, this work focuses on recycling waste tires into reclaimed rubber and chemically modifying its structure to reduce flammability without relying on heavy filler loadings [14]. In this study, reclaimed rubber was first devulcanized and then grafted with PCA and ECH to introduce chlorine-containing groups that serve as halogen-containing flame-retardant sites. The flame-retardancy results show that the LOI of the reference rubber (R-0) is 18.4%, and this value increases stepwise to 18.7% for RF-GTR, 18.9% for RF-GTRECH4, and 19.0% for RF-GTRECH9, while all samples retain a UL-94 V-2 rating with no dripping. Considering the amount of chlorine in the system (0.6–1.3% by EDX), the halogen loading is relatively small, and the LOI value increasing by 0.3–0.6 is thus reasonable. According to Patarapaiboolchai *et al.* [15], a required 30:10 phr of chlorinated paraffin:antimony oxide is for UL-94 V-0 in natural rubber, while this Cl-grafting achieves V-2 at ~3 times lower halogen. Although these LOI values are still below 21% and therefore in the flammable range, the 0.6 percentage-point gain from 18.4% to 19.0% is comparable to improvements reported for rubber systems using low levels of halogen-based additives [16]. This indicates that the chlorine introduced by ECH already provides a practical, lightweight flame-retardant contribution. The modest LOI increase is consistent with a gas-phase halogen mechanism, in which C – Cl group decomposes during burning to produce chlorine-containing species that quench flame radicals [3]. Thus, ECH-modified reclaimed rubber is a promising starting matrix for further enhancement of flame resistance.

Table 4. Flame retardancy properties of RF-GTRs.

Sample code	LOI%	UL94	
		Rating	Dripping
R-0	18.4	V-2	No
RF-GTR	18.7	V-2	No
RF-GTRECH4	18.9	V-2	No
RF-GTRECH9	19.0	V-2	No

4. Conclusions

Devulcanization was confirmed by the significant increase in sol fraction and swelling, the drop in crosslink density from 18.1×10^{-5} to about $4–5\times10^{-5}$ mol/cm³, high devulcanization degrees of ~72–78%, and the substantial decrease in torque compared with raw GTR, indicating that many sulfur crosslinks were broken while a re-crosslinkable rubber phase remained. Structural analyses (DSC, ATR-FTIR, and EDX) showed the disappearance of epoxide bands, retention of C–Cl signals, and a rise in chlorine content from 0 to 0.56 and 1.28 wt% for FD-GTRECH4 and FD-GTRECH9, confirming the grafting of ECH onto the reclaimed rubber. As a result, the LOI increased from 18.4% (R-0) to 19.0% (RF-GTRECH9). At the same time, all samples maintained a UL-94 V-2 rating with no dripping, demonstrating a modest but clear improvement in the flame resistance of the reclaimed rubber.

5. Acknowledgements

The authors would like to thank the National Research Council of Thailand (NRCT) for the financial support for this research. The scholarship program for ASEAN and non-ASEAN countries at Chulalongkorn University also supported this research. We thank Union Commercial Development Co., Ltd., for their support for waste tire rubber, and AGC Vinuthai Public Company Limited (AVT) for their support for bio-based ECH.

6. References

1. Hopewell, J.; Dvorak, R.; Kosior, E. Plastics recycling: challenges and opportunities. *Philos Trans R Soc Lond B Biol Sci*. **2009**, *364* (1526), 2115-2126.
2. Molanorouzi, M.; Mohaved, S. O. Reclaiming waste tire rubber by an irradiation technique. *Polymer Degradation and Stability*. **2016**, *128*, 115-125.
3. Georlette, P. Applications of halogen flame retardants. *Fire retardant materials*. **2001**, 264-292.
4. Wang, X.; Tu, H.; Xiao, H.; Lu, J.; Xu, J.; Gu, G. A novel halogen-free flame-retardant fabrication for the study of smoke suppression and flame retardancy of polystyrene. *Polymer*. **2023**, *283*.
5. Bukowska, A.; Bukowski, W.; Noworól, J. A study on the addition of some carboxylic acids to epichlorohydrin in the presence of salen chromium (III) complexes. *Journal of Molecular Catalysis A: Chemical*. **2003**, *203* (1-2), 95-99.
6. Sirisinha, C.; Phoowakeereewiwat, S; Saeoui, P. Cure and dynamic mechanical properties in peoxide-cured isoprene rubber: effects of stearic acid and amine-based antioxidant. *European Polymer Journal*. **2004**, *40* (8), 1779-1785.
7. Xiao, L.; Shan, H.; Wu, Y. Chitosan cross-linked and grafted with epichlorohydrin and 2, 4-dichlorobenzaldehyde as an efficient adsorbent for removal of Pb (II) ions from aqueous solution. *International Journal of Biological Macromolecules*. **2023**, *247*, 125503.
8. Wang, W.; Hao, K.; Guo, X.; Liu, F.; Xu, Y.; Guo, S.; Bai, L.; Liu, G.; Qu, L.; Liu, M. Mechano-chemical rubber reclamation using aminolysis products of waste flexible polyurethane foams as the devulcanizing agent. *Journal of Cleaner Production*. **2023**, *384*, 135421.
9. Intharapat, P.; Nakason, C.; Kongnoo, A. Preparation of boric acid supported natural rubber as a reactive flame retardant and its properties. *Polymer Degradation and Stability*. **2016**, *128*, 217-227.
10. Chidara, V. K.; Gnanou, Y.; Feng, X. Exploring borinane-based multi-ammonium salts for epoxide (co) polymerization: insights into the structure–activity relationship. *Polymer Chemistry*. **2024**, *15* (24), 2492-2501.
11. Saito, T.; Klinklai, W.; Kawahara, S. Characterization of epoxidized natural rubber by 2D NMR spectroscopy. *Polymer*. **2007**, *48* (3), 750-757.
12. Zhou, S.; Xu, X.; Ma, N.; Jung, F.; Lendlein, A. Prediction of the epichlorohydrin derived cytotoxic substances from the eluent of poly(glycerol glycidyl ether) films. *MRS Advances*. **2021**, *7* (16-17), 354-359.

13. Keya, K. N.; Li, Z.; Xu, L.; Xia, W. Exploring cross-link density and additive effects on mechanical and morphological behaviors of cross-linked polymers. *Macromolecular Materials and Engineering*. **2025**, *310* (5), 2400383.
14. Marvin, C. H.; Sverko, E.; Tomy, G. T. Analysis of chlorinated and phosphorus flame retardants. In *Dioxin and Related Compounds*, Springer, **2016,** 411-456.
15. Patarapaiboolchai, O.; Chaiyaphate, S. Improvements of natural rubber for flame resistance. *Songklanakarin Journal of Science and Technology*. **2010**, *32* (3), 299.
16. Jiang, J.; Zhang, J.; Kong, L.; Zhao, D.; Feng, Y. Flame retardant chloroprene rubbers with high tensile strength and elongation at break via dual cross-linked networks. *RSC advances*. **2022**, *12* (42), 27633-27640.
17. Toshtemirova, G.; Tokhirov, M.; Adilov, R. Study of the properties of sulfur obtained by devulcanization of aged rubber waste. *Science and Innovation*. **2025**, *4*, 174-181.
18. Sugano, M.; Tsubosaka, M.; Shimizu, S.; Fujita, M; Fukumoto, T.; Hirano, K.; Mashimo, K. Dechlorination of chloroprene rubber by coliquefaction with natural rubber containing zinc oxide. *Energy and Fuels*. **2008**, *22* (3), 1986-1990.
19. Kindrick, R. H. Zinc oxide-zinc salt smoke suppressant/flame retardants. *U.S. Patent*. **1984**, No. 4.439.572.
20. Liu, L; Zhang, Y.; Wang, T.; Ma, C.; Fang, Z; Wang, D. Dependence of flame retardancy and smoke suppression properties of chloroprene rubber on zinc borate and antimony trioxide loadings. *Material Today Chemistry*. **2024**, *36*, 101966.
21. Innes, J. R.; Siddique, N.; Thompson, G.; Wang, X.; Coates, P.; Whiteside, B.; Kelly, A. The influence of devulcanization and revulcanization on sulfur crosslink type/rank: recycling of ground tire rubber. *ACS omega*. **2024**, *9* (40), 41797-41806.

Author